History of ice sheets surrounding Baffin Bay and its link with oceanic conditions since MIS3

zur Erlangung des Doktorgrades der Naturwissenschaften
am Fachbereich Geowissenschaften
der Universität Bremen/

submitted for the doctoral degree in natural sciences
at the faculty of Geosciences
of Bremen University

vorgelegt von/
by

Rebecca Jackson
Bremen, 14.08.2017

marum ArcTrain Universität Bremen

Erstgutachter/ First Reviewer

Prof. Dr. Michal Kucera, Universität Bremen

Zweitgutachter/ Second Reviewer

Dr. Matthias Moros, Leibniz Institute for Baltic Sea Research Warnemünde

Tag des Prüfungskolloquiums/ Date of PhD defence

14. December 2017

Versicherung an Eides Statt

gem. § 5 Abs. 5 der Promotionsordnung vom 15.07.2015

Ich, _____
(Vorname, Name, Anschrift, ggf. Matr.-Nr.)

versichere an Eides Statt durch meine Unterschrift, dass ich die vorstehende Arbeit selbständig und ohne fremde Hilfe angefertigt und alle Stellen, die ich wörtlich dem Sinne nach aus Veröffentlichungen entnommen habe, als solche kenntlich gemacht habe, mich auch keiner anderen als der angegebenen Literatur oder sonstiger Hilfsmittel bedient habe, und die zu Prüfungszwecken beigelegte elektronische Version der Dissertation mit der abgegebenen gedruckten Version identisch ist.

Ich versichere an Eides Statt, dass ich die vorgenannten Angaben nach bestem Wissen und Gewissen gemacht habe und dass die Angaben der Wahrheit entsprechen und ich nichts verschwiegen habe.

Die Strafbarkeit einer falschen eidesstattlichen Versicherung ist mir bekannt, namentlich die Strafandrohung gemäß § 156 StGB bis zu drei Jahren Freiheitsstrafe oder Geldstrafe bei vorsätzlicher Begehung der Tat bzw. gemäß § 161 Abs. 1 StGB bis zu einem Jahr Freiheitsstrafe oder Geldstrafe bei fahrlässiger Begehung.

_____ _____

Ort, Datum Unterschrift

Abstract

Many of the climatic changes we are witnessing in the present day are amplified in the Arctic regions. Rising atmospheric and ocean temperatures and the recession of the Greenland Ice Sheet, so called 'Polar Amplification', make it more important than ever to understand the interaction between the different components of the Earths' system. Reconstructing past climate is not only a vital means of understanding the history of these interactions and the processes behind them; it in turn serves to strengthen future projections of the fate of climatically sensitive regions.

Baffin Bay is a semi-enclosed ocean basin that lies between Greenland and the Canadian Arctic Archipelago and provides the ideal setting for studying the interaction between the marine realm and the cryosphere. Up until the transition from the last glacial period into the warm Holocene period, Baffin Bay was flanked by three major northern hemisphere ice sheets: the Innuitian, Laurentide and Greenland ice sheets, the latter of which persists today. It is an important, but often overlooked, conduit for meltwater into the Labrador Sea and North Atlantic; a key site for deep-water formation and thus climate modulation. Baffin Bay is fed from the south by waters from the North Atlantic Ocean and from the north by cool and fresh waters from the Arctic Ocean. Marine sediment archives capture characteristics of both ice sheet behaviour and oceanic conditions. Layers of detrital material, brought into the bay by iceberg and meltwater discharge, provide a record of ice sheet retreat. Marine organisms, preserved in this same sediment, provide information on the conditions of the waters which they inhabited. However, one of the key hindrances to reconstructing paleoclimatic conditions in this region is pervasive carbonate dissolution in the corrosive waters of deep Baffin Bay. Not only does this hinder multi-proxy paleoceanographic studies but prevents the construction of robust, radiocarbon-dated chronologies.

In this study we utilise two sediment cores collected from both the central western and central eastern Baffin Bay and both with good preservation of biogenic carbonate. The first aim of the study was to produce robust age models for the last deglaciation and early Holocene ($\sim$17-10kyr BP) in Baffin Bay and accurately constrain the timing of ice sheet instabilities, termed Baffin Bay Detrital Carbonate events (BBDCs). There were two periods of meltwater and iceberg discharge during this period, with a significant

contribution from the ice sheets surrounding northern Baffin Bay. These events (BBDC 1 and 0) were synchronous across the Baffin Bay but occurred during both stadial and interstadial periods, highlighting the need to consider regional responses of ice sheets to climatic changes.

In light of this, the second aim of the study was to establish changes in paleoceanographic conditions off the west coast of Greenland throughout the deglacial and early Holocene and to assess whether these changes were a potential trigger or product of ice-sheet instabilities (BBDCs). The multi-proxy study indicated the presence of persistent sea ice throughout this period and that the sub-surface water masses had similar characteristics to the wider region. Prior to $\sim$14kyr BP Baffin Bay was relatively well-ventilated compared to modern conditions and a strong inflow of the West Greenland Current is only observed after this time. These changes post-date the onset of BBDC 1 and no major change in oceanic conditions predated BBDC 0.

The third aim was to establish the timing of BBDC events further back in time, to Marine Isotope Stage 3 (MIS 3). Utilising the longer core from central west Baffin Bay, we combined radiocarbon and paleomagnetic dating to establish a chronology. Results indicate that there were 7 BBDC events between $\sim$52 and 0.9kyr BP, that occurred during both stadial (cold) and interstadial (warm) periods. Sedimentary properties outside these layers suggest a change in source area and/or mechanism of delivery of sediment from surrounding ice sheets to central west Baffin Bay from $\sim$44 kyr BP up until the onset of the Holocene, when the Innuitian and north-eastern Laurentide ice sheets had likely retreated from their marine-terminating position thus exhausting the supply of detrital material to Baffin Bay.

Zusammenfassung

Viele der klimatischen Veränderungen, die wir heutzutage beobachten, treten in verstärkter Form in den Polregionen auf. Steigende Temperaturen der Atmosphäre und des Ozeans, sowie der Rückgang des Grönlandeisschildes gehören zu den sogenannten "Polaren Verstärkunge" und machen es wichtiger als je zuvor, die Interaktionen zwischen verschiedenen Komponenten des Erdsystems zu verstehen. Die Rekonstruktion des Klimas der Vergangenheit ist nicht nur ein unverzichtbares Instrument, um die Entwicklung dieser Interaktionen und die Prozesse dahinter zu verstehen, es trägt auch zur Verbesserung von Zukunftsprognosen über deren Auswirkung auf klimatisch sensible Regionen bei. Die Baffinbucht ist ein halb geschlossenes Ozeanbecken zwischen Grönland und dem kanadisch-arktischen Archipel und bietet ideale Bedingungen, um die Interaktion zwischen der Meereswelt und der Kryosphäre zu untersuchen. Bis zum Übergang von dem letzten Deglazial zum warmen Holozän war die Baffinbucht umgeben von drei für die Nordhalbkugel bedeutenden Eisschilden: dem Innuitian, dem Laurentidischen und dem Grönländischen Eisschild, letzterer existiert auch heute noch. Auch wenn es oft übersehen wird, ist die Baffinbucht ein wichtiger Zufluss von Schmelzwasser in die Labradorsee und in den Nordatlantik, welcher eine Schlüsselregion für die Tiefenwasserformierung und daher auch für die Klimamodellierung ist. Die Baffinbucht wird im Süden von dem Nord-atlantischen Ozean und im Norden von dem kalten Süßwasser des Arktischen Ozeans gespeist. Marine Sedimentablagerungen archivieren sowohl die Eigenschaften und das Verhalten der Eisschilde als auch Ozeanbedingungen. Durch den Eintrag von Eisbergen und Schmelzwasserabfluss in die Bucht entstanden Detriuslagen, welche Auskunft über den Eisschildrückgang geben. Marine Organismen, die in demselben Sediment abgelagert wurden, bieten Informationen über die Eigenschaften des Wassers, in welchem sie lebten. Eines der größten Hindernisse für die Paleoklimarekonstruktion ist die allgegenwärtige Karbonatlüsung in dem korrosiven Tiefenwasser der Baffinbucht. Dieses beeinträchtigt nicht nur Multi-Proxy paleozeanographische Untersuchungen, sondern auch die Erstellung von verlässlichen Radiokarbon Altersdatierungen. Für diese Arbeit wurden zwei Sedimentkerne verwendet, die in der zentral-östlichen und der zentral-westlichen Baffinbucht genommen wurden. Beide weisen eine gute Erhaltung von biogenem Karbonat auf. Das erste Ziel dieser Arbeit war es, verlässliche Altersmodelle für das Deglazial und das frühe Holozän (ca. 17.000-10.000 v. h.) zu erstellen

und die genaue Datierung von Phasen der Instabilität der Eisschilde, sogenannte Baffin Bay Detrital Carbonate Events (BBDCs). Während dieser Zeit gab es zwei Phasen von Süßwasser- und Eisberg-Eintrag, bei denen die umliegenden Eisschilde der nördlichen Baffinbucht einen deutlichen Beitrag leisteten. BBDC 1 und 0 verliefen in der gesamten Baffinbucht synchron aber traten sowohl während eines Stadials als auch während eines Interstadials auf, was zeigt, dass es wichtig ist, regionale Feedbacks von Eisbergen auf das Klima zu berücksichtigen. Daher war das zweite Ziel dieser Arbeit, eine Begründung für Änderungen der Paläozeanografischen Bedingungen vor der westlichen Küste Grönlands während des Deglazials und des frühen Holozäns zu finden und zu bewerten, ob diese Veränderungen potentielle Verursacher für oder ein Ergebnis der Eisschildinstabilitäten (BBDCs) waren. Diese Multi-Proxy Studie zeigt, dass während dieser Zeit beständiges Meereis vorhanden war und dass das Oberflächenwasser (bis ca. 150 m Tiefe) ähnliche Eigenschaften hatte wie das der umliegenden Region. In der Zeit bis 14.000 v. h. war die Baffinbucht relativ gut durchlüftet verglichen zu jüngeren Bedingungen und der starke Einfluss des Westgrönland Stroms wird erst nach diesem Zeitpunkt beobachtet. Diese Veränderungen begannen nach dem Beginn des BBDC 1 und es gab keine grösseren Veränderungen der Ozeanischen Bedingungen vor dem BBDC 0. Das dritte Ziel war es, auch frühere BBDC Events rückreichend bis zum Marinen Isotopenstadium 3 (MIS 3) zu datieren. Für die Erstellung einer Chronologie wurden an dem längeren der Kerne aus der zentral-westlichen Baffinbucht Radiokarbon und Paleomagnetische Altersdatierung durchgeführt. Die Daten zeigen, dass es sieben BBDC Events zwischen ca. 52.000 und 00.900 v. h. gab, die sich sowohl während Stadialen (kalt) als auch während der Interstadialen (warm) ereigneten. Die Sedimentablagerungen zwischen diesen Lagen deuten auf eine Änderung der Quelle und/oder der Transportmechanismen des Sedimentes von den umgebenden Eisschilden zu der zentral-westlichen Baffinbucht in dem Zeitraum von 44.000 v. h. bis zum Anfang des Holozäns hin, als sich das Innuitian und das nordöstliche Laurentidische Eisschild vermutlich von ihrer ins Meer mündenden Position zurückzogen und dadurch der Eintrag von Detius in die Baffinbucht versiegte.

Acknowledgements

Where to begin...there have been so many people, institutes and projects that have brought this PhD thesis to fruition.

I'll start at the beginning. I would like to thank the scientists and crew on the *Maria S. Merian* resarch cruise MSM/09 in 2008 for collecting the cores as well as the staff at University of Tübingen for curating them.

This project was one of many completed as part of the International Research Training Group ArcTrain (ITRG 1904) so firstly I acknowledge the Deutsche Forschungsgemeinschaft (DFG) for its funding. Secondly, the ArcTrain project would not have existed without its proponents, Prof.Dr. Michal Kucera and Prof.Anne de Vernal. As members of my thesis committee these two people also deserve acknowledgement for their supervision, support and advice throughout this project. As a newcomer to Arctic research their combined experience was invaluable asset to this project. I would also like to thank Anne de Vernal and the GEOTOP institute at the Université du Québec à Montréal for sharing their labs and hosting my research stay.

Many different analyses were carried out as part of this project. Thanks go to the Crystallography, Marine Geophysics Group and the mass spectrometry laboratory at the Univerisität Bremen/MARUM, as well as the ETH Zürich, for their role in this analysis as well as for advice and resulting co-authorship. I also would like to thank other co-authors on the published manuscript, Anders E. Carlson and Claude Hillaire-Marcel for their feedback which helped lead to the successful publishing of the manuscript.

On a more personal level, I would like to thank the AG Kucera for hosting me in the MARUM for the last three (nearly four) years. They have all been incredibly supportive and welcoming. I regard the other ArcTrain students not only as lovely colleagues but also great friends; they provided not only a great scientific network but support and advice (and a kind ear) whenever I needed it. I hope to keep in touch with them all and I truly wish them all the best for the future.

My family deserve a special mention too. I am the first one in my family to attend university: they always say I don't do things by halves. For the being proud, the late night Skype conversations, the surprise visit and the stream of nephew photos...thank

you. The many friends I have made outside of work in Bremen deserve a special mention too for their encouragement, their patience, sharing a bottle of wine/kiosk beer every now and then, and of course their love. You know who you are.

Last but not least, I would like to acknowledge myself, if that's not too self serving. Completing a PhD has been an amazing/stressful/challenging/ experience all at the same time and something that at some points I wasn't sure I was capable of achieving. So to you Becky: you did it. Well done.

Contents

1 Introduction **1**

1.1 Regional Setting . . . 1
1.2 Modern oceanography . . . 1
1.3 Glacial History . . . 3
1.4 Baffin Bay Detrital Carbonate Events (BBDCs) . . . 4
1.5 Paleoceanography of Baffin Bay during the last deglaciation and early Holocene . . . 6
1.6 Chronological issues . . . 8
1.7 Materials used in this study . . . 8
1.8 Research Objectives . . . 9

2 Thesis outline and author contributions **11**

2.1 Thesis outline . . . 11
2.2 Description of own contributions . . . 13

3 Asynchronous instability of the North American-Arctic and Greenland ice sheets during the last deglaciation **15**

3.1 Published paper . . . 15
3.2 Supplementary Information . . . 31
3.2.1 PARASOUND surveys and magnetic susceptibility . . . 31
3.2.2 Chronology: outliers in SL 170 age model . . . 31
3.2.3 Sedimentation rates . . . 33
3.2.4 Computerised tomography (CT) scanning . . . 33
3.2.5 X-ray fluorescence (XRF) analysis . . . 33
3.2.6 X-ray diffraction (XRD) analysis . . . 35

4 Paleoceanographic changes during the last deglaciation and early Holocene in Baffin Bay: links with ice sheet instabilities? **37**

4.1 Introduction . . . 38
4.2 Methods and material . . . 39
4.2.1 Coring and construction of the age model . . . 39
4.2.2 Physical sediment properties and X-ray florescence (XRF) analysis 41

4.2.3 Palynomorph analysis . . . 41
4.2.4 Foraminiferal analysis . . . 41
4.2.5 Multivariate statistics . . . 42
4.2.6 Stable isotope analysis . . . 42
4.3 Results . . . 42
4.3.1 Chronology . . . 42
4.3.2 Surface ocean conditions: palynomorph analysis . . . 44
4.3.3 Sub-surface ocean conditions . . . 45
4.3.4 Bottom water conditions . . . 45
4.4 Discussion . . . 50
4.4.1 Changes in surface conditions during the deglaciation and early Holocene . . . 50
4.4.2 Sub-surface conditions in Baffin Bay: a regional δ^{18}O signal? . . . 51
4.4.3 Changes in deeper waters throughout the deglaciation and early Holocene . . . 53
4.4.4 Relationship between ice sheet instabilities (BBDCs) and paleoceonographic changes . . . 57
4.5 Conclusions . . . 61
4.6 Supplementary Figures . . . 63

5 A new chronology of ice sheet retreat in Baffin Bay since Marine Isotope Stage 3 67
5.1 Introduction . . . 68
5.1.1 Regional setting and glacial history . . . 68
5.1.2 Previous work . . . 70
5.2 Methods and Materials . . . 71
5.2.1 Core GeoTü SL 174 . . . 71
5.2.2 Physical and elemental properties . . . 71
5.2.3 Magnetic Susceptibility measurements . . . 72
5.2.4 Rock and Paleomagnetic measurements . . . 72
5.2.5 Relative Paleointensity (RPI) dating . . . 73
5.2.6 Radiocarbon dating . . . 73
5.2.7 Age Modelling . . . 74
5.2.8 Multivariate Analysis . . . 76
5.3 Results . . . 76
5.3.1 Lithology, physical and geochemical properties . . . 76
5.3.2 Magnetic Susceptibility and magnetic remanence properties . . . 78
5.3.3 Multivariate analysis . . . 79
5.3.4 Chronology . . . 82

5.4 Discussion 85
5.4.1 BBDC events: identification and timing 85
5.4.2 BBDC events: a link with climatic variation? 87
5.4.3 'Non-event' layers and background sedimentation in Baffin Bay . 90
5.5 Conclusions 93
5.6 Supplementary figures 94

6 Conclusions and outlook **95**
6.1 Conclusions 95
6.2 Outlook 97

References **99**

List of Figures

1.1 Location and geology surrounding Baffin Bay 2
1.2 Modern oceanography 3
1.3 Last Glacial Maximum (LGM) ice sheet extent 4
1.4 Timing of BBDC events 6
1.5 Links between ice sheet instabilites and paleoceangraphic conditions . . . 7

3.1 Location of study sites and modern oceanography of Baffin Bay 18
3.2 Chronology and lithostratigraphy of core SL 174 20
3.3 Chronology and lithostratigraphy of core SL 170 21
3.4 Timing of BBDC events during the last deglaciation and early Holocene . 23
3.5 Detrital carbonate composition during BBDC events 24
3.6 Testing the effect of local reservoir age on the timing off BBDCs 25
3.7 Compilation of ice-rafting and detrital carbonate events in and around Baffin Bay 26
S3.1 PARASOUND profiles at core sites 31
S3.2 Age-depth relationship for core SL170 32
S3.3 Downcore properties of Baffin Bay sediment cores 34

4.1 Core location of SL 170 and modern oceanography of Baffin Bay 40
4.2 Chronology and lithostratigraphy for core SL 170 43
4.3 Palynomorph concentrations in core SL 170 44
4.4 Sub-surface ocean conditions 46
4.5 Benthic foraminifera assemblages in core SL 170 48
4.6 Correspondence Analysis cross plot of benthic foraminifera assemblages . 49
4.7 Changes in bottom ocean conditions 50
4.8 Compilation of Npl δ^{18}O from the Greenland margins and Labrador Sea . 54
4.9 BBDC events and the timing of paleoceanographic change in Baffin Bay 60
S4.1 Corss plot: Pb ratios in different size fractions 63
S4.2 Cross plot: benthic δ^{18}O and δ^{13}C 64
S4.3 Cross plot: $\Delta\delta^{18}$O and planktonic to benthic ratio 65

5.1 Geology surround Baffin Bay and core SL 174 location 69
5.2 Summary of lithostratigraphy, physical and geochemical paratemter . . . 77

5.3 Mineral magnetic parameters downcore in SL 174 79
5.4 PCA analysis of core SL 174 80
5.5 Linear Discriminant Analysis of DC-rich layers 81
5.6 Linear Discriminant Analysis (LDA) results of 'non-event' layers 82
5.7 Directional magnetic measurements for core SL 174 83
5.8 Chronology of core SL 174 84
5.9 Timing of BBDC events in core SL 174 88
5.10 'Non-event' layers and background sedimentation in core SL 174 91
S5.1 Cross plots of L-ratio/S-ratio and L-ratio/HIRM 94

List of Tables

3.1 Radiocarbon dates and modelled ages for core SL 174 22
3.2 Radiocarbon dates and modelled ages for core SL 170 22

4.1 Benthic foraminifera species and their environmental preferences 47

5.1 Relative Paleointensity tie-points: GLOPIS and SL 174 74
5.2 Radiocarbon dates and RPI tie points for core SL 174 75
5.3 SL 174 PCA scores 80

Chapter 1

Introduction

1.1 Regional Setting

Baffin Bay is a narrow oceanic basin situated between Greenland and Canada, stretching from ∼67°N-76°N (Fig. 1.1). The 1300 km long and 450 km wide basin, covering a total area of ∼690.000 km^2, is a product of the North Atlantic-Labrador Sea rift system [*Maclean et al.*, 1990]. Baffin Bay is a semi-enclosed basin, with connections to the North Atlantic via the Davis Strait (∼650 m water depth) and with the Arctic Ocean via the Nares Strait and various channels through the Canadian Arctic Archipelago. The central abyssal plain is 2000-2500 m deep and in the eastern margin gives way to steep continental slopes that extend from the Greenland shelf by >250 km and are characterised by submarine fans and cross-shelf troughs (e.g. *Ò Cofaigh et al.* [2013]). These features are not found adjacent to the Baffin Island coast, mostly likely due to smaller fjord outlets along the narrower shelf (25–50 km) [*Ó Cofaigh et al.*, 2013].

Very few outcrops of young rock are observed in the landmasses surrounding Baffin Bay. The geology of the Greenland landmass consists the of Archaean Block and Nagssugtoquidian Mobile Belt on the south east and central west coast. To the north and west, the Ellesmere Island, Nares Strait/Smith Sound and Lancaster Sound regions are characterised by extensive outcrops of Palaeozoic limestones and dolostones [*Hiscott et al.*, 1989] whilst the Baffin Island region is predominantly composed of Paleoproterozoic granites, gneisses and siliciclastic rocks.

1.2 Modern oceanography

Modern circulation in Baffin Bay is anti-cyclonic (Fig. 1.2). The cool and fresh polar East Greenland Current (EGC) flows southward along the coast of east Greenland, where it is met by the warmer and more saline northward flowing Irminger Current (IC), an

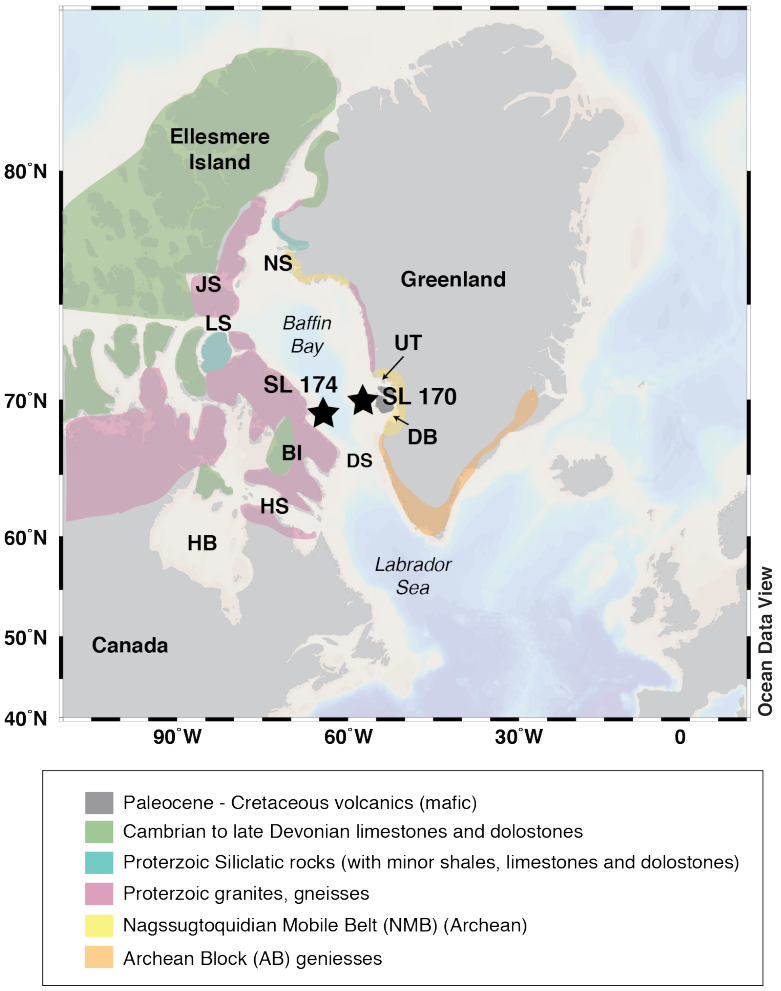

Figure 1.1: Location of Baffin Bay, surrounding landmasses, geology and the location of cores in this study (black stars). Simplified geology is adapted from *Harrison et al.* [2011]. Modern inlets into the Baffin Bay are indicated: DS = Davis Strait, DB = Disko Bugt, UT = Uummannaq Trough, NS = Nares Strait, JS = Jones Sound; LS = Lancaster Sound, BI = Baffin Island, HB = Hudson Bay, HS = Hudson Strait.

offshoot of the North Atlantic Current, which flows beneath the EGC. These currents continue to follow the Greenland coastline and enter into Baffin Bay, becoming the West Greenland Current (WGC) that is increasingly mixed as it travels up the west Greenland coast [*Tang et al.*, 2004]. The WGC forms a subsurface water layer between ∼150-600m, termed West Greenland Intermediate Water and this layer caps the Baffin Bay 'Deep water'; a monotonously cool ($\leq 0\,^{\circ}C$) and saline water mass that penetrates to the deepest parts of Baffin Bay (Fig. 1.2) [*Tang et al.*, 2004]. The top ∼150 m of the water column remain cool and fresh due to both input of meltwater from the Greenland Ice Sheet (GIS) and the southward flow of polar water via the Baffin Island Current, which enters Baffin Bay via the main conduits in the north of the basin, such as the Nares Strait and Lancaster and Jones Sound. Thus the water column is relatively well

stratified throughout Baffin Bay. As the WGC loses strength as it travels north, the eastern portion of the Baffin Bay is cooler throughout the water column. The inflow of Atlantic-sourced waters thus explains the asymmetric distribution of sea ice in Baffin Bay; sea ice cover is more persistent and extensive in the western portions of Baffin Bay than along the west Greenland margins. However, sea ice is persistent throughout most of the year with the exception of September and August [*Tang et al.*, 2004].

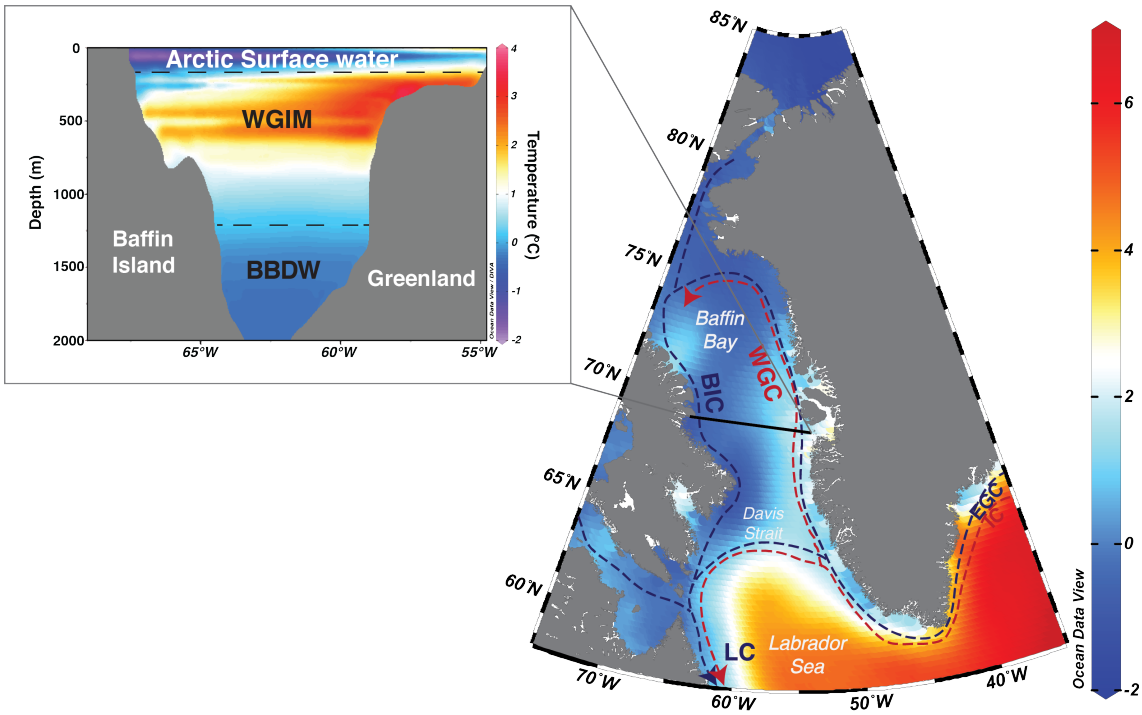

Figure 1.2: Modern Oceanography in Baffin Bay. Coloured map (left) indicates modern sea surface temperatures and major ocean currents entering the Baffin Bay (EGC = East Greenland Current IC = Irminger Current, WGC = West Greenland Current). Colder surface waters enter the basin in the north and travel along the coast, travelling south and into the Labrador Sea (BIC = Baffin Island Current, LC = Labrador Current). The insert shows water column temperatures and water masses cross section of the basin (WGIM = West Greenland Intermediate Water, BBDW = Baffin Bay Deep Water). All data complied in Ocean Data View using the World Ocean Atlas (WOA) dataset.

1.3 Glacial History

During the Last Glacial Maximum (LGM), Baffin Bay was flanked by the Greenland Ice Sheet (GIS) to the east and the north-eastern Laurentide Ice Sheet (LIS) to the west [*Dyke et al.*, 2002]. The Innuitian Ice Sheet (IIS) formed a bridge between the GIS and LIS across the northern sector of Baffin Bay [*England et al.*, 2006], encapsulating the basin in a near-continuous belt of ice (Fig. 1.3). The GIS extended westward onto the shelf edge and according to geological and seismic investigation as far as the shelf break in the Uummannaq Trough and Disko Bugt [*Ò Cofaigh et al.*, 2013; *Ó Cofaigh et al.*,

2013; *Funder et al.*, 2011; *Jennings et al.*, 2014] and remained at this maximum extent until ∼15 kyr BP. The retreat of the central west GIS margin to its current position was not linear; this dynamic ice margin re-advanced at least once during the Younger Dryas stadial at ∼12.2 kyr BP via the Jakobshavn Isbrae (Fig. 1.1), supplying the adjacent area with ice-rafted detrital material [*Jennings et al.*, 2014]. However further north in the Uummannaq Trough region, retreat was already underway ∼14.8 kyr BP [*Ò Cofaigh et al.*, 2013; *Sheldon et al.*, 2016].

The IIS advanced later than the GIS, reaching its maximum extent ∼19 kyr BP and along with the LIS, these ice streams filled the Nares Strait/Smith Sound, Jones Sound and Lancaster Sound (e.g. *Marcott et al.* [2011]), as well as extending through Baffin Island [*Briner et al.*, 2007, 2016]. However, an LGM grounding line, deposited 270 km from the mouth of Lancaster Sound suggests that the LIS reached its maximum extent between 24 and 20 kyr BP [*Li et al.*, 2011], earlier than the IIS. The total discharge of icebergs from the ice sheets that surrounded Baffin Bay during the LGM has been estimated at $\sim 1.86 \times 10^{-6} \mathrm{km}^3$ [*Marshall and Koutnik*, 2006].

Figure 1.3: Last Glacial Maximum (LGM) extent of the Greenland, Innuitian and Laurentide ice sheets, adapted from *Dyke et al.* [2002].

1.4 Baffin Bay Detrital Carbonate Events (BBDCs)

The retreat of the IIS and LIS is archived in sedimentary deposits throughout Baffin Bay. These layers are often composed of coarse, ice-rafted material that has a distinct, detrital carbonate-rich composition. The discovery of these layers is not new; work by *Aksu and Piper* [1987] and *Hiscott et al.* [1989] described these facies in detail and proposed that this detrital material originated from northern Baffin Bay and was transported southward as ice-rafted debris, following a current path similar to the modern day Baffin

Island Current (Fig. 1.2). This early research suggested that these events occurred during periods of stronger influx of Atlantic-sourced waters and ice melt as indicated by planktonic δ^{18}O records (Fig. 1.4). The sequence of these layers, termed Baffin Bay Detrital Carbonate Events (BBDCs, *Andrews et al.* [1998]), appeared to be offset from the record of Heinrich Events, the latter documenting the discharge of icebergs armadas from the LIS via the Hudson Strait [*Heinrich*, 1988; *Hemming*, 2004; *Channell et al.*, 2012]. More recent sedimentary records confirm this hypothesis, indicating that the behaviour of the IIS and north-eastern LIS was out of phase with the LIS and that this asynchronicity was a potentially persistent feature of the late Quaternary period [*Andrews et al.*, 2014; *Simon et al.*, 2012, 2014]. BBDC events are likely a response to Dansgaard-Oeschger oscillations observed in Greenland ice core δ^{18}O records, but unlike Heinrich events which occurred during stadial periods [*Bond et al.*, 1993; *Broecker et al.*, 1992], BBDC events have been suggested to be linked to interstadials (e.g. *Simon et al.* [2014]).

Heinrich Event layers deposited in the Labrador Sea and further afield in the North Atlantic are also characterised by a high proportion of detrital carbonate (e.g. *Channell et al.* [2012]; *Rashid et al.* [2003]); however, if the modern day circulation (Fig. 1.2) persisted in the past then icebergs expelled by the LIS via the Hudson Strait would be driven south-east and likely not redirected into Baffin Bay. Furthermore, a large proportion of the carbonate found within BBDC layers is dolomite, as opposed to the calcite-rich signature of Heinrich event layers. Mineralogical analysis of box-core samples throughout Baffin Bay indicate a 'plume' of dolomite-rich detrital carbonate that extends south and west throughout Baffin Bay from the axial point of its north-eastern Baffin Bay source area [*Andrews et al.*, 2011]. Evidence of these dolomite-rich BBDC layers have been found in the Disko Bugt area during the last deglaciation and early Holocene [*Jennings et al.*, 2014, 2017], as far south as the Labrador Sea during the last $\sim$40 kyr BP [*Andrews et al.*, 2014, 2012] and off the coast of Newfoundland in the early Holocene [*Pearce et al.*, 2015].

Heinrich events and associated meltwater discharge from the LIS have been a major focus of research for number of years and their timing and potential impacts on climate are well documented (e.g. *Bond et al.* [1992]; *Heinrich* [1988]; *Bond et al.* [1995]; *Broecker et al.* [1992]; *Carlson and Clark* [2012]; *Channell et al.* [2012]; *Hemming* [2004]). In comparison, Baffin Bay has received relatively little attention. Baffin Bay acted as a corridor for meltwater delivery from north-eastern LIS and IIS, as well as the GIS which flowed into the Labrador Sea, an important area for deepwater formation and thus climate modulation. Although progress has been made on defining the timing of these ice sheet instabilities since they were first discovered, absolute chronologies, beyond the Younger Dryas and Holocene periods, are absent. Without such a chronology, the role and/or

response of the ice sheets surrounding Baffin Bay in the wider climatic context and oceanic circulation cannot be fully assessed.

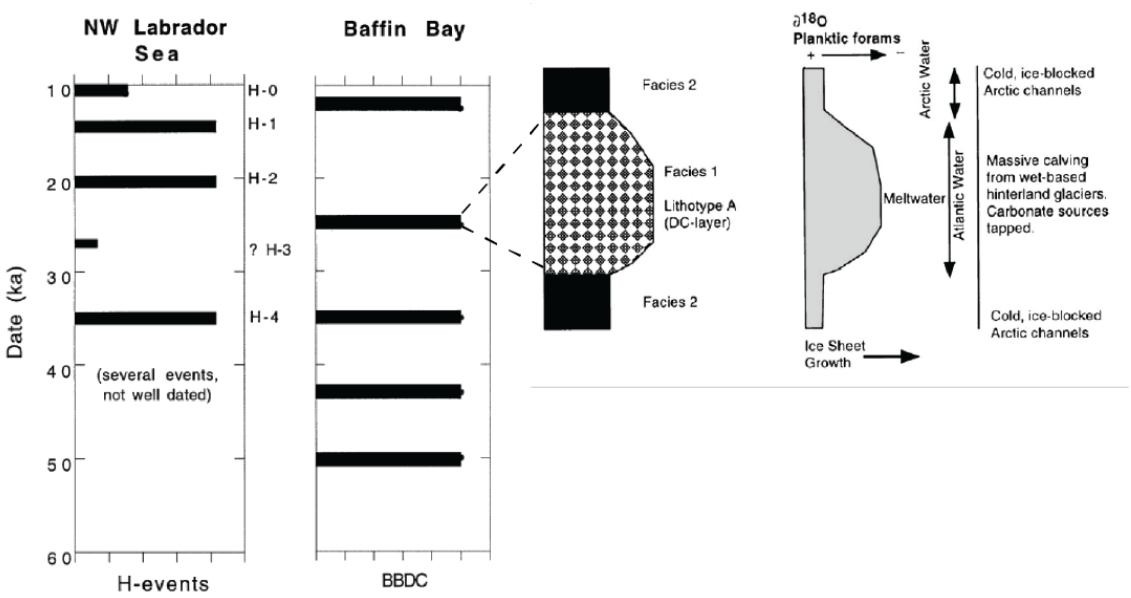

Figure 1.4: Timing of BBDC events, modified from *Andrews et al.* [1998], who proposed that Baffin Bay Detrital Carbonate Events were likely asynchronous with Heinrich Events and occurred at the same time as influxes of Atlantic water.

1.5 Paleoceanography of Baffin Bay during the last deglaciation and early Holocene

Reconstruction of paleoceanographic conditions in Baffin Bay is vital to understanding the behaviour of the marine-terminating outlets of the GIS, IIS and LIS. Much work has focussed on the fjord areas of the GIS such as Disko Bugt where the abundance of biogenic carbonate allows for not only radiocarbon dating, but for combined sedimentological studies with a reconstruction of sub-surface and deeper water conditions using foraminifera (e.g. *Ouellet-Bernier et al.* [2014]; *Perner et al.* [2011, 2013]; *Seidenkrantz et al.* [2013]). However, these records contain extensive local influence and only extend back to the Younger Dryas.

Early studies of sediments from the deeper portions of Baffin Bay, using dinoflagellate cysts and planktonic foraminifera where available, suggested that detrital carbonate layers are related to the increasing influence of Atlantic water [*de Vernal et al.*, 1987]. More recent work [*Sheldon et al.*, 2016] supported this assertion in the Uummannaq Trough region; the retreat of the GIS through the trough mouth fan made way for the inflow of 'warm' Atlantic-sourced water ∼15 kyr BP, which prompted further retreat. However these records only contain sparse dating. The increased strength of North

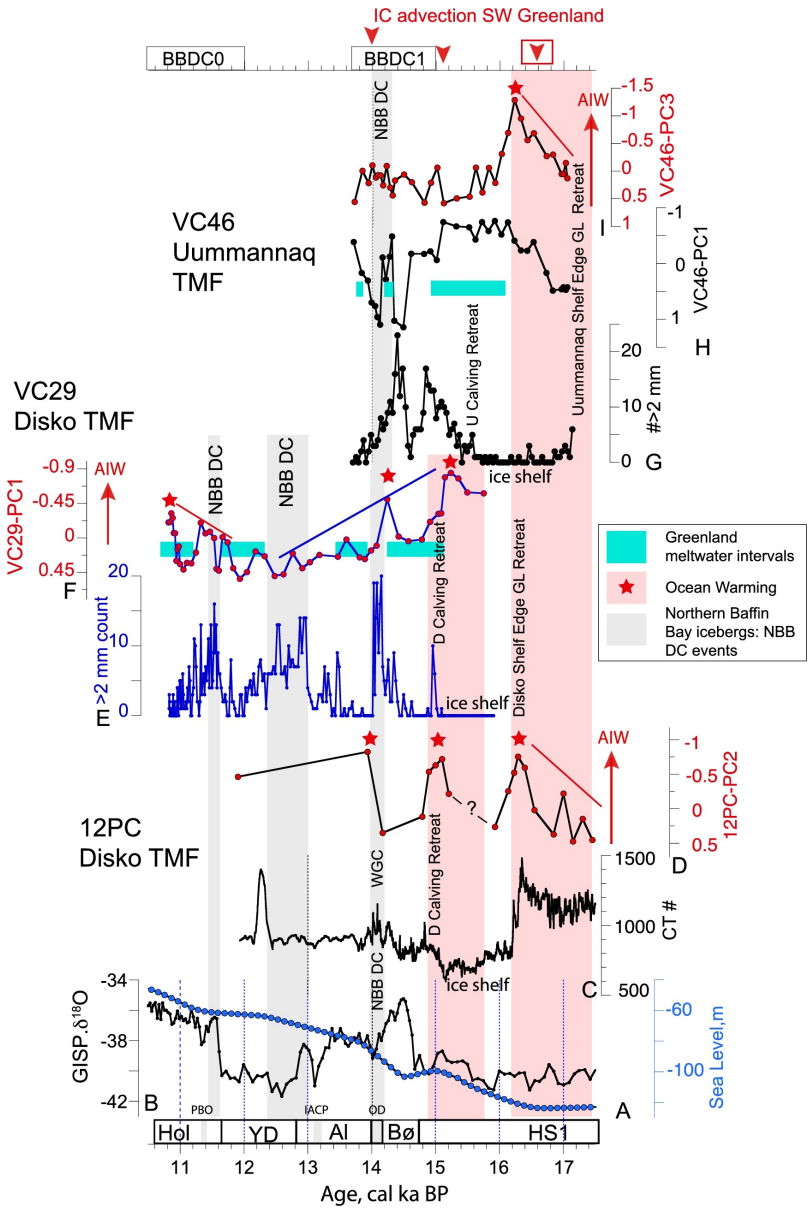

Figure 1.5: Links between ice sheet instabilities and paleoceanographic conditions, indicted by principal component analysis (PCA) of benthic foraminifera assemblages along the central west Greenland margin. Figure taken from *Jennings et al.* [2017].

Atlantic water inflow via the WGC prompted the onset of GIS instabilities according to studies from the Disko Bugt (Fig. 1.5) [*Jennings et al.*, 2014, 2017]. This area also received detrital material from the northern Baffin Bay, but there was no apparent oceanic warming prior to the latest two BBDC events, one of which occurred during the Younger Dryas stadial and thus require an explanation different to that of the initial ice-calving, followed by increased influence of the WGC and subsequent basal melting at the ice margins. A multi-proxy approach, including analysis of surface, sub-surface and deeper oceanic conditions, in an area that is within the influence of regional climatic changes, would be needed to assess the role or phase relationship of oceanographic conditions on ice-sheet retreat around Baffin Bay.

1.6 Chronological issues

Correctly assigning a chronology to the retreat of ice sheets in Baffin Bay is imperative not only for the study of GIS, IIS and LIS behaviour in response to rapid climate changes throughout the last deglaciation and beyond, but also for this information to be meaningful for overarching studies, such as, for example, modelling the effect of meltwater discharge into regions such as the Labrador Sea.

In this respect, Baffin Bay is a challenging place to work. Radiocarbon-dated records in fjord areas are often limited to the Younger Dryas and the Holocene, capturing only the final stages of ice sheet retreat. Deeper records, that are of lower resolution but cover longer time periods such as the last interglacial (e.g. *Hiscott et al.* [1989]; *Simon et al.* [2012, 2014]) lack an absolute chronology. Deeper sections of Baffin Bay are plagued by carbonate dissolution; the carbonate compensation depth (CCD) is between ∼600–900 m in Baffin Bay [*Aksu*, 1983] and in the present day, low saturation state surface water reaches Baffin Bay via the conduits of the Canadian Arctic Archipelago [*Azetsu-Scott et al.*, 2010]. This results in extensive carbonate dissolution and thus poor preservation of biogenic carbonate (foraminifera) at deep core sites (e.g. *Gibb* [2014]).

This has lead to a research gap in Baffin Bay. First, these chronological issues make it difficult to reconstruct paleo-ice sheet retreat on consistent time-scales with consistent accuracy. Coupling high resolution Holocene cores that are well dated with those from the more central and deeper Baffin Bay which provide greater temporal coverage but are difficult to date is problematic. Secondly, a lack of biogenic carbonate to date means a lack of biogenic carbonate to analyse, ruling out some of the paleoceanographic proxies commonly used to reconstruct sub-surface and deeper ocean conditions (e.g. benthic foraminifera assembladges, planktonic and benthic δ^{18}O).

1.7 Materials used in this study

We use two sediment cores in this study, collected with a gravity corer. Both cores were retrieved aboard the RV *Maria S. Merian* on research cruise MSM09/02 in 2008 [*Kucera et al.*, 2014]. GeoTü SL 174 (68° 31.88' N 63° 19.82' W, MSM09/02-0467/3) was collected from central western Baffin Bay from 1559 m water depth and is 777.5 cm in length. GeoTü SL 170 (68° 58.15' N 59° 23.58' W, MSM09/02-0455/13) off the coast of Greenland in the vicinity of Disko Bugt. Geo Tü SL 170 was collected at 1087 m water depth and is 683 cm long. Previous work on this core included provisional XRF data and limited radiocarbon dating [*de Groot*, 2013] (unpublished). Only the top ∼280 cm of core GeoTü SL 174 was analysed. This initial work indicated that this section of GeoTü

SL 174 and the full length of core GeoTü SL 170 covered roughly the last deglaciation to the present day (∼18–0 kyr BP) and revealed the presence of several intervals of elevated calcium counts.

1.8 Research Objectives

Despite the growing wealth of research in the Baffin Bay region, there are still unanswered questions with regards to the timing and nature of ice-sheet instabilities and paleoceanographic conditions. With these uncertainties in mind, we use the two sediment cores described above to address three main objectives in this study:

1) To define the timing of Baffin Bay Detrital Carbonate Events (BBDCs) during the last deglaciation and early Holocene by creating a detailed, radiocarbon-dated age model

2) To reconstruct paleoceanographic conditions in Baffin Bay during the last deglacial and early Holocene, with a multi-proxy investigation of surface, subsurface, and bottom ocean conditions, to assess if there is a link between changing paleoceanographic conditions and BBDC events

3) To construct an expanded chronology of BBDC events from Marine Isotope Stage 3 through to the early Holocene, combining radiocarbon and palaeomagnetic dating methods. To assess the link between paleoclimatic conditions and BBDC events, as well as assessing changes in background sedimentation

Chapter 2

Thesis outline and author contributions

This thesis is presented in a cumulative fashion and consists of three chapters that are either published [*Jackson et al.*, 2017] or in preparation for submission to international peer-reviewed scientific journals. A short outline of the manuscripts and details of co-author contributions is given below.

2.1 Thesis outline

Chapter 3: Asynchronous Instability of the North-American Arctic and Greenland ice sheets during the last deglaciation

Rebecca Jackson, Anders E.Carlson, Claude Hillaire-Marcel, Christoph Vogt, Lukas Waker and Michal Kucera

Published in *Quaternary Science Reviews* 2017, Volume 164, pp.140-153

doi:10.1016/j.quascirev.2017.03.020

MK helped design the study and suggested analytical techniques to use. CV carried out the XRD measurements. LK performed radiocarbon dating. AEC, CHM and MK provided feedback on the manuscript and suggested further lines of discussion. RJ wrote the manuscript with contributions from all co-authors.

This manuscript deals with the construction of a radiocarbon-dated chronology for Baffin Bay during the last deglaciation and early Holocene. Radiocarbon-dating was performed on two sediment cores from Baffin Bay. Physical, elemental and mineralogical properties were measured and from this, layers of elevated detrital dolomite-rich carbonate input were identified. This information, in combination with the new chronology, provides a revised timing of so-called Baffin Bay Detrital Carbonate Events (BBDC's), periods of ice sheet instability and delivery of material from the ice-sheets surrounding Baffin Bay via iceberg rafting and basal melting. Results indicate that there is no event equivalent

to Heinrich Event 1 and the first event of the deglaciation (BBDC 1, 14.2-13.7 kyr BP) actually occurred during an interstadial. The onset of the second event (BBDC 0, 12.7-11 kyr BP) was concurrent with the onset of the Younger Dryas stadial and predates revised timing of Heinrich Event 0. The asynchronicity of the North-American Arctic discharge with that of the Laurentide ice sheet highlights the need to consider the regional response of major ice sheets to climatic variability.

Chapter 4: Paleoceanographic changes during the last deglaciation and early Holocene in Baffin Bay: a link with ice-sheet instabilities?

Rebecca Jackson, Anne de Vernal, Marit-Solveig Seidenkrantz and Michal Kucera

In preparation for submission (e.g. Paleoceanography or Climate of the Past)

MK helped design the study. AdV provided facilities to process and analyse sediment samples for palynomorph analysis, as well as expertise on taxonomy and interpretation of the data. MSS provided help with benthic foraminifera taxonomy and interpretation of assemblages found. RJ wrote the manuscript with feedback from AdV and MMS.

This manuscript deals with the reconstruction of paleoceanographic conditions in Baffin Bay during the last deglaciation and early Holocene ($\sim$17-10 kyr BP). It utilises the preservation of biogenic carbonate and high temporal resolution of core SL 170, situated off the coast of Greenland. Dinoflagellate cyst concentration and assemblage composition were used to evaluate surface ocean conditions. Sub-surface conditions were reconstructed using the δ^{18}O of planktonic foraminifera. Benthic foraminifera assemblages and stable isotopes (δ^{18}O and δ^{13}C) provided information on deep ocean conditions. Utilising the chronology presented in *Jackson et al.* [2017], we were able to assess possible links and phase relationships between the ice-sheet instabilities (BBDC events) and oceanographic changes throughout the entire deglaciation and early Holocene. Results indicate that throughout the deglacial and early Holocene there was persistent extensive sea ice cover and sub-surface conditions contain a regional δ^{18}O signal. Deeper waters appeared to be better ventilated in the early deglacial until the first signs of a strong influx of the West Greenland Current $\sim$14 kyr BP. Changes in oceanic conditions do not pre-date the onset of BBDC 1 and by the onset of BBDC 0 conditions in Baffin Bay were already evolving toward present conditions of a more stratified water column.

Chapter 5: A new chronology of ice sheet retreat in Baffin Bay since Marine Isotope Stage 3

Rebecca Jackson, Thomas Frederichs and Michal Kucera

In preparation for submission (e.g. Earth and Planetary Science letters)

MK suggested the analysis.TF carried out the rock and paleomagnetic measurements.TF produced the Relative Paleointensity based age model and RPI tie points of the combined model with radiocarbon dates from RJ. TF also provided help with interpretation of rock and paleomagnetic data. RJ interpreted the data and wrote the manuscript.

This manuscript deals with the construction of a chronology of BBDC events from Marine Isotope Stage 3 through to the Holocene. We build on the work of *Jackson et al.* [2017] on core SL 174 by adding additional radiocarbon dates and combining this with Relative Paleointensity dating. Within the framework of this new age model we use physical, geochemical and rock magnetic parameters, along with multivariate statistics, to define BBDC events and their timing. Results confirm the presence of 7 BBDC events between ∼52–0.9 kyr BP that track the retreat of the ice sheets surrounding northern Baffin Bay. The timing of BBDC events was not consistent with abrupt climate change, with events occurring during both stadial and interstadial periods as indicated by the Greenland ice core record. Furthermore, after removing these layers and their characteristic properties from the analysis, it was found that there were intervals with distinct sedimentary characteristics, likely related to changes in the source or delivery mechanism of detrital material delivered from elsewhere in Baffin Bay.

2.2 Description of own contributions

All of the aforementioned chapters were written by myself with contributions from co-authors. The designation of datasets to certain chapters was done largely by myself with advice from M. Kucera. Below is a detailed overview of my contribution to the sampling, laboratory work and analysis of the sediment cores.

Both cores presented in this thesis were collected on board the RV *Maria S. Merian* on cruise MSM09/2 in 2008. Applicable to all chapters, the working halves of sediment cores SL 174 and SL 170 were sampled by myself and the help of colleagues H.Kolling and V.Kirillova at 1 cm intervals. The entirety of the working halves were sampled and I organised the system by which they were labelled, weighed and stored. I performed the high-resolution linescan imaging (LS), computerised tomography (CT) scans and performed the XRF analysis on the archive halves. I designed the protocol for preparation of the working half samples and conducted the freeze-drying of samples. For radiocarbon dating I processed the samples (freeze-drying, washing, wet sieving, oven-drying and weighing) and picked the foraminifera from these. Due to the large number of samples I had assistance from a student helper with the wet sieving and picking. I weighed and prepared the picked samples to be sent for radiocarbon dating. I constructed the age model for both cores with the results of the radiocarbon dating. Additional to the

above for the first chapter, I selected intervals of interest for XRD analysis, subsampled these sections and prepared them for the analyses (homogenisation of samples by manual crushing).

For the second chapter (SL 170 only), I performed the sample preparation for palynomorph analysis and did the microscope work of counting and identifying marine and terrestrial palynomorphs at UQAM, Montreal with consultation from A. de Vernal. Additional samples were processed for foraminiferal analysis, as above, with additional help in washing and initial picking by students. I counted the foraminifera and in the case of benthic foraminifers, learnt the taxonomy at Aarhus University with M.S. Seidenkrantz and subsequently analysed the benthic species assemblage and conducted the multivariate analysis. Following this I chose, picked and weighed foraminifera samples for stable isotope analysis.

For the third chapter (SL 174 only) I measured the magnetic susceptibility in the laboratory of the Marine Geophysics group of the Geoscience Department, University of Bremen. I sampled the core for palaeomagnetic and magnetic remanence measurements, which were done by T.Frederichs and colleagues. I prepared additional down-core samples for radiocarbon dating. I constructed the age model, this time for the whole core, with a combination of radiocarbon dates and Relative Paleointensity tie points provided by T.Frederichs. I performed the multivariate analysis on the datasets.

Chapter 3

Asynchronous instability of the North American-Arctic and Greenland ice sheets during the last deglaciation

Published in Quaternary Science Reviews, April 2017

3.1 Published paper

Quaternary Science Reviews 164 (2017) 140–153

Contents lists available at ScienceDirect

Quaternary Science Reviews

journal homepage: www.elsevier.com/locate/quascirev

Asynchronous instability of the North American-Arctic and Greenland ice sheets during the last deglaciation

Rebecca Jackson [a, *], Anders E. Carlson [b], Claude Hillaire-Marcel [c], Lukas Wacker [d], Christoph Vogt [e], Michal Kucera [a]

[a] MARUM – Centre for Marine Environmental Sciences, Leobener Straße 8, Bremen, 28359, Germany
[b] College of Earth, Ocean, and Atmospheric Sciences, Oregon State University, Corvallis, OR, 97331, USA
[c] GEOTOP, Université du Québec à Montréal, CP 8888, Succ. Centre-Ville, Montréal, Québec, H3C 3P8, Canada
[d] Laboratory of Ion Beam Physics, ETHZ, Otto-Stern-Weg 5, Zürich, 8093, Switzerland
[e] Zentrallabor für Kristallographie und Angewandte Materialwissenschaften (ZEKAM), Department of Geoscience, Universität Bremen, Klagenfurter Str., Bremen, 28359, Germany

ARTICLE INFO

Article history:
Received 5 December 2016
Received in revised form
17 March 2017
Accepted 21 March 2017

Keywords:
Quaternary
Glaciology (inc. paleo-ice sheets)
Sedimentology – marine cores
Baffin Bay
Last deglaciation
Ice-sheet retreat
Radiocarbon dating
Detrital carbonate events

ABSTRACT

The chronology of deglacial meltwater pulses from the Laurentide Ice Sheet is well documented. However, the deglacial history of the North American-Arctic (north-eastern Laurentide and Innuitian) and western Greenland ice sheets draining into the Labrador Sea via Baffin Bay is less well constrained. Here we present new high-resolution, radiocarbon-dated records from the central Baffin Bay spanning ~17 to 10 kyr BP and documenting the full deglacial history of Baffin Bay. Sedimentological and geochemical data confirm the presence of two periods of enhanced detrital carbonate delivery, termed Baffin Bay Detrital Carbonate Events (BBDCs). These events are dated to ~14.2–13.7 kyr BP and ~12.7–11 kyr BP. They are synchronous across Baffin Bay and their mineralogical signature indicates a common source of detrital carbonate from northern Baffin Bay. The first event, BBDC 1, postdates Heinrich Event 1 and the second event, BBDC 0, predates the recently revised timing of Heinrich Event 0. The onset of the BBDC events appears not to be systematically linked to Greenland temperature change as they occur during both interstadial and stadial periods. This indicates that deglaciation of North American-Arctic and western Greenland ice sheets with the associated iceberg and meltwater discharge were decoupled from the dominant North Atlantic climate mode, where iceberg discharge events from the Laurentide Ice Sheet occurred during stadial periods.

1. Introduction

The transition from the Last Glacial Maximum to the Holocene was characterised by rapid changes in temperature, ice sheet volume and ocean circulation (Carlson and Clark, 2012; Clark et al., 2012; Shakun and Carlson, 2010). In the Arctic and sub-Arctic regions, this transition is associated with two distinct events of ice sheet instability, known as Heinrich Events 1 and 0 (see a review in Clark et al., 2012). Heinrich Events, massive discharges of icebergs mostly from surges of the Laurentide Ice Sheet (Heinrich, 1988), are well documented in Labrador Sea (Andrews et al., 2012; Pearce et al., 2015; Stoner et al., 1996) and North Atlantic (Bond et al., 1997; Channell et al., 2012; Hemming, 2004) sedimentary records and their timing is well constrained. Heinrich Events are associated with cold stadial conditions in the North Atlantic, but their causal relationship to stadial coolings is unclear (Bond et al., 1993; Broecker, 1994; Marcott et al., 2011). Notwithstanding their exact relationship with the regional climate evolution, these events were associated with large meltwater injections into the North Atlantic and as such are likely to have had an impact on deep-water formation, especially in the Labrador Sea, thus modulating the global climate evolution of the last deglaciation (McManus et al., 2004; Thornalley et al., 2011). Most climate hypotheses and paleoclimate models assume that deglacial meltwater discharge into the North Atlantic was associated with Heinrich Events sourced from the Hudson Bay. However, there exists a second potential meltwater route, from Baffin Bay (e.g. Simon et al., 2014). Compared to the well-known chronology of late glacial meltwater discharges

* Corresponding author.
E-mail addresses: rjackson@marum.de (R. Jackson), acarlson@coas.oregonstate.edu (A.E. Carlson), hillaire-marcel.claude@uqam.ca (C. Hillaire-Marcel), wacker@phys.ethz.ch (L. Wacker), cvogt@uni-bremen.de (C. Vogt), mkucera@marum.de (M. Kucera).

http://dx.doi.org/10.1016/j.quascirev.2017.03.020
0277-3791/

from the Labrador Dome of the Laurentide Ice Sheet since the Last Glacial Maximum (LGM), meltwater discharges from ice sheets that drain into Baffin Bay are less well documented and still loosely dated: a gap we intend to fill here.

1.1. Regional setting and previous work

During the LGM, Baffin Bay was flanked by three major ice sheets that flowed into it: the Greenland Ice Sheet (GIS), the north-eastern sector of the Laurentide Ice Sheet (LIS) and the south-eastern sector of the Innuitian Ice Sheet (IIS) (Dyke et al., 2002; England et al., 2006). We will term these as the North American-Arctic and western Greenland ice sheets. These ice sheets expanded into the fjord systems surrounding Baffin Bay and filled marine channels such as the Nares Strait/Smith Sound, and Lancaster and Jones Sound (Fig. 1) (Dyke et al., 2002; Li et al., 2011) as well as resulting in the spreading of an ice shelf across the northern Baffin Bay (Marcott et al., 2011). The GIS advanced through Disko Bugt and the Uummannaq Trough as far as the shelf edge on the western Greenland margin (Ó Cofaigh et al., 2013b; Ò Cofaigh et al., 2013a).

Baffin Bay has a counter-clockwise oceanic circulation (Tang et al., 2004). The colder East Greenland Current and warmer Irminger Current join to form the West Greenland Current (WGC) that enters Baffin Bay via the Davis Strait and travels north along the west coast of Greenland. Paleoceaongraphic records from the Uummannaq region of the west Greenland shelf suggest the establishment of 'warm' WGC prior to 14 kyr BP (Sheldon et al., 2016). At the head of Baffin Bay the WGC recirculates south, incorporating Arctic waters and forming the Baffin Island Current (BIC). The BIC travels south along Baffin Island, with some recirculation east towards Greenland, while the rest flows into the Labrador Sea via the Davis Strait, forming part of the Labrador Current (Fig. 1).

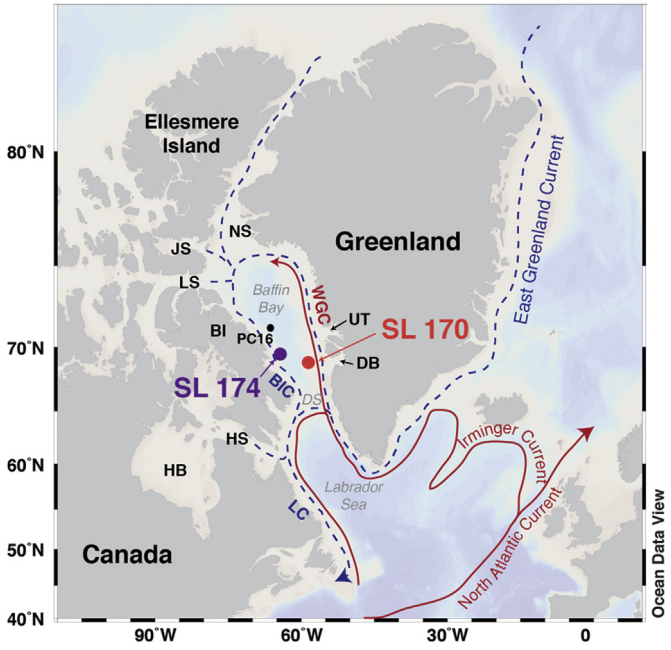

Fig. 1. Location of Baffin Bay, surrounding land masses (BI = Baffin Island), 'modern' oceanography and core location used in this study (SL 170 and SL 174). The location of core PC 16 (Simon et al., 2014, 2012) is also shown. Warm currents originating in the North Atlantic are shown by solid red lines (WGC = West Greenland Current). Cooler currents of Arctic origin are shown by blue dashed line (BIC = Baffin Island Current; LC = Labrador Current). Areas of meltwater/water influx into the Baffin Bay are also shown (DS = Davis Strait; DB = Disko Bugt; UT = Uummannaq Trough; NS = Nares Strait; JS = Jones Sound; LS = Lancaster Sound; HB = Hudson Bay; HS = Hudson Strait). (For interpretation of the references to colour in this figure legend, the reader is referred to the web version of this article.)

As well as the direct sources of sediment from the adjacent landmasses and shelves, this ocean current configuration provided a southerly path for iceberg-rafting and meltwater discharge from the North American-Arctic ice sheets (England et al., 2006; Simon et al., 2014), as well as a northerly path from the western GIS and its previously glaciated shelf (Jennings et al., 2014; Ò Cofaigh et al., 2013b). In the northern region of Baffin Bay, many of the major paleo-ice streams draining the IIS and north-eastern LIS, such as the Nares Strait/Smith Sound and Lancaster Sound (Fig. 1) are flanked by large areas of Palaeozoic limestones and dolostones (Hiscott et al., 1989). This is in contrast to the older Archean Nagssugtoqidian Mobile Belt (NMB) of the central west Greenland coast. Discrete discharge events originating from northern Baffin Bay are hence recorded in marine sedimentary records as layers rich in detrital carbonate, generally ice-rafted southward along the path of the BIC (Andrews et al., 2011). In contrast with the calcite-rich mineralogical signature of detrital carbonate layers originating from the Hudson Strait, ice-rafted detrital carbonate layers found in Baffin Bay are characterised by a calcite/dolomite ratio ~0.25:1 (Andrews et al., 2014, 1998, 1995; Simon et al., 2014).

Two BBDC events have been previously identified during the last deglaciation (Aksu and Piper, 1987; Andrews et al., 1998; Hiscott et al., 1989; Simon et al., 2014, 2012). Magnetostratigraphic dating of these records has been recently used to suggest that these events were not in phase with the North Atlantic Heinrich Events (Simon et al., 2014, 2012) but much uncertainty exists in such a paleomagnetic-based chronology, demonstrated by its recent revision (Simon et al., 2016). This uncertainty derives from the ambiguity in tuning noisy curves to a target curve that, in itself, includes dating uncertainty. If periods of iceberg and meltwater discharge from the ice sheets draining into Baffin Bay (i.e. BBDCs) were asynchronous with Heinrich Events, this could have implications for the history of meltwater delivery into the Labrador Sea and North Atlantic. Obviously, a robust chronology would allow here for a better evaluation of the relationship between iceberg discharge and deglacial climate change (Bond et al., 1993; Broecker, 1994).

Deep sea sediments in Baffin Bay are affected by poor preservation of biogenic carbonate, particularly during the Holocene (Aksu, 1983), which has so far hindered the construction of a radiocarbon chronology for the deglaciation and thus a robust assessment of the melting history of the surrounding ice sheets. Here we present two new deglacial records from Baffin Bay (Fig. 1), from sites where a better preservation of benthic and planktonic foraminifera is observed. Better preservation is likely due here to the cored sediment depths near the carbonate compensation depth (CCD), ranging from 600 to 900 m in Baffin Bay (Aksu, 1983), as compared to deeper cores (>2000 m water depth, e.g. Simon et al., 2012). Combined with the use of a new preparation technique for radiocarbon dating of ultra-small samples (Bard et al., 2015; Wacker et al., 2013), we are now in a situation to (i) precisely determine the ages and durations of BBDC events and (ii) set a reliable deglacial chronology of iceberg and meltwater discharge events from the North American-Arctic and western Greenland ice sheets.

2. Methods and material

2.1. Core locations

Gravity cores GeoTü SL 174 (68° 31.88′ N 63° 19.82′ W, MSM09/02-0467/3) and GeoTü SL 170 (68° 58.15′ N 59° 23.58′ W, MSM09/

02-0455/13) were retrieved aboard the *RV Maria S. Merian* research cruise MSM09/02 (Kucera et al., 2014) in 2008. Cores are herein referred to by number only. SL 174 (777.5 cm in length) was retrieved from 1559 m water depth off the coast of Baffin Island. SL 170 (683 cm in length) was retrieved from 1078 m water depth in the eastern region of Baffin Bay, to the west of Disko Bugt (Fig. 1). PARASOUND™ surveys at the core sites and magnetic susceptibility profiles (Fig. S1) carried out at 1 cm intervals on board, show no evidence of turbidites or hiatuses in sediment deposition, thus indicating promising records for a cross-basinal study of deglacial history of the ice sheets surrounding Baffin Bay. Sediment cores were stored at <4 °C and split lengthways into archive and working halves.

2.2. Chronology

Age models were constructed for both cores using Accelerator Mass Spectrometry (AMS) ^{14}C dating of biogenic carbonate. To this end, foraminifera were picked from the >150 μm fraction of processed sediment samples in both cores. Either planktonic (*Neogloboquadrina pachyderma* sinistral) or mixed benthic foraminifera samples were dated. The selection depended on availability of sufficient material at the intervals of interest and where possible, replicate dates based on planktonic and benthic foraminifera within the same sample were obtained. Also included are two dates based on mollusc fragments from core SL 170. Two methods were used for the radiocarbon dating; traditional ^{14}C measurements with AMS on samples converted to graphite and a new method, where CO_2 from ultra-small amounts (~0.5 mg) of carbonate (Wacker et al., 2013) were directly analysed with a compact AMS facility equipped with a gas ion source at the Laboratory for Ion Beam Physics, ETH Zurich. Some of these samples were also leached before measurement (Bard et al., 2015). There is good agreement between the methods, suggesting the dating procedure is robust.

The chronology for both cores was constructed using BACON (Blaauw and Christen, 2011), a Bayesian accumulation model code using an autoregressive gamma process. The code is open-source and run in the program 'R'. This method of constructing an age-depth model is more flexible than classical age-depth modelling, such as CLAM (Blaauw, 2010), as it allows for variable sedimentation rates between radiocarbon dates. Initially, all AMS ^{14}C radiocarbon dates were considered in the development of the age model. The AMS ^{14}C ages and their associated errors were calibrated within the age-depth modelling process, using the Marine13 radiocarbon age calibration curve (Reimer, 2013). In addition, we applied a local reservoir correction (ΔR) of 140 ± 35 years as estimated from historical but pre-bomb samples (Lloyd et al., 2011), currently used for radiocarbon date calibrations of Disko Bugt sedimentary sequences (Jennings et al., 2014; Lloyd et al., 2011; Ouellet-Bernier et al., 2014; Perner et al., 2013, 2011). Since the local reservoir correction in high latitude regions remains poorly constrained during the deglaciation, we carried out a detailed sensitivity assessment of the chronology of the two cores against the choice of local reservoir correction. These results are thoroughly addressed and the effects of changing local reservoir correction are evaluated in the discussion section 4.2.

2.3. Physical sediment properties

Computerised tomography (CT) and high-resolution colour linescan (LS) imaging were carried out on the archive halves of both cores at the University of Bremen, Germany. Lithofacies were determined from these along with visual analysis, with particular interest in areas of coarser, potentially ice-rafted sediment (Figs. 2 and 3). L*, a measure of lightness and component of the CIE/L*a*b* colour space, was measured during linescan image acquisition. L* is unit-less value, but represents lightness (in this case of sediment) on a scale from darkest black (L* = 0) to brightest white (L* = 100). L* values are often used as a proxy for relative carbonate content in marine sediment cores; high L* values indicating higher carbonate content (e.g. Balsam et al., 1999). To determine grain size distribution throughout the core and also to obtain samples for radiocarbon dating, the working half of both cores was continuously sampled in slices of 1 cm thickness. A portion of the slice corresponding approximately to 10 g dry weight was freeze dried, weighed, washed over 0.063 mm screen until all fine fraction was removed. The sieve residue was then collected, dried and weighed again. The proportion of sediment in this >63 μm fraction was calculated as the ratio between the dry weight of the residue and dry weight of the bulk sample.

2.4. X-ray fluorescence (XRF) and quantitative X-ray diffraction (qXRD) analysis

XRF scanning was used to determine elemental properties in the cores. Data were collected every 1 cm along the archive half surface of both cores with the XRF Core Scanner II™ (AVAATECH™ serial No. 2) at MARUM, University of Bremen. Sediment intervals containing large amounts of calcium (Ca) were noted, as in previous studies, as an indication of detrital input from source areas surrounding northern Baffin Bay (Aksu and Piper, 1987; Andrews et al., 2014, 1985; Simon et al., 2014). These potential detrital carbonate layers were sub-sampled for qXRD analysis to establish their mineralogy. qXRD was measured on a Bruker D8 Advance™ diffractometer at the University of Bremen. Of particular interest was the proportion of dolomite and calcite within detrital carbonate rich layers. For full details of XRF and qXRD methods see supplementary information.

3. Results

3.1. Deglacial chronology

The chronology of the two sediment cores is based on a total of 28 radiocarbon dates (Tables 1 and 2). The distribution of the calibrated ages reveals that the uppermost portions of both cores, which contained fine-grained sediment and were barren of biogenic carbonate, corresponds to the later part of the Holocene with oldest ages being >10 kyr BP (Tables 1 and 2). The age models of both cores reveal continuous deposition during the last deglacial and early Holocene period (~17–10 kyr BP), albeit at different resolutions. The interval of highest sedimentation rates and thus of clastic delivery appears synchronous across the two cores (~12.6 kyr BP).

In core SL 174, the barren Holocene section corresponds to the top 98 cm. Further downcore, the progression of ages indicates undisturbed sedimentation (Fig. 2). As a result, the Bayesian age model could be constructed using all ages, including a replicate age measurement on both planktonic and benthic foraminifera in one sample interval. A large amount of planktonic foraminifera in the sample interval 384–385 cm allowed for a technical replicate; the extracted foraminifera were split and resulting aliquots were dated separately. The replicate planktonic-benthic age differed by about the same amount as the technical replicate in the oldest dated sample at 384–385 cm (260 ^{14}C years) (Table 1). A (calibrated) date of ~17.6 kyr BP at 294–295 cm is the first date bracketing the deglacial period. An older (calibrated) ^{14}C age of ~26.2 kyr BP obtained from 384 – 385 cm indicates that the lower part of the sediment sequence in the core is older than the LGM. The overlying 10 radiocarbon dates included in the age model indicate that the

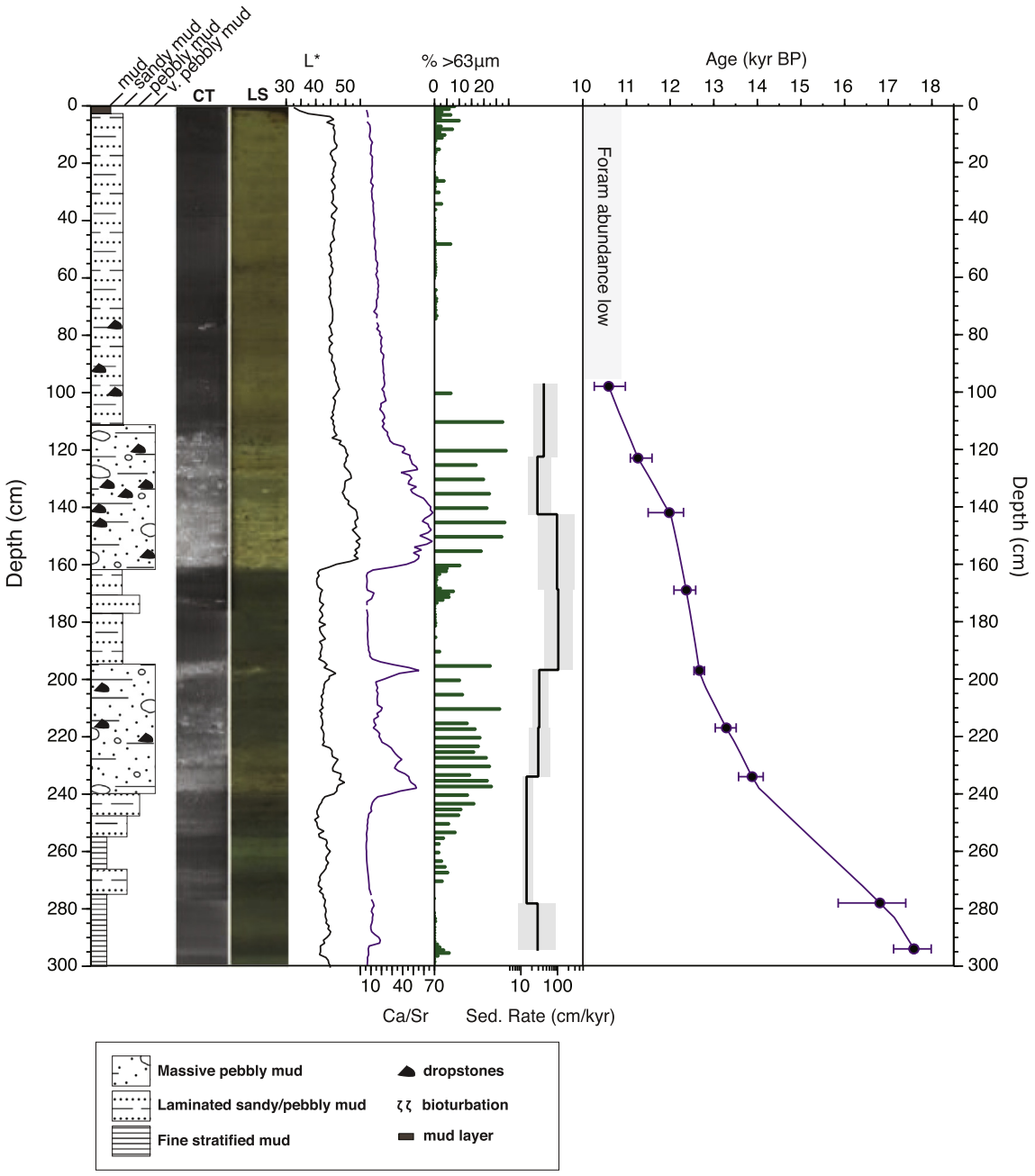

Fig. 2. Chronology and lithostratigraphy for core SL 174. The age-depth relationship is based on 10 ^{14}C dates (filled circles). Error bars indicate minimum and maximum ages (95% uncertainty, 2σ) for dated intervals from the age model. Sedimentation rate (shown on log scale) was calculated between each dated interval, the black line indicating the mean sedimentation rate and grey area indicating the error (95% uncertainty). Computerised tomography (CT) and colour linescan images (LS) are shown as well as sediment lightness (L*) measurements. The percentage of sediment >63 µm is shown in green. Ca/Sr ratio downcore is shown in purple. The lithofacies are defined from CT, LS images and visual inspection of the core. (For interpretation of the references to colour in this figure legend, the reader is referred to the web version of this article.)

corresponding 197 cm-long interval covers the period ~17.6–10.6 kyr BP (Fig. 2). The initial part of the deglacial record of SL 174 is characterised by low sedimentation rates of 14–23 cm kyr^{-1} up to 234 cm downcore (~13.9 kyr BP), above it increasing about twofold to 28–32 cm kyr^{-1}. Highest sedimentation rates of 85–95 cm kyr^{-1} are observed between 197 and 143 cm (~12.7–12.0 kyr BP).

A total of 21 ^{14}C ages, including 3 planktonic-benthic replicate ages, 2 benthic (technical) replicates and 2 benthic-mollusc fragment replicate ages were obtained for core SL 170 (Table 2). There were insufficient foraminifera in the top 24 cm and bottom 46 cm of the core for radiocarbon dating. Three radiocarbon ages fell outside the 95% uncertainty range of the age-depth model (see Fig. S2 and supplementary information for details). These ages were removed from the final age model run, including one replicate planktonic age (116–118 cm) and two replicate benthic-mollusc fragment ages (136–139 cm). The remaining replicates showed excellent reproducibility, with plankton-benthos age differences of the same size as differences between benthic replicates. Based on the retained 18 ages, the corresponding 613 cm sedimentary sequence could be dated to the period ~17.0–10.2 kyr BP (Fig. 3). The calculated sedimentation rate was low (~56 cm kyr^{-1}) during the deposition of the 636–486 cm interval (~17.0–14.1 kyr BP). A twofold increase in sedimentation rate (up to ~96 cm kyr^{-1}) occurred at ~14.1 kyr BP, and from then on the sedimentation rate remained high, varying

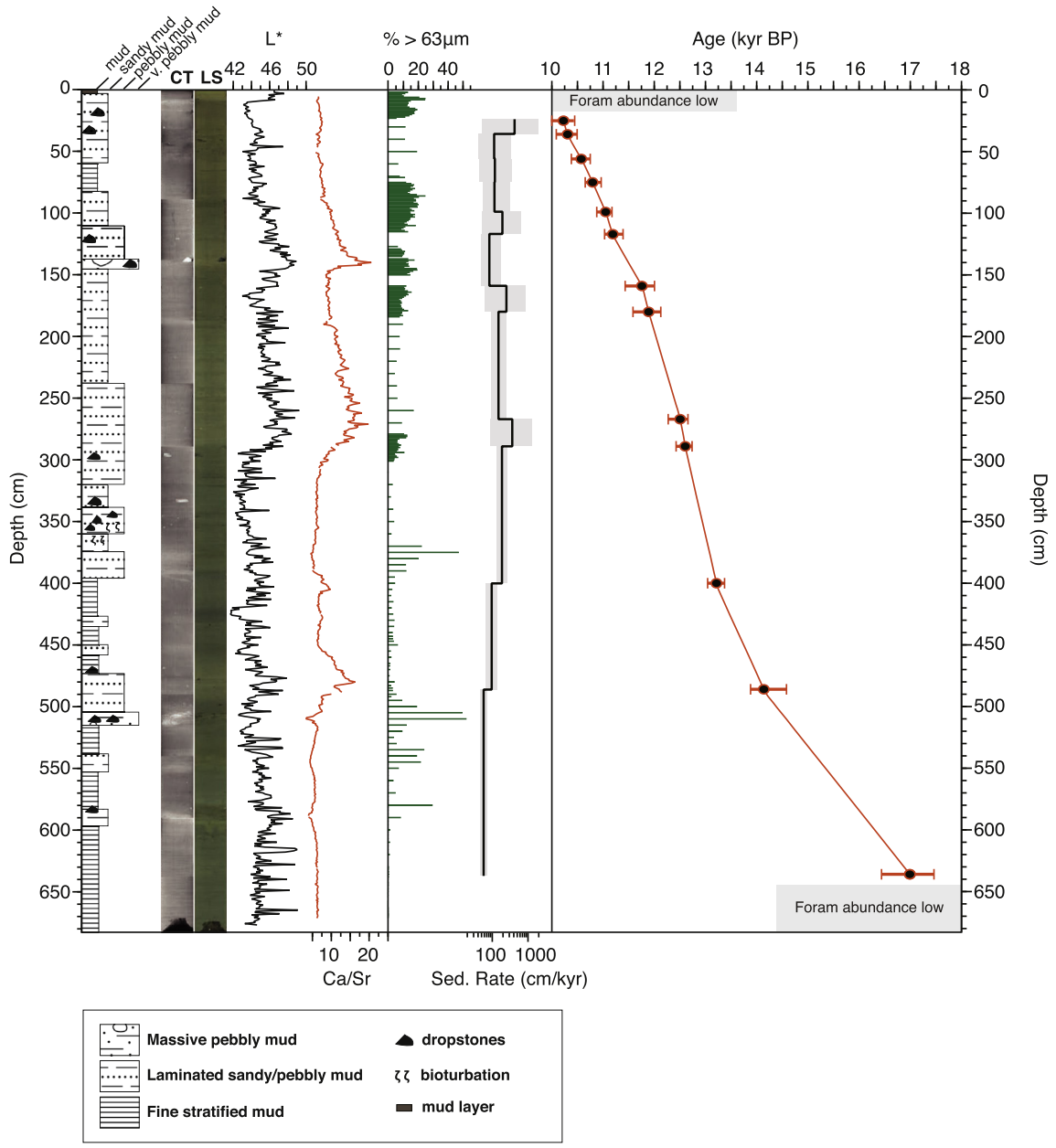

Fig. 3. Chronology and lithostratigraphy for core SL 170. The age-depth relationship is based on 18 ^{14}C dates (filled circles). Error bars indicate minimum and maximum ages (95% uncertainty, 2σ) for dated intervals from the age model. Sedimentation rate (shown on log scale) was calculated between each dated interval, the black line indicating the mean sedimentation rate and grey area indicating the error (95% uncertainty). Computerised tomography (CT) and colour linescan images (LS) are shown as well as sediment lightness (L*) measurements. The percentage of sediment >63 μm is shown in green. Ca/Sr ratio downcore is shown in orange. The lithofacies are defined from CT, LS images and visual inspection of the core. (For interpretation of the references to colour in this figure legend, the reader is referred to the web version of this article.)

between 87 and 257 cm kyr^{-1} (Fig. 3).

3.2. Physical sediment properties

In core SL 174 the interval 295–240 cm (~17.6–14.2 kyr BP) is characterised by laminated muds (Fig. 2). Within this interval, the >63 μm fraction remains below 20% and L* values fluctuate around 45. The following section is coarsening upward towards a thick layer of massive pebbly mud between 240 and 195 cm (~14.2–12.6 kyr BP). Gravel-sized clasts embedded in the finer matrix, likely representing dropstones, are abundant within this interval. Between 195 and 163 cm (~12.6–12.2 kyr BP), a layer of darker sediment (L* value ~40) composed of a finer laminated mud, with lower > 63 μm fraction content (≤10%) is observed. A layer of massive pebbly mud, with dropstones, 30% > 63 μm fraction and L* values of 50–60, are found between 163 and 111 cm (~12.2–10.9 kyr BP). The rest of the core is composed of laminated mud and a much reduced content of the >63 μm fraction. Occasional dropstones are found until 75 cm. A brown mud layer of less than 5 cm caps the top of the core.

The base of core SL 170 to 510 cm depth (~17.0–14.6 kyr BP) is characterised by fine stratified mud (Fig. 3) with a very low content of the >63 μm fraction. Above 510 cm, a thin layer of pebbly mud with dropstones is followed by a sandy mud layer with a >63 μm fraction content of up to 50% (505–470 cm; ~14.5–13.9 kyr BP). Up to 393 cm (~13.2 kyr BP), the core then consists of stratified fine muds. Laminated sandy and pebbly muds characterise the sediment from this point on, with abundant dropstones and

Table 1
Radiocarbon dates and modelled ages for core SL 174. All ^{14}C radiocarbon dates with the ETH lab code were measured as gas samples for this study at the Laboratory for Ion Beam Physics, ETHZ; other codes are for ^{14}C dates measured using the traditional AMS ^{14}C method. All ^{14}C ages were calibrated using the Marine13 dataset (Reimer, 2013) and a ΔR of 140 ± 35 years was applied in the age modelling software BACON. Maximum and minimum ages represent the 95% (2σ uncertainty) in the age model. No dates were considered outliers by the BACON age model. *The ages obtained from sample interval 384–385 cm were not included in the deglacial age model (see text for details).

Lab code	Depth (cm)	Material	Weight (mg)	^{14}C age (yrs)	^{14}C (+/− yrs)	^{14}C age benthic - planktonic	Min age (yrs BP)	Max age (yrs BP)	Mean age (yrs BP)
ETH-55690	97–100	planktonic (*N.pachyderma*) and mixed benthic	0.32	9793	120		10,262	10,961	**10,592**
Beta-344508	122–125	planktonic (*N.pachyderma*) and mixed benthic	4.16	10,390	40		11,089	11,585	**11,262**
ETH-55691	142–145	mixed benthic	0.56	10,997	110		11,512	12,346	**12,018**
ETH-58356	169–170	mixed benthic	0.91	11,010	85		12,088	12,586	**12,370**
Beta - 344505	196–199	planktonic (*N. pachyderma*)	8.54	11,410	50		12,547	12,787	**12,672**
Beta - 344506	196–199	mixed benthic	12.72	11,150	50	−260			
KIA 40767	215–219	planktonic (*N. pachyderma*)	1.1	12,000	80		13,035	13,514	**13,288**
Beta - 344507	233–236	planktonic (*N. pachyderma*)	3.42	12,580	60		13,569	14,134	**13.879**
ETH-58357	278–279	planktonic (*N. pachyderma*)	0.91	14,510	120		15,852	17,401	**16,807**
ETH-58358	294–295	planktonic (*N. pachyderma*)	0.98	15,060	110		17,122	17,984	**17,587**
*ETH-58360.1	384–385	planktonic (*N. pachyderma*)	0.57	22,380	289		25,831	26,701	**26,235**
*ETH-58360.3	384–385	planktonic (*N. pachyderma*) replicate	0.73	22,640	190				

Table 2
Radiocarbon dates and modelled ages for core SL 170. All ^{14}C radiocarbon dates with the ETH lab code were measured for this study as gas samples at the Laboratory for Ion Beam Physics, ETHZ; other codes are for ^{14}C dates measured using the traditional AMS ^{14}C method. All ^{14}C were calibrated using the Marine13 dataset (Reimer, 2013) and a ΔR of 140 ± 35 years was applied in the age modelling software BACON. Maximum and minimum ages represent the 95% (2σ uncertainty) in the age model.

Lab code	Depth (cm)	Material	Weight (mg)	^{14}C age (yrs)	^{14}C (+/− yrs)	^{14}C age benthic - planktonic	Min age (yrs BP)	Max age (yrs BP)	Mean age (yrs BP)
ETH-55678	24–27	mixed benthic	0.47	9668	112		9930	10,432	**10,226**
ETH-55679	35–37	mixed benthic	0.81	9460	80		10,095	10,500	**10,310**
ETH-55680	55–57	mixed benthic	1.03	9833	83		10,376	10,747	**10,572**
ETH-55681	74–76	planktonic (*N. pachyderma*)	0.79	9901	82		10,652	10,966	**10,797**
ETH-55682.1	74–76	mixed benthic	0.87	10,028	87	127			
ETH-55682.2	74–76	mixed benthic (replicate)	0.86	10,090	97	189			
ETH-55683.1	98–100	mixed benthic	0.81	10,243	80		10,877	11,200	**11,059**
ETH-55683.2	98–100	mixed benthic (replicate)	0.90	10,232	137				
**ETH-55684	116–118	planktonic (*N. pachyderma*)	0.44	11,042	107				
ETH-55685	116–118	mixed benthic	0.93	10,274	86		11,012	11,471	**11,213**
**Beta - 344504	136–139	mollusc fragments	12.22	10,080	50				
**ETH-55686	136–139	mixed benthic	0.71	12,990	117				
ETH-58351	159–160	mollusc fragments	0.85	10,755	85		11,380	11,974	**11,694**
ETH-58352	159–160	mixed benthic	0.96	10,905	85				
ETH-58353	180–181	mixed benthic	1.08	10671	85		11,516	12,105	**11,845**
ETH-55687	266–269	mixed benthic	0.92	11,267	100		12,251	12,656	**12,498**
ETH-58354	288–290	mixed benthic	0.97	11,150	75		12,414	12,739	**12,601**
ETH-55688	399–402	planktonic (*N. pachyderma*)	0.69	11,597	104		13,040	13,369	**13,213**
ETH-55689	399–402	mixed benthic	0.87	11,944	92	347			
KIA 40766	484–488	planktonic (*N. pachyderma*)	1.20	12,730	60		13,879	14,573	**14,138**
ETH-58355	636–637	planktonic (*N. pachyderma*)	0.85	14,640	130		16,435	17,462	**16,992**

** ^{14}C dates that were considered outliers and thus removed from the final age model presented here (see supplementary information for details).

recognisable bioturbation between 360 and 320 cm (~12.9–12.7 kyr BP). Another pebbly layer corresponds to the period ~11.5 to 11.1 kyr BP (145–110 cm). The top 60 cm of the core is characterised by a sandy mud layer (>63 μm 10–25%) with occasional dropstones. While L* values fluctuate here more frequently than in SL 174, coarser layers between 320 and 70 cm are composed of consistently lighter sediment (L* ~47–49). The top of the core is capped with a ~4 cm thick brown mud layer.

3.3. Detrital carbonate layers: XRF and XRD analysis

X-ray fluorescence (XRF) scans were used to characterise elemental properties of the sediment and thus identify detrital carbonate layers that were found in this time interval in Baffin Bay sediments during previous studies. We use the ratio of calcium (Ca) to strontium (Sr) counts to define these layers, as used in studies of North Atlantic and Labrador Sea sedimentary sequences, to identify detrital carbonate layers (Channell et al., 2012; Hodell et al., 2008; Pearce et al., 2013; Winsor et al., 2012). In core SL 174, the first increase in Ca/Sr (>30) occurs between 240 and 217 cm. A subsequent peak is seen between 200 and 185 cm, and the thickest one between 165 and 115 cm (Fig. 2). Outside these intervals, Ca/Sr values remain between 5 and 30. In core SL 170, three intervals with high Ca/Sr ratios (>15) are observed at depths of 510–460, 285–190 and 145–110 cm (Fig. 3). Outside these intervals Ca/Sr ratios remain between 5 and 13.

qXRD measurements were carried out on a subset of samples where high Ca/Sr values were observed. Of particular interest was the proportion of dolomite and calcite within layers with high Ca/Sr values, which were expected to contain detrital carbonate. The results of qXRD analyses indicate that in these carbonate-rich layers from SL 174, total carbonate percentages are between 23 and 55% with a high proportion of dolomite (17–40%) relative to calcite (7–17%). The proportion of total carbonate in detrital carbonate layers is lower in SL 170 (4–16%). However as found in SL 174, there is a consistently higher proportion of dolomite (4–12%) as

compared to calcite (1–4%) in all samples analysed. All data presented here will be made available online at the PANGEA portal.

4. Discussion

4.1. Identification and timing of Baffin Bay detrital carbonate (BBDC) events

In both cores, the base of the oldest detrital carbonate layer is associated with an almost twofold increase in sedimentation rates. In core SL 174, the detrital carbonate delivery event is characterised by a very pebbly mud layer with abundant dropstones, possibly indicating iceberg rafting (Fig. 2). In SL 170 this layer is associated with the deposition of a less coarse, sandy layer, with occasional dropstones (Fig. 3). Within the age model uncertainty, this layer (and thus the event that led to its deposition) appears synchronous on both sides of Baffin Bay, beginning ~14.2 kyr BP and ending ~13.7 kyr BP (Fig. 4). This event corresponds to the first observed detrital carbonate delivery in Baffin Bay during the last deglaciation and thus appears to correspond to BBDC 1 as described in previous Baffin Bay records (Andrews et al., 2014, 1998, Simon et al., 2014, 2012).

A subsequent increase in detrital carbonate input is inferred to start at ~12.7 kyr BP in SL 174 and ~12.6 kyr BP in SL 170, i.e. at about the same time within the age model uncertainty. This second detrital carbonate layer is associated with an almost four-fold increase in sedimentation rates in both cores, peaking at ~12.6 kyr BP (Figs. 2 and 3) and by lithology and physical properties similar to those of the older BBDC 1 in each core. However, peak accumulation rates at ~12.6 kyr BP are associated with different geochemical signatures on both sides of Baffin Bay. On the Greenland side, the Ca/Sr values are at their maximum, whereas on the Baffin Island side, there is a distinct minimum in Ca/Sr (Fig. 4). The manifestation of this event in SL 174 is almost identical to that observed in the deeper and more northern core PC 16 (Fig. 1; Simon et al., 2014, 2012). In both western Baffin Bay cores, this event is characterised by a decrease in the proportion of >63 μm fraction (Fig. 2) and an increase in Ti/Sr ratios (Fig. S3), a proxy for increased terrigenous (vs. biogenic) input. The common internal structure of this event in both PC 16 and SL 174 could therefore reflect a regional change in the source and pattern of sediment delivery to the basin. Indeed, this finer, Ti-rich sediment is thought to indicate a lateral mode of sediment delivery from ice stream advance/retreat in Baffin Bay (Aksu and Piper, 1987; Hiscott et al., 1989). More recent provenance studies identify a predominantly western Greenland (Uummannaq) source of these fine grained layers (Simon et al.,

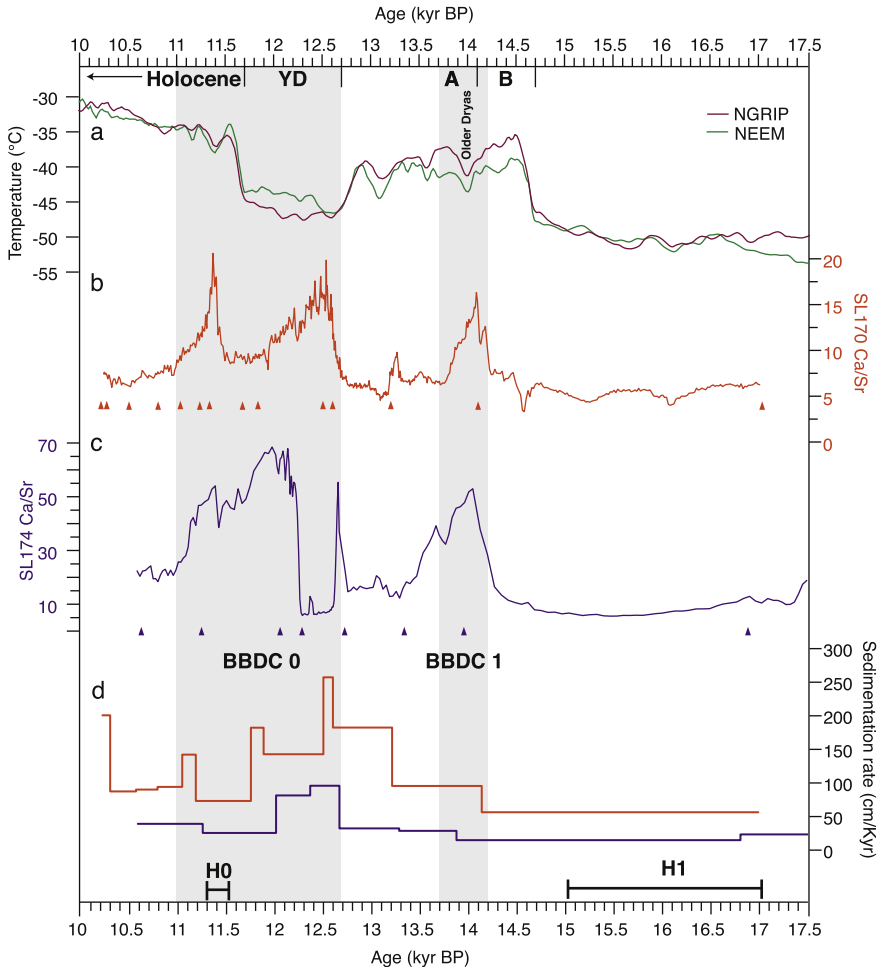

Fig. 4. Timing of BBDC events in central Baffin Bay during the last deglaciation. Elevated Ca/Sr ratios for SL 170 (b) and SL 174 (c) depict the two major BBDC events during the deglaciation, highlighted by grey shading. Radiocarbon dates for each record are shown by triangles of corresponding colour. Average sedimentation rates are also shown for both cores in the corresponding colour (d). BBDC 1 post-dates the onset of Bølling warming (B) and continues into the Allerød (A) indicated by new analysis of Greenland ice core records (a) (Buizert et al., 2014) and the Heinrich 1 Event (H1) in the Atlantic (Carlson and Clark, 2012) (d). BBDC 0 occurs at the onset of the Younger Dryas (YD) stadial and ends apparently slightly after the YD-end, possibly overlapping the newest timing of North Atlantic Heinrich Event 0 in the Labrador Sea (d) (Jennings et al., 2015; Pearce et al., 2015). (For interpretation of the references to colour in this figure legend, the reader is referred to the web version of this article.)

2014). The end of this event in both cores studied here is characterised by a secondary peak in Ca/Sr at ~11.4 kyr BP followed by a gradual decline in Ca/Sr until ~11.0 kyr BP. The timing of this event and its structure on the Baffin Island side suggests it is the previously identified BBDC 0 event (Andrews et al., 1995; Jennings et al., 2014; Simon et al., 2014, 2012).

Our identification of these detrital carbonate layers as BBDC layers is further supported by qXRD results (Fig. 5). The bulk sediment composition in both BBDC events shows calcite/dolomite ratios consistently lower than ~0.25:1 in cores SL 174 and SL 170. When compared with core PC 16, the total carbonate and dolomite therein decreases with increasing distance from the northern Baffin Bay source area, to which core PC 16 is most proximal and core SL 170 most distal along the path of the counter-clockwise circulation (Fig. 1). This suggests that ice-rafting of dolomite rich carbonates from the major northern ice streams, such as Nares Strait/Smith Sound and Lancaster Sound, followed the southward path of the present-day Baffin Island current and re-circulated east toward the centre of Baffin Bay north of Davis Strait (Fig. 1), as also suggested by Andrews et al. (2011). The composition of the BBDC 1 layer is distinctly different from Heinrich Event 1 layers from the Hudson Strait (Andrews et al., 2012, 1995) and from this we can assume that icebergs discharged from the Hudson Strait did not recirculate north into Baffin Bay (Fig. 5). BBDC 0 has a higher proportion of carbonate (and dolomite) perhaps indicating larger amounts of detrital carbonate among the ice rafted debris than during the deposition of BBDC 1. In fact, composition of the presumed H0 event in the Labrador Sea has a distinct signature more closely following that of BBDC events in the Baffin Bay (Fig. 5).

The synchronous nature of the BBDC 1 and 0 events that span Baffin Bay provides evidence for two periods of major North American-Arctic ice-sheet instability events Baffin Bay during the last deglaciation. This model of sediment delivery (Andrews et al., 1998; Hiscott et al., 1989) explains the sedimentation pattern along the Baffin Island margin (PC 16 and SL 174), but the higher sedimentation rate in SL 170 during both BBDC events requires an additional, local source of sediment during these events. The proximity of SL 170 to the paleo-ice streams of Disko Bugt suggests material delivered by the dynamic Jakobshavn Isbrae as the most likely local source of clastic sediment. Indeed, these ice streams retreated via iceberg calving during the interval of BBDC 0 (Jennings et al., 2014) and sediment originating from nearby west Greenland could have potentially caused dilution of the carbonate-rich signal in SL 170.

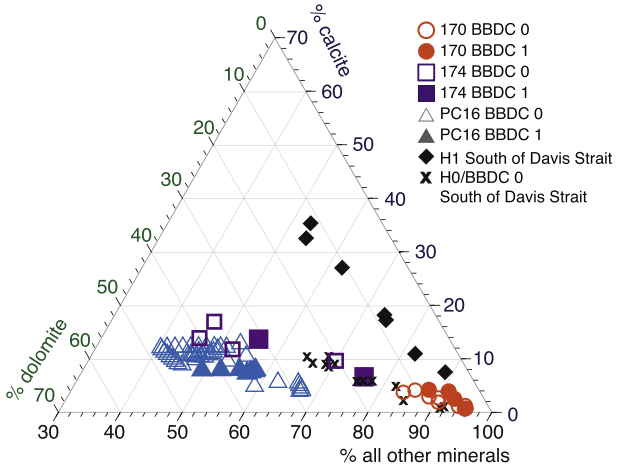

Fig. 5. Detrital carbonate composition during BBDC events in central Baffin Bay. Core PC 16 (Simon et al., 2014) has the highest concentration of carbonate and dolomite whilst the most distal core (SL170, this study) has the lowest. Composition of detrital carbonate layers found south of the Davis Strait (HU97048-007 PC and HU87033-009) during Heinrich Event 1 are shown for comparison. Layers depositing during the presumed H0/BBDC 0 event have a higher dolomite component within detrital carbonate layers (Andrews et al., 2014, 2012). Allocation of these sediments to Heinrich layer timing is based on the original age models for these cores.

4.2. Age uncertainty due to variable local ^{14}C reservoir effect in Baffin Bay

The construction of a radiocarbon chronology and dating of the observed abrupt ice-sheet instabilities are associated with uncertainties, which deserve consideration prior to full discussion of their relation to regional as well as global climatic changes. Of particular importance is the effect of a local ^{14}C reservoir age (ΔR) in Baffin Bay; the magnitude and variability of which is not well constrained (e.g. Pearce et al., 2015). Previous radiocarbon chronologies in Baffin Bay and surrounding regions have employed ΔR values ranging from 0 years (e.g. Levac et al., 2001; Knudsen et al., 2008; Gibb et al., 2015) to 400 years in the northern Baffin Bay (e.g. Ledu et al., 2010). Recent studies in the Disko Bugt area use a ΔR of 140 ± 35 yrs (Jennings et al., 2014; Lloyd et al., 2011; Ouellet-Bernier et al., 2014; Perner et al., 2013, 2011), estimated from historical but pre-bomb samples. Using $\Delta R = 140 \pm 35$ yrs at the site of SL 174 is also in line with studies of regional reservoir correction in Arctic Canada, that indicate local reservoir correction of $\Delta R = 150 \pm 60$ yrs in the south east Baffin Island region (Coulthard et al., 2010). No studies to-date address radiocarbon dating and the effect of ΔR in the region of the deeper cores used here. Furthermore, we lack dateable material independent of any reservoir effect (e.g., pollen or tephra), in order to test for reservoir effects.

Instead, to assess potential variability in the timing of the observed BBDC events, we generated multiple age models with BACON under same settings but varying the ΔR and its associated uncertainty (±). Due to the higher resolution and higher number of available ^{14}C dates we focused on the core SL 170 and tested the impact of changing ΔR on the onset and termination of BBDC events (at cm depth). The results can be seen in Fig. 6. While increasing ΔR from the published standard of $\Delta R = 140 \pm 35$ yrs (total correction = ~540 ± 35 yrs) to $\Delta R = 400 \pm 100$ yrs (total correction = ~800 ± 100 yrs) has the expected effect of making these events younger, the onset of the events even after application of these variable corrections remains within the 95% confidence intervals of the original age model. Importantly, none of the corrections align the timing of these events with Greenland temperature changes or Hudson Strait Heinrich Events (Fig. 6).

Three sample intervals at depths 74–76 cm (SL 170), 399–402 cm (SL 170) and 196–199 cm (SL 174) yielded enough material for planktonic and benthic radiocarbon dating, providing potentially another means of assessing ΔR (Tables 1 and 2). The (uncalibrated) difference in ^{14}C ages between planktonic and benthic ranges from 127 to 347 yrs (mean = 221, standard deviation = 113) in core SL 170, whereas the planktonic age from SL 174 is 260 years older than the benthic age. This is a feature occasionally observed in deep sea sediments and assigned either to the export of fresh young carbon from the photic zone to the sea floor or to distinct ventilation ages of sub-surface versus bottom waters (Bauer et al., 1995; Lund et al., 2011; Wu and Hillaire-Marcel, 1994). Whilst this does not permit a quantitative assessment of the offset between planktonic and benthic radiocarbon dates, it gives an indication that the difference does not vary by more than a few centuries. This small difference also allows us to accept the two-topmost dates (Holocene) for SL 174, which, due to low abundance of planktonic and benthic foraminifera, required a mixed sample for dating (Table 1).

A $\Delta R = 140 \pm 35$ yrs (total correction = 540 ± 35 yrs) is more

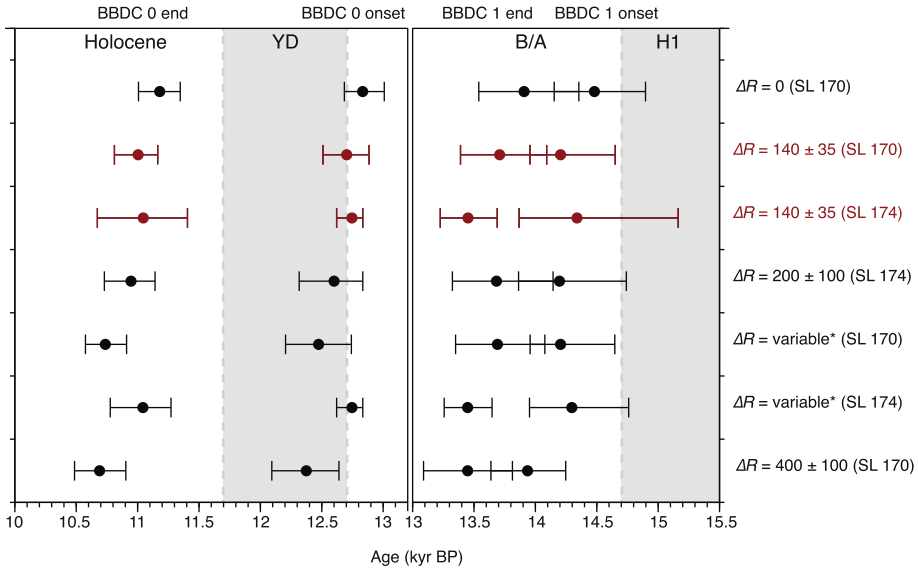

Fig. 6. Testing the effect of local reservoir age on the timing of detrital carbonate events in the studied central Baffin Bay cores. Modelled age (kyr BP) for the onset and end of BBDC events 1 and 0 in both cores, using differing local reservoir age (ΔR) and associated uncertainty ($\Delta R \pm$) are shown. All other model-run parameters were kept the same. *variable ΔR run applied a $\Delta R = 140 \pm 35$ yrs to planktonics and $\Delta R = 400 \pm 50$ yrs to benthics ^{14}C dates. Shaded intervals refer to climatic events during the Holocene; YD = Younger Dryas, B/A = Bølling/Allerød, H1 = Heinrich Event 1.

than likely sufficient for correcting ages based on planktonic foraminifera. While Baffin Bay is and was subject to extensive and persistent sea-ice cover, planktonic foraminifera would inhabit the top ~150 m of the water column, with well ventilated water (Fig. 1). Although our planktonic and benthic dates agree with each other (Tables 1 and 2), we nonetheless tested the difference between applying $\Delta R = 140 \pm 35$ yrs to all radiocarbon dates (age model presented here) and keeping the ΔR the same for radiocarbon ages based on planktonic foraminifera, while increasing it to $\Delta R = 400 \pm 50$ yrs for radiocarbon ages based on benthic foraminifera (Fig. 6; variable ΔR). This also has the effect of making the onset and termination of the BBDC 0 event younger, but the new dates remain within the uncertainty (95% confidence interval) of the original age model. Differences are minimal in the deeper sections of both cores (BBDC 1), where most pre-Younger Dryas ^{14}C dates are based on planktonic foraminifera. Small differences between models for core SL 174 (Fig. 6), where most dates are based on planktonic material, also supports this finding. The disintegration of the Greenland and Innuitian (Ellesmere) ice sheets and subsequent opening of the Nares Strait was not achieved before ~10 kyr BP (Jennings et al., 2011; Zreda et al., 1999), so the effect on the age model of poorly-ventilated (older) Arctic water entering Baffin Bay can be largely disregarded.

The variability of ΔR through time is unknown in Baffin Bay. A larger ΔR correction of 700–800 yrs was found to be appropriate for the North Atlantic during the Younger Dryas stadial, owing to enhanced sea ice cover and reduced advection of surface waters into the area (Bard et al., 1994). The potential that ΔR could have been larger during the Younger Dryas and the early part of the last deglacial period is something that we cannot quantify in this study. However previous studies in Baffin Bay indicate that extensive sea ice conditions persisted throughout the deglacial until the early Holocene ~7.4–7.3 kyr BP (Gibb et al., 2015; Ouellet-Bernier et al., 2014). From this we could make the assumption that if there is an additional sea-ice correction needed, it would remain relatively constant during the period studied here. Nonetheless, the age model, run with various reservoir ages (Fig. 6), gives us an indication as to the effect of increasing reservoir ages on the timing of the recorded BBDC events. Unless using a very high negative reservoir correction, it is not possible to align BBDC 1 with Heinrich Event 1 as recorded in the North Atlantic (Fig. 4). The possibility that BBDC 1 was synchronous with the North Atlantic Heinrich Event 0 can also be rejected. Although Bond et al. (1997) suggested H0 onset at ~12.8 kyr BP, more recent work (Hillaire-Marcel and de Vernal, 2008; Jennings et al., 2015; Pearce et al., 2015), points to a much younger age ~11.5 kyr BP, at the very end of the Younger Dryas (Figs. 4 and 7). The onset of BBDC 1 inferred in this study (~14.1 kyr BP) is ~2400 years younger than the revised onset of H0. This would require applying an extremely high $\Delta R > 2000$ years to planktonic radiocarbon dates, which we consider unrealistic. Applying such high reservoir correction would imply that BBDC 0 post-dated the main discharge events from the Disko Bay (Jennings et al., 2014).

In summary, the sensitivity study indicates that the age model using the published local reservoir ($\Delta R = 140 \pm 35$ yrs) on all radiocarbon dates is unlikely to be affected by variable reservoir age effects to such degree that it would allow an alternative phase relationship with Greenland temperatures and Labrador Sea Heinrich Events (Fig. 4).

Besides local reservoir correction, the possibility of detrital carbonate contamination of the foraminifera tests used for radiocarbon dating, particularly within BBDC layers, also requires discussion. We noted previously that detrital carbonate delivered to the study core sites is likely of Paleozoic age; thus even a minute amount of contamination would yield either substantially older or 'blank' ^{14}C ages, i.e. beyond the range of radiocarbon dating. Radiocarbon dates within a detrital carbonate layer representing the 8.2 kyr BP event in Laurentian Fan sedimentary sequences, for example, required additional reservoir correction; Lake Agassiz waters were depleted in ^{14}C due to underlying Palaeozoic carbonates (Hoffman et al., 2012). Only three radiocarbon ages (including one replicate) had to be removed from the final age model of SL 170 (Table 2) as they caused small reversals (Fig. S2). No age reversals occurred in SL 174 (Table 1). Comparisons of dates within BBDC layers with those outside them are consistently well within the error of the age-depth relationship and we can conclude from this that there was little contamination effect. Although the potential impact of a contamination by Palaeozoic carbonate would be significantly more important on ^{14}C-dating than on stable isotope

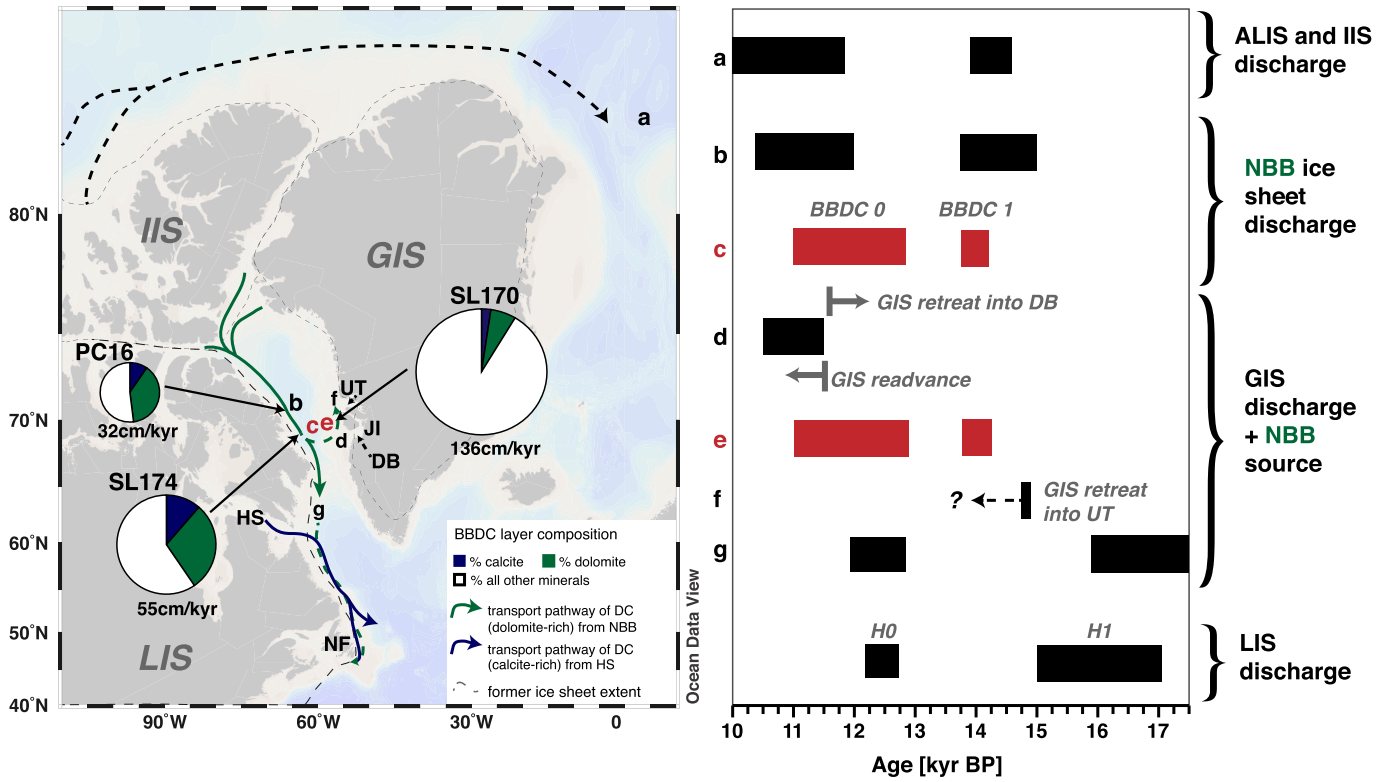

Fig. 7. Compilation of the timing of ice-rafted and detrital carbonate events in and around Baffin Bay during the late deglacial period. Map (left) shows the paths of detrital carbonate delivery in the Baffin Bay corridor region. Pie charts indicate the composition of BBDC layers in SL 174 and SL 170 (red, this study) and PC 16 (Simon et al., 2014); pie size is relative to the sedimentation rate during these periods. Letters indicate positions of other cores with detrital layers at various locations. The timing of these events according to their respective age models is shown right. Records used: Fram Strait (a) (Darby and Zimmerman, 2008); NW Baffin Bay (b) (Simon et al., 2014, 2012); SL 174 (c, this study); Disko Bugt Shelf (d) (Jennings et al., 2014); SL 170 (e, this study); Uummannaq Trough (f) (Ò Cofaigh et al., 2013b; Sheldon et al., 2016); Labrador Sea (g) (Andrews et al., 2014) and North Atlantic Heinrich Events 1 (Carlson and Clark, 2012) and 0 (Pearce et al., 2015). The comparison of records suggests stochastic behaviour (discharge and iceberg rafting) of the ice sheets surrounding the Baffin Bay. IIS = Innuitian Ice Sheet, LIS = Laurentide Ice Sheet and GIS = Greenland Ice Sheet. (For interpretation of the references to colour in this figure legend, the reader is referred to the web version of this article.)

compositions of foraminifera, it is noteworthy that stable isotopes measurements in the northwest Labrador Sea of 'dirty' vs. 'clean' foraminifera tests, did not yield significant differences. The 'dirty' foraminifera tests, extracted from detrital carbonate-rich layers, contained mostly clay-sized grains and minerals and there was little offset between these and the clean foraminifera (Gibb, 2014).

4.3. Asynchronous ice sheet instability during the last deglaciation

From the Last Glacial Maximum until BBDC 1, there is no evidence for enhanced detrital carbonate delivery to the Baffin Bay (see also Simon et al., 2014), suggesting only minimal discharge from any of the surrounding ice sheets until ~14.2 kyr BP. Our results confirm earlier inferences about the unlikeliness of a Heinrich Event 1 equivalent in Baffin Bay (Andrews et al., 2014, 1998, Simon et al., 2014, 2012) (Figs. 4 and 7). Outside of BBDC layers, we observe no sedimentary evidence for any major ice sheet instability. Although precise sediment provenance data are not available, it appears that there is an out-of-phase relationship between the North American Arctic and western Greenland ice sheets discharging into Baffin Bay and the Laurentide Ice Sheet calving via the Hudson Strait. Our age model test runs (see section 4.2) indicate that this out of phase behaviour is unlikely to be caused by variable local reservoir ages. The conclusion is further supported by the ^{14}C date in SL 174 at 384–385 cm, with an (uncalibrated) age of ~22.3–22.6 kyr BP. Although not included in the age model, it indicates the continuation of low sedimentation rates during the glacial period and thus no enhanced detrital input during Heinrich stadial 1. Furthermore, no Heinrich Event 1 equivalent event was noted in PC 16, north of SL 174 (Simon et al., 2014, 2012).

Contrary to earlier inferences (Simon et al., 2014, 2012), our high-resolution age model indicates that the onset of BBDC 1 postdates the onset of the Bølling interstadial as expressed in northern Greenland atmospheric temperatures (Buizert et al., 2014) by ~500 years (Fig. 4). This difference is outside the 95% uncertainty in SL 170 and marginally within uncertainty in SL 174, indicating that the observed phase relationship may reflect a real temporal succession. In this scenario, the onset of the BBDC 1 event could reflect a lagged-nonlinear response (Carlson and Winsor, 2012) of the marine-terminating portions of the North American Arctic and western Greenland ice sheets to the Bølling warming. On the one hand, the onset of BBDC 1 occurred at the very end of meltwater pulse 1A (e.g. Deschamps et al., 2012), at the end of a period of rapid postglacial sea level rise. This would potentially deepen sills such as Davis Strait (e.g. Tarasov et al., 2012) (Fig. 1) which in turn could have flooded ice margins. However the role of this mechanism would depend on the source of the meltwater pulse (North American and/or Antarctic ice sheets), which is still under debate (e.g. Liu et al., 2015). Thus we cannot directly implicate this as a mechanism for the onset of BBDC 1 in Baffin Bay. On the other hand, the timing of the BBDC 1 onset follows the spreading of warm water in the deep North Atlantic (Thiagarajan et al., 2014) and invigorated circulation (Liu et al., 2009) at the transition into the Bølling interstadial. This could have resulted in a greater inflow of the warm Irminger component of the West Greenland Current into Baffin Bay (Fig. 1). The incursion of warmer

sub-surface water was observed off St. Lawrence (Obbink et al., 2010) and the incursion of warmer Irminger Water was observed off southern Greenland at ~14 kyr BP (Jennings et al., 2006; Knutz et al., 2011; Winsor et al., 2012), and there is potential evidence for this incursion prior to 14 kyr BP in the Uummannaq Trough region (Sheldon et al., 2016). This incursion of warm sub-surface water has been implicated as a mechanism for enhancing basal melting of the Uummannaq Trough ice stream (Sheldon et al., 2016) situated to the north of SL 170. There is little evidence of extensive ice-rafted debris in the BBDC 1 layer in SL 170, but the increased sedimentation rate at ~14.1 kyr BP could reflect increased delivery of local sediment driven by enhanced basal melting along the West Greenland margin (Fig. 3), but this requires further investigation.

In western Baffin Bay, BBDC 1 sediments contain significant amounts of detrital carbonates (and abundant dolomite, Fig. 5). The coarser sediment, containing abundant dropstones, is more characteristic of ice-rafted deposition. This layer is similar in timing and properties to a DC layer observed in cores from the Uummannauq Trough region (Sheldon et al., 2016) and in PC 16, north of SL 174 (Simon et al., 2014, 2012). Evidence of detrital carbonate layers are also found in sediments from the Lancaster Sound Trough mouth (Li et al., 2011), although these layers remain undated, the authors assigning these events to the Heinrich Event timescale (Li et al., 2011). Similarly, records of detrital deposition in the Fram Strait, originating from the Arctic-Innuitian and -Laurentide ice sheets, are roughly in line with the timing of the BBDC 1 (Darby and Zimmerman, 2008) (Fig. 7). However, Darby and Zimmerman (2008) also suggest that Fram Strait ice-rafted debris (IRD) events could be (with age model uncertainties) a manifestation of Heinrich Events, a suggestion weakened by the chronology proposed here.

Although we cannot identify specific source areas in this study, it appears that the BBDC 1 event follows the model of sediment dispersal first proposed by Aksu and Piper (1987) and Hiscott et al. (1989). In this scenario, massive calving from destabilised ice sheets and glaciers surrounding northern Baffin Bay (North American-Arctic and north-western Greenland) resulted in the deposition of detrital carbonate layers along the path of the WGC/BIC (Fig. 7). Whether the destabilisation of the North American-Arctic and western Greenland ice sheets and associated discharge were driven by the incursion of a warmer and stronger WGC (Fig. 1) at the study sites requires further investigation. Alternatively, BBDC 1 could be a product of some internal ice-sheet instability as has been proposed for Heinrich events. However, we cannot assess these mechanisms (e.g. binge/purge oscillations (MacAyeal, 1993), the subglacial outburst-flow model or catastrophic ice shelf breakup model, summarised by Hesse and Khodabakhsh, 2016; Marcott et al., 2011) with the data presented here.

In contrast, the onset of BBDC 0 (~12.7 kyr BP) is coincident, within uncertainty, with the onset of the Younger Dryas stadial. Unlike the BBDC 1 event that, even with age model uncertainties, clearly postdates Heinrich Event 1, the difference between the timing of BBDC 0 and Heinrich Event 0 is not so clear. This rests on the uncertainties regarding the representation of Heinrich Event 0 in previously studied marine records. In earlier Labrador Sea core studies, the onset of Heinrich Event 0 was seen as coincident with the Younger Dryas (~12.8 kyr BP) (e.g. Andrews et al., 2012, 1995; Hillaire-Marcel et al., 1994; Stoner et al., 1996), but only a small number of these cores in shallower regions show clear evidence of a discrete Heinrich Event 0. Many cores from the deeper north-western Labrador Sea lack a detrital carbonate peak in this late deglacial interval (Andrews et al., 1995; Gibb et al., 2014; Rashid et al., 2011). Of the few cores with a distinct Heinrich-type layer and adequate radiocarbon dating to constrain the upper and lower limit of the event, the duration of Heinrich 0 is ~12.8 to between 12.0 and 8.7 kyr BP (as summarised by Rashid et al., 2011). Within these poorly constrained age brackets, BBDC 0 from our records would then be coeval with the start of Heinrich Event 0. However all higher resolution cores present a revised timing of the Heinrich Event 0 onset following the Younger Dryas interval at ~11.5 kyr BP (Hillaire-Marcel and de Vernal, 2008; Jennings et al., 2015; Pearce et al., 2015) (Figs. 4 and 7). This suggests that the onset of ice-sheet instabilities of the northern Baffin Bay predates the H0 discharge from Hudson Strait recorded mostly in the western Labrador Sea.

Evidence from geochemical data and sedimentation rates points to two modes of detrital deposition during the BBDC 0 event in western Baffin Bay (SL 174). Here, the initial carbonate rich and ice-proximal layer is followed by layer of Ti-enriched finer material (Fig. S3), followed again by a layer more enriched in carbonate that persisted until the end of the event (Fig. 4). While the coarser and more carbonate rich layers were likely transported by iceberg rafting as during BBDC 1 (Fig. 2), the fine-grained layer in between requires a different transport mechanism.

Sediments with such characteristics have been previously attributed to lateral mass flows resulting from rapid basal melting of ocean-terminating glaciers (Aksu and Piper, 1987; Simon et al., 2012). This characteristic composition and sedimentation sequence of BBDC 0 in west Baffin Bay is also seen in the more central PC 16, ruling out this layer as a turbidite. This rapidly deposited sub-layer of BBDC 0 could be seen as a dilution event of the more or less continuous deposition of the detrital carbonate-rich ice-rafted debris from northern Baffin Bay sources. A SedUnMix sediment analysis (c.f Andrews and Eberl, 2012; Simon et al., 2014) concluded that at least during the earlier part of the deglaciation, these Ti-rich, finer layers may have been laterally transported from the Uummannaq Trough area (Simon et al., 2014). Although paleoceanographic reconstructions in north-western Baffin Bay are sparse and do not quite cover the onset of BBDC 0, the dominance of the Atlantic Water species *Cassidulina neoteretis* (Perner et al., 2013; Seidenkrantz, 1995) at ~12.5 kyr BP in a sediment core located south of the Nares Strait, suggests some influence of the WGC this far north by this time (Knudsen et al., 2008).

Eastward, re-advance of the GIS through Disko Bugt to the shelf edge during the early Younger Dryas and its subsequent retreat around 12.2 kyr BP would be a large source of ice rafted debris. Evidence from sediment cores suggest initial retreat was via calving (Hogan et al., 2016; Jennings et al., 2014; Ó Cofaigh et al., 2013b; Rinterknecht et al., 2014), accounting for the elevated sedimentation rates on the Greenland side of Baffin Bay recorded in SL 170 (Figs. 3 and 7). This local source would have amplified the effect of enhanced deposition of northern Baffin Bay-sourced detrital carbonate as found in SL 170 and other cores in the Disko Bugt area (Jennings et al., 2014). Whatever the mechanism, the effects of the discharge event from the North American-Arctic ice sheets surrounding the northern portion of Baffin Bay was far-reaching; evidence of a dolomite-rich detrital carbonate component are seen on the Greenland side of Baffin Bay in SL 170 (Fig. 7e) and the nearby Disko Bugt shelf (Jennings et al., 2014) (Fig. 7d). Furthermore, evidence of a dolomite-rich detrital carbonate layer in the Labrador Sea indicates that these events can overspill the Davis Strait (Andrews et al., 2014, 2012, 1995) (Figs. 5 and 7g).

The end of BBDC 0 at ~11 kyr BP appears concurrent with ice retreat from the carbonate terranes of northern Baffin Bay (Zreda et al., 1999) and coincides with exposure dates of ~11.1–10.8 kyr BP from the Lancaster Sound area (Ledu et al., 2010). By this time, transport of detrital carbonate from the northern source of BBDC events was severely diminished. On the west Greenland margin, exposure dates indicate that ice retreated across the Assiaat Sill (south of Disko Bugt) ~11 kyr BP and reached the mainland ~10 kyr

BP (Kelley et al., 2013; Young et al., 2013). In northern Disko Bugt, older exposure ages ~11 kyr BP were found at the head of Vagait Strait, indicating that retreat was somewhat faster in this area (Kelley et al., 2015). Similarly Rinterknecht et al. (2014) dated the collapse of the Jakobshavn Isbrae ice stream at 12.2 ± 0.6 kyr BP. However, after correcting for the improper uplift adjustment used, by accounting for the gravitational attraction of water towards ice (Cuzzone et al., 2016; Ullman et al., 2016), would place this collapse at the end of the Younger Dryas. Landward retreat of these ice streams would trap detrital material in fjord areas, exhausting the source of clastic material along this portion of the West Greenland coast to the seafloor at site SL 170.

5. Conclusions

Our new radiocarbon-based chronology indicates centennial synchronicity in the deposition of two distinct detrital carbonate layers across Baffin Bay during the last deglaciation and early Holocene (~17–10 kyr BP). We have determined that these layers represent the previously identified Baffin Bay Detrital Carbonate Events (BBDCs). Using the new chronology, we redefine the timing of these events as occurring between ~14.2–13.7 kyr BP (BBDC 1) and ~12.7–11 kyr BP (BBDC 0). The onset of BBDC 1 (~14.2 kyr BP) appears to have lagged Greenland warming and the event occurred completely out of phase with Heinrich Event 1. Iceberg and meltwater discharge from the North American-Arctic ice sheets during the latter part of the Bølling and into the Allerød interstadial implies the presence of significant amounts of icebergs and meltwater, which could have been channelled into the Labrador Sea through the Davis Strait. This finding questions the common assumption that iceberg discharge events caused reductions in Atlantic meridional overturning circulation and cold stadial conditions (Broecker, 1994).

The onset of BBDC 0 (~12.7 kyr BP) in the Younger Dryas stadial and its continuation into the Holocene (~11 kyr BP) suggests that instability of the North American-Arctic ice sheets could have been stochastic and independent of temperature change. This event was far-reaching and evidence of BBDC 0 is found in other cores on the western Greenland margin (Jennings et al., 2014) and the northwest Labrador Sea (Andrews et al., 2012, 1995). New records from the Labrador Sea suggest that BBDC 0 may have pre-dated the major discharge event from the Laurentide Ice Sheet via the Hudson Strait, Heinrich Event 0 (Pearce et al., 2015). The different timing of iceberg discharge events between Baffin Bay and the Labrador Sea therefore adds to the complexity of our understanding of abrupt climate change. Our results also highlight the importance of considering regional responses/linkages of ice sheets to/with abrupt climatic changes not only during the last deglacial period, but likely during earlier ice retreat intervals.

Acknowledgements

We thank the captain and crew of *RV Maria S. Merian* for support during the expedition MSM09/2 and Hartmut Schulz for help with curation of the sediment cores. The manuscript benefited from comments by Paul Knutz and two anonymous referees of an earlier version and comments from David Piper and an anonymous referee. R. Jackson would also like to thank S. Mulitza for help with the BACON age-modelling. This project was supported by the Deutsche Forschungsgemeinschaft (DFG) (Grant no. 1904) through the International Research Training Group "Processes and impacts of climate change in the North Atlantic Ocean and the Canadian Arctic" (IRTG 1904 ArcTrain). A.E. Carlson notes support from the U.S. National Science Foundation Polar Programs (ANS-1418074).

Appendix A. Supplementary data

Supplementary data related to this article can be found at http://dx.doi.org/10.1016/j.quascirev.2017.03.020.

References

Aksu, A.E., 1983. Holocene and Pleistocene dissolution cycles in deep-sea cores of Baffin Bay and Davis Strait: Palaeoceano-graphic implications. Mar. Geol. 53, 331–348.
Aksu, A.E., Piper, D.J.W., 1987. Late Quaternary sedimentation in Baffin Bay. Can. J. Earth Sci. 24, 1833–1846. http://dx.doi.org/10.1139/e87-174.
Andrews, J.T., Aksu, A., Kelly, M., Klassen, R., Miller, G.H., Mode, W.N., Mudie, P., 1985. Land/ocean correlations during the last interglacial/glacial transition, Baffin Bay, northwestern North Atlantic: a review. Quat. Sci. Rev. 4, 333–355.
Andrews, J.T., Barber, D.C., Jennings, A.E., Eberl, D.D., Maclean, B., Kirby, M.E., Stoner, J.S., 2012. Varying sediment sources (Hudson Strait, Cumberland Sound, Baffin Bay) to the NW Labrador Sea slope between and during Heinrich events 0 to 4. J. Quat. Sci. 27, 475–484. http://dx.doi.org/10.1002/jqs.2535.
Andrews, J.T., Eberl, D.D., 2012. Determination of sediment provenance by unmixing the mineralogy of source-area sediments: the "SedUnMix" program. Mar. Geol. 291–294, 24–33. http://dx.doi.org/10.1016/j.margeo.2011.10.007.
Andrews, J.T., Eberl, D.D., Scott, D., 2011. Surface (sea floor) and near-surface (box cores) sediment mineralogy in Baffin Bay as a key to sediment provenance and ice sheet variations. Can. J. Earth Sci. 48, 1307–1328. http://dx.doi.org/10.1139/e11-021.
Andrews, J.T., Gibb, O.T., Jennings, A.E., Simon, Q., 2014. Variations in the provenance of sediment from ice sheets surrounding Baffin Bay during MIS 2 and 3 and export to the Labrador Shelf Sea: site HU2008029-0008 Davis Strait. J. Quat. Sci. 29, 3–13. http://dx.doi.org/10.1002/jqs.2643.
Andrews, J.T., Jennings, A.E., Kerwin, M., Kirby, M., Manley, W., Miller, G.H., Bond, G., MacLean, B., 1995. A Heinrich-like event, H-0 (DC-0): Source(s) for detrital carbonate in the North Atlantic during the Younger Dryas Chronozone. Paleoceanography 10, 943–952. http://dx.doi.org/10.1029/95PA01426.
Andrews, J.T., Kirby, M.E., Aksu, A., Barber, D.C., Messe, D., 1998. Late Quaternary Detrital carbonate (DC-) layers in Baffin Bay marine sediments (67°–74°N): Correlation with Heinrich events in the North Atlantic? Quat. Sci. Rev. 17, 1125–1137.
Balsam, W.L., Deaton, B.C., Damuth, J.E., 1999. Evaluating optical lightness as a proxy for carbonate content in marine sediment cores. Mar. Geol. 161, 141–153. http://dx.doi.org/10.1016/S0025-3227(99)00037-7.
Bard, E., Arnold, M., Mangerud, J., Paterne, M., Labeyrie, L., Duprat, J., Mélières, M.-A., Sønstegaard, E., Duplessy, J.-C., 1994. The North Atlantic atmosphere-sea surface 14C gradient during the Younger Dryas climatic event. Earth Planet. Sci. Lett. 126, 275–287. http://dx.doi.org/10.1016/0012-821X(94)90112-0.
Bard, E., Tuna, T., Fagault, Y., Bonvalot, L., Wacker, L., Fahrni, S., Synal, H.-A., 2015. AixMICADAS, the accelerator mass spectrometer dedicated to 14C recently installed in Aix-en-Provence, France. Nucl. Instrum. Methods Phys. Res. Sect. B Beam Interact. Mater. Atoms 361, 80–86. http://dx.doi.org/10.1016/j.nimb.2015.01.075.
Bauer, J.E., Reimers, C.E., Druffel, E.R.M., Williams, P.M., 1995. Isotopic constraints on carbon exchange between deep ocean sediments and sea water. Nature 373, 686–689. http://dx.doi.org/10.1038/373686a0.
Blaauw, M., 2010. Methods and code for "classical" age-modelling of radiocarbon sequences. Quat. Geochronol. 5, 512–518. http://dx.doi.org/10.1016/j.quageo.2010.01.002.
Blaauw, M., Christen, J.A., 2011. Flexible paleoclimate age-depth models using an autoregressive gamma process. Bayesian Anal. 6, 457–474.
Bond, G., Broecker, W., Johnsen, S., McManus, J., Labeyrie, L., Jouzel, J., Bonani, G., 1993. Correlations between climate records from North Atlantic sediments and Greenland ice. Nature 365, 143–147. http://dx.doi.org/10.1038/365143a0.
Bond, G., Showers, W., Chesby, M., Lotti, R., Almasi, P., deMenocal, P., Priore, P., Cullen, H., Hajdas, I., Bonani, G., 1997. A Pervasive Millennial-Scale cycle in North Atlantic Holocene and Glacial climates. Science 278, 1257–1266. http://dx.doi.org/10.1126/science.278.5341.1257, 80.
Broecker, W.S., 1994. Massive iceberg discharges as triggers for global climate change. Nature 372, 421–424. http://dx.doi.org/10.1038/372421a0.
Buizert, C., Gkinis, V., Severinghaus, J.P., He, F., Lecavalier, B.S., Kindler, P., Leuenberger, M., Carlson, A.E., Vinther, B., Masson-Delmotte, V., White, J.W.C., Liu, Z., Otto-Bliesner, B., Brook, E.J., 2014. Greenland temperature response to climate forcing during the last deglaciation. Science 345, 1177–1180. http://dx.doi.org/10.1126/science.1254961.
Carlson, A.E., Clark, P.U., 2012. Ice sheet sources of sea level rise and freshwater discharge during the last deglaciation. Rev. Geophys. 50, RG4007. http://dx.doi.org/10.1029/2011RG000371.
Carlson, A.E., Winsor, K., 2012. Northern Hemisphere ice-sheet responses to past climate warming. Nat. Geosci. 5, 607–613. http://dx.doi.org/10.1038/ngeo1528.
Channell, J.E.T., Hodell, D.A., Romero, O., Hillaire-Marcel, C., de Vernal, A., Stoner, J.S., Mazaud, A., Röhl, U., 2012. A 750-kyr detrital-layer stratigraphy for the North Atlantic (IODP Sites U1302–U1303, Orphan Knoll, Labrador Sea). Earth Planet. Sci. Lett. 317–318, 218–230. http://dx.doi.org/10.1016/j.epsl.2011.11.029.
Clark, P.U., Shakun, J.D., Baker, P.A., Bartlein, P.J., Brewer, S., Brook, E., Carlson, A.E., Cheng, H., Kaufman, D.S., Liu, Z., Marchitto, T.M., Mix, A.C., Morrill, C., Otto-

Bliesner, B.L., Pahnke, K., Russell, J.M., Whitlock, C., Adkins, J.F., Blois, J.L., Clark, J., Colman, S.M., Curry, W.B., Flower, B.P., He, F., Johnson, T.C., Lynch-Stieglitz, J., Markgraf, V., McManus, J., Mitrovica, J.X., Moreno, P.I., Williams, J.W., 2012. Global climate evolution during the last deglaciation. Proc. Natl. Acad. Sci. 109, E1134–E1142. http://dx.doi.org/10.1073/pnas.1116619109.

Coulthard, R.D., Furze, M.F.A., Pieńkowski, A.J., Chantel Nixon, F., England, J.H., 2010. New marine ΔR values for Arctic Canada☆. Quat. Geochronol. 5, 419–434. http://dx.doi.org/10.1016/j.quageo.2010.03.002.

Cuzzone, J.K., Clark, P.U., Carlson, A.E., Ullman, D.J., Rinterknecht, V.R., Milne, G.A., Lunkka, J.-P., Wohlfarth, B., Marcott, S.A., Caffee, M., 2016. Final deglaciation of the Scandinavian Ice Sheet and implications for the Holocene global sea-level budget. Earth Planet. Sci. Lett. 448, 34–41. http://dx.doi.org/10.1016/j.epsl.2016.05.019.

Darby, D.A., Zimmerman, P., 2008. Ice-rafted detritus events in the Arctic during the last glacial interval, and the timing of the Innuitian and Laurentide ice sheet calving events. Polar Res. 27, 114–127. http://dx.doi.org/10.1111/j.1751-8369.2008.00057.x.

Deschamps, P., Durand, N., Bard, E., Hamelin, B., Camoin, G., Thomas, A.L., Henderson, G.M., Okuno, J., Yokoyama, Y., 2012. Ice-sheet collapse and sea-level rise at the Bølling warming 14,600 years ago. Nature 483, 559–564. http://dx.doi.org/10.1038/nature10902.

Dyke, A.S., Andrews, J.T., Clark, P.U., England, J.H., Miller, G.H., Shaw, J., Veillette, J.J., 2002. The Laurentide and Innuitian ice sheets during the last Glacial maximum. Quat. Sci. Rev. 21, 9–31. http://dx.doi.org/10.1016/S0277-3791(01)00095-6.

England, J., Atkinson, N., Bednarski, J., Dyke, A.S., Hodgson, D.A., Ó Cofaigh, C., 2006. The Innuitian Ice Sheet: configuration, dynamics and chronology. Quat. Sci. Rev. 25, 689–703. http://dx.doi.org/10.1016/j.quascirev.2005.08.007.

Gibb, O.T., 2014. Paleohydrography of Baffin Bay, Davis Strait, and the Northwest Labrador Sea during the Last Climatic Cycle. UNIVERSITÉ DU QUÉBEC À MONTRÉAL.

Gibb, O.T., Hillaire-Marcel, C., de Vernal, A., 2014. Oceanographic regimes in the northwest Labrador Sea since Marine Isotope Stage 3 based on dinocyst and stable isotope proxy records. Quat. Sci. Rev. http://dx.doi.org/10.1016/j.quascirev.2013.12.010.

Gibb, O.T., Steinhauer, S., Frechette, B., de Vernal, A., Hillaire-Marcel, C., 2015. Diachronous evolution of sea surface conditions in the Labrador Sea and Baffin Bay since the last deglaciation. Holocene 25, 1882–1897. http://dx.doi.org/10.1177/0959683615591352.

Heinrich, H., 1988. Origin and consequences of cyclic ice rafting in the Northeast Atlantic Ocean during the past 130,000 years. Quat. Res. 29, 142–152. http://dx.doi.org/10.1016/0033-5894(88)90057-9.

Hemming, S.R., 2004. Heinrich events: massive late Pleistocene detritus layers of the North Atlantic and their global climate imprint. Rev. Geophys. 42, RG1005. http://dx.doi.org/10.1029/2003RG000128.

Hesse, R., Khodabakhsh, S., 2016. Anatomy of Labrador Sea Heinrich layers. Mar. Geol. http://dx.doi.org/10.1016/j.margeo.2016.05.019.

Hillaire-Marcel, C., de Vernal, A., 2008. Stable isotope clue to episodic sea ice formation in the glacial North Atlantic. Earth Planet. Sci. Lett. 268, 143–150.

Hillaire-Marcel, C., de Vernal, A., Bilodeau, G., Wu, G., 1994. Isotope stratigraphy, sedimentation rates, deep circulation, and carbonate events in the Labrador Sea during the last ~ 200 ka. Can. J. Earth Sci. 31, 63–89. http://dx.doi.org/10.1139/e94-007.

Hiscott, R., Aksu, A., Nielsen, O., 1989. Provenance and dispersal patterns, Pliocene-Pleistocene section at site 645, Baffin Bay. Proc. Ocean Drill. Progr. 105, 31–52.

Hodell, D.A., Channell, J.E.T., Curtis, J.H., Romero, O.E., Röhl, U., 2008. Onset of "Hudson Strait" Heinrich events in the eastern North Atlantic at the end of the middle pleistocene transition (~640 ka)? Paleoceanography 23. http://dx.doi.org/10.1029/2008PA001591 n/a-n/a.

Hoffman, J.S., Carlson, A.E., Winsor, K., Klinkhammer, G.P., LeGrande, A.N., Andrews, J.T., Strasser, J.C., 2012. Linking the 8.2 ka event and its freshwater forcing in the Labrador Sea. Geophys. Res. Lett. 39 http://dx.doi.org/10.1029/2012GL053047.

Hogan, K.A., Jennings, A.E., Dowdeswell, J.A., Hiemstra, J.F., 2016. Deglaciation of a major palaeo-ice stream in Disko trough, West Greenland. Quat. Sci. Rev. 147, 5–26. http://dx.doi.org/10.1016/j.quascirev.2016.01.018.

Jennings, A., Andrews, J., Pearce, C., Wilson, L., Ólfasdóttir, S., 2015. Detrital carbonate peaks on the Labrador shelf, a 13–7ka template for freshwater forcing from the Hudson Strait outlet of the Laurentide Ice Sheet into the subpolar gyre. Quat. Sci. Rev. 107, 62–80. http://dx.doi.org/10.1016/j.quascirev.2014.10.022.

Jennings, A., Sheldon, C., Cronin, T., Francus, P., Stoner, J., Andrews, J., 2011. The Holocene history of Nares Strait: transition from Glacial Bay to Arctic-Atlantic Throughflow. Oceanography 24, 26–41. http://dx.doi.org/10.5670/oceanog.2011.52.

Jennings, A.E., Hald, M., Smith, M., Andrews, J.T., 2006. Freshwater forcing from the Greenland Ice Sheet during the Younger Dryas: evidence from southeastern Greenland shelf cores. Quat. Sci. Rev. 25, 282–298.

Jennings, A.E., Walton, M.E., Ó Cofaigh, C., Kilfeather, A., Andrews, J.T., Ortiz, J.D., De Vernal, A., Dowdeswell, J.A., 2014. Paleoenvironments during Younger Dryas-Early Holocene retreat of the Greenland Ice Sheet from outer Disko trough, central west Greenland. J. Quat. Sci. 29, 27–40. http://dx.doi.org/10.1002/jqs.2652.

Kelley, S.E., Briner, J.P., Young, N.E., 2013. Rapid ice retreat in Disko Bugt supported by 10Be dating of the last recession of the western Greenland Ice Sheet. Quat. Sci. Rev. 82, 13–22. http://dx.doi.org/10.1016/j.quascirev.2013.09.018.

Kelley, S.E., Briner, J.P., Zimmerman, S.R.H., 2015. The influence of ice marginal setting on early Holocene retreat rates in central West Greenland. J. Quat. Sci. 30, 271–280. http://dx.doi.org/10.1002/jqs.2778.

Knudsen, K.-L., Stabell, B., Seidenkrantz, M.-S., Eiriksson, J., Blake Jr., W., 2008. Deglacial and Holocene conditions in northernmost Baffin Bay: sediments, foraminifera, diatoms and stable isotopes. Boreas 37, 346–376. http://dx.doi.org/10.1111/j.1502-3885.2008.00035.x.

Knutz, P.C., Sicre, M.-A., Ebbesen, H., Christiansen, S., Kuijpers, A., 2011. Multiple-stage deglacial retreat of the southern Greenland Ice Sheet linked with Irminger Current warm water transport. Paleoceanography 26. http://dx.doi.org/10.1029/2010PA002053 n/a-n/a.

Kucera, M., Rhein, M., Gohl, K., 2014. Oceanography and Geodynamics in the NW Atlantic and the Baffin Bay – Cruise No. MSM09-July 23 – October 29, 2008-Bremen (Germany). http://dx.doi.org/10.2312/cr_msm09. Ponta Delgada (Azores).

Ledu, D., Rochon, A., de Vernal, A., St-Onge, G., 2010. Holocene paleoceanography of the northwest passage, Canadian Arctic Archipelago. Quat. Sci. Rev. 29, 3468–3488. http://dx.doi.org/10.1016/j.quascirev.2010.06.018.

Levac, E., De Vernal, A., Blake Jr., W., 2001. Sea-surface conditions in northernmost Baffin Bay during the Holocene: palynological evidence. J. Quat. Sci. 16, 353–363. http://dx.doi.org/10.1002/jqs.614.

Li, G., Piper, D.J.W., Calvin Campbell, D., 2011. The Quaternary Lancaster Sound Trough-mouth fan, NW Baffin Bay. J. Quat. Sci. 26, 511–522. http://dx.doi.org/10.1002/jqs.1479.

Liu, J., Milne, G.A., Kopp, R.E., Clark, P.U., Shennan, I., 2015. Sea-level constraints on the amplitude and source distribution of Meltwater Pulse 1A. Nat. Geosci. 9, 130–134. http://dx.doi.org/10.1038/ngeo2616.

Liu, Z., Otto-Bliesner, B.L., He, F., Brady, E.C., Tomas, R., Clark, P.U., Carlson, A.E., Lynch-Stieglitz, J., Curry, W., Brook, E., Erickson, D., Jacob, R., Kutzbach, J., Cheng, J., 2009. Transient simulation of last deglaciation with a new mechanism for Bolling-Allerod warming. Science 325, 310–314. http://dx.doi.org/10.1126/science.1171041.

Lloyd, J., Moros, M., Perner, K., Telford, R.J., Kuijpers, A., Jansen, E., McCarthy, D., 2011. A 100 yr record of ocean temperature control on the stability of Jakobshavn Isbrae, West Greenland. Geology 39, 867–870. http://dx.doi.org/10.1130/G32076.1.

Lund, D.C., Mix, A.C., Southon, J., 2011. Increased ventilation age of the deep northeast Pacific Ocean during the last deglaciation. Nat. Geosci. 4, 771–774. http://dx.doi.org/10.1038/ngeo1272.

MacAyeal, D.R., 1993. Binge/purge oscillations of the Laurentide Ice Sheet as a cause of the North Atlantic's Heinrich events. Paleoceanography 8, 775–784. http://dx.doi.org/10.1029/93PA02200.

Marcott, S.A., Clark, P.U., Padman, L., Klinkhammer, G.P., Springer, S.R., Liu, Z., Otto-Bliesner, B.L., Carlson, A.E., Ungerer, A., Padman, J., He, F., Cheng, J., Schmittner, A., 2011. Ice-shelf collapse from subsurface warming as a trigger for Heinrich events. Proc. Natl. Acad. Sci. U. S. A. 108, 13415–13419. http://dx.doi.org/10.1073/pnas.1104772108.

McManus, J.F., Francois, R., Gherardi, J.-M., Keigwin, L.D., Brown-Leger, S., 2004. Collapse and rapid resumption of Atlantic meridional circulation linked to deglacial climate changes. Nature 428, 834–837. http://dx.doi.org/10.1038/nature02494.

Ó Cofaigh, C., Andrews, J.T., Jennings, A.E., Dowdeswell, J.A., Hogan, K.A., Kilfeather, A.A., Sheldon, C., 2013a. Glacimarine lithofacies, provenance and depositional processes on a West Greenland trough-mouth fan. J. Quat. Sci. 28, 13–26. http://dx.doi.org/10.1002/jqs.2569.

Ó Cofaigh, C., Dowdeswell, J.A., Jennings, A.E., Hogan, K.A., Kilfeather, A., Hiemstra, J.F., Noormets, R., Evans, J., McCarthy, D.J., Andrews, J.T., Lloyd, J.M., Moros, M., 2013b. An extensive and dynamic ice sheet on the West Greenland shelf during the last glacial cycle. Geology 41, 219–222. http://dx.doi.org/10.1130/G33759.1.

Obbink, E.A., Carlson, A.E., Klinkhammer, G.P., 2010. Eastern North American freshwater discharge during the Bolling-Allerod warm periods. Geology 38, 171–174. http://dx.doi.org/10.1130/G30389.1.

Ouellet-Bernier, M.-M., de Vernal, A., Hillaire-Marcel, C., Moros, M., 2014. Paleoceanographic changes in the Disko Bugt area, West Greenland, during the Holocene. Holocene 24, 1573–1583. http://dx.doi.org/10.1177/0959683614544060.

Pearce, C., Andrews, J.T., Bouloubassi, I., Hillaire-Marcel, C., Jennings, A.E., Olsen, J., Kuijpers, A., Seidenkrantz, M.-S., 2015. Heinrich 0 on the east Canadian margin: Source, distribution, and timing. Paleoceanography 30, 1613–1624. http://dx.doi.org/10.1002/2015PA002884.

Pearce, C., Seidenkrantz, M.-S., Kuijpers, A., Massé, G., Reynisson, N.F., Kristiansen, S.M., 2013. Ocean lead at the termination of the Younger Dryas cold spell. Nat. Commun. 4, 1664. http://dx.doi.org/10.1038/ncomms2686.

Perner, K., Moros, M., Jennings, A., Lloyd, J., Knudsen, K., 2013. Holocene palaeoceanographic evolution off West Greenland. Holocene 23, 374–387. http://dx.doi.org/10.1177/0959683612460785.

Perner, K., Moros, M., Lloyd, J.M., Kuijpers, A., Telford, R.J., Harff, J., 2011. Centennial scale benthic foraminiferal record of late Holocene oceanographic variability in Disko Bugt, West Greenland. Quat. Sci. Rev. 30, 2815–2826.

Rashid, H., Piper, D.J.W., Flower, B.P., 2011. The role of Hudson Strait outlet in Younger Dryas Sedimentation in the Labrador Sea. In: Abrupt Climate Change: Mechanisms, Patterns, and Impacts. American Geophysical Union, pp. 93–110. http://dx.doi.org/10.1029/2010GM001011.

Reimer, P., 2013. IntCal13 and Marine13 radiocarbon age calibration curves 0–50,000 Years cal BP. Radiocarbon 55, 1869–1887. http://dx.doi.org/10.2458/

azu_js_rc.55.16947.
Rinterknecht, V., Jomelli, V., Brunstein, D., Favier, V., Masson-Delmotte, V., Bourles, D., Leanni, L., Schlappy, R., 2014. Unstable ice stream in Greenland during the Younger Dryas cold event. Geology 42, 759–762. http://dx.doi.org/10.1130/G35929.1.
Seidenkrantz, M.-S., 1995. Cassidulina teretis Tappan and Cassidulina neoteretis new species (Foraminifera): stratigraphic markers for deep sea and outer shelf areas. J. Micropalaeontol. 14, 145–157. http://dx.doi.org/10.1144/jm.14.2.145.
Shakun, J.D., Carlson, A.E., 2010. A global perspective on Last Glacial Maximum to Holocene climate change. Quat. Sci. Rev. 29, 1801–1816. http://dx.doi.org/10.1016/j.quascirev.2010.03.016.
Sheldon, C., Jennings, A., Andrews, J.T., Hogan, K., Dowdeswell, J.A., Seidenkrantz, M.-S., 2016. Ice stream retreat following the LGM and onset of the west Greenland current in Uummannaq Trough, west Greenland. Quat. Sci. Rev. 147, 27–46. http://dx.doi.org/10.1016/j.quascirev.2016.01.019.
Simon, Q., Hillaire-Marcel, C., St-Onge, G., Andrews, J.T., 2014. North-eastern Laurentide, western Greenland and southern Innuitian ice stream dynamics during the last glacial cycle. J. Quat. Sci. 29, 14–26. http://dx.doi.org/10.1002/jqs.2648.
Simon, Q., St-Onge, G., Hillaire-Marcel, C., 2012. Late Quaternary chronostratigraphic framework of deep Baffin Bay glaciomarine sediments from high-resolution paleomagnetic data. Geochem. Geophys. Geosyst. 13 http://dx.doi.org/10.1029/2012GC004272.
Simon, Q., Thouveny, N., Bourlès, D.L., Nuttin, L., Hillaire-Marcel, C., St-Onge, G., 2016. Authigenic 10Be/9Be ratios and 10Be-fluxes (230Thxs-normalized) in central Baffin Bay sediments during the last glacial cycle: paleoenvironmental implications. Quat. Sci. Rev. 140, 142–162. http://dx.doi.org/10.1016/j.quascirev.2016.03.027.
Stoner, J.S., Channell, J.E.T., Hillaire-Marcel, C., 1996. The magnetic signature of rapidly deposited detrital layers from the Deep Labrador Sea: relationship to North Atlantic Heinrich layers. Paleoceanography 11, 309–325. http://dx.doi.org/10.1029/96PA00583.
Tang, C.C., Ross, C.K., Yao, T., Petrie, B., DeTracey, B.M., Dunlap, E., 2004. The circulation, water masses and sea-ice of Baffin Bay. Prog. Oceanogr. 63, 183–228.
Tarasov, L., Dyke, A.S., Neal, R.M., Peltier, W.R., 2012. A data-calibrated distribution of deglacial chronologies for the North American ice complex from glaciological modeling. Earth Planet. Sci. Lett. 315–316, 30–40. http://dx.doi.org/10.1016/j.epsl.2011.09.010.
Thiagarajan, N., Subhas, A.V., Southon, J.R., Eiler, J.M., Adkins, J.F., 2014. Abrupt pre-Bølling-Allerød warming and circulation changes in the deep ocean. Nature 511, 75–78. http://dx.doi.org/10.1038/nature13472.
Thornalley, D.J.R., Barker, S., Broecker, W.S., Elderfield, H., McCave, I.N., 2011. The deglacial evolution of North Atlantic deep convection. Science 331, 202–205. http://dx.doi.org/10.1126/science.1196812.
Ullman, D.J., Carlson, A.E., Hostetler, S.W., Clark, P.U., Cuzzone, J., Milne, G.A., Winsor, K., Caffee, M., 2016. Final Laurentide ice-sheet deglaciation and Holocene climate-sea level change. Quat. Sci. Rev. 152, 49–59. http://dx.doi.org/10.1016/j.quascirev.2016.09.014.
Wacker, L., Lippold, J., Molnár, M., Schulz, H., 2013. Towards radiocarbon dating of single foraminifera with a gas ion source. Nucl. Instrum. Methods Phys. Res. Sect. B Beam Interact. Mater. Atoms 294, 307–310. http://dx.doi.org/10.1016/j.nimb.2012.08.038.
Winsor, K., Carlson, A.E., Klinkhammer, G.P., Stoner, J.S., Hatfield, R.G., 2012. Evolution of the northeast Labrador Sea during the last interglaciation. Geochem. Geophys. Geosyst. 13 http://dx.doi.org/10.1029/2012GC004263 n/a-n/a.
Wu, G., Hillaire-Marcel, C., 1994. Accelerator mass spectrometry radiocarbon stratigraphies in deep Labrador Sea cores: paleoceanographic implications. Can. J. Earth Sci. 31, 38–47.
Young, N.E., Briner, J.P., Rood, D.H., Finkel, R.C., Corbett, L.B., Bierman, P.R., 2013. Age of the Fjord Stade moraines in the Disko Bugt region, western Greenland, and the 9.3 and 8.2 ka cooling events. Quat. Sci. Rev. 60, 76–90. http://dx.doi.org/10.1016/j.quascirev.2012.09.028.
Zreda, M., England, J., Phillips, F., Elmore, D., Sharma, P., 1999. Unblocking of the Nares Strait by Greenland and Ellesmere ice-sheet retreat 10,000 years ago. Nature 398, 139–142. http://dx.doi.org/10.1038/18197.

3.2 Supplementary Information

3.2.1 PARASOUND surveys and magnetic susceptibility

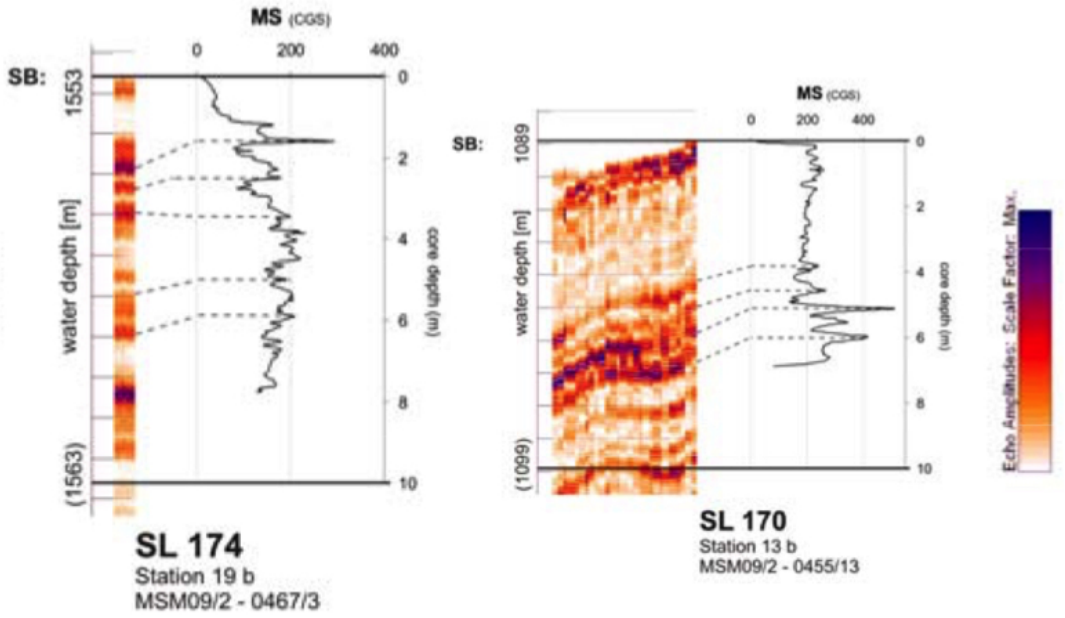

Figure S3.1: PARASOUND profiles at site of core recovery (left) correlated with (dashed lines) 1 cm resolution magnetic susceptibility curves for each core, measured on board (right). Image adapted from *Kucera et al.* [2014].

3.2.2 Chronology: outliers in SL 170 age model

Three of the ^{14}C ages obtained for core SL 170 were not included in the final age model. Fig. S3.2 shows the age-depth model calculated in BACON [*Blaauw and Christen*, 2011] that initially included these δ^{13}C dates. The dates that lie outside the 95% uncertainty interval are 116–118 cm (planktic), 136–139 cm (fragments) and 136–139 cm (benthic).

The first excluded date is a planktonic ^{14}C date (calibrated) at 116-118 cm which is 260 years older than the benthic date at the same depth (Fig. S3.2). This is a feature occasionally observed in deep sea sediments and assigned either to the export of fresh young carbon from the photic zone to the sea floor or to distinct ventilation ages of sub-surface versus bottom waters [*Bauer et al.*, 1995; *Lund et al.*, 2011; *Wu and Hillaire-Marcel*, 1994]. The ^{14}C date based on (unidentified) shell fragments at 136-139 cm could be an outlier for two reasons: the sample was measured via conventional ^{14}C

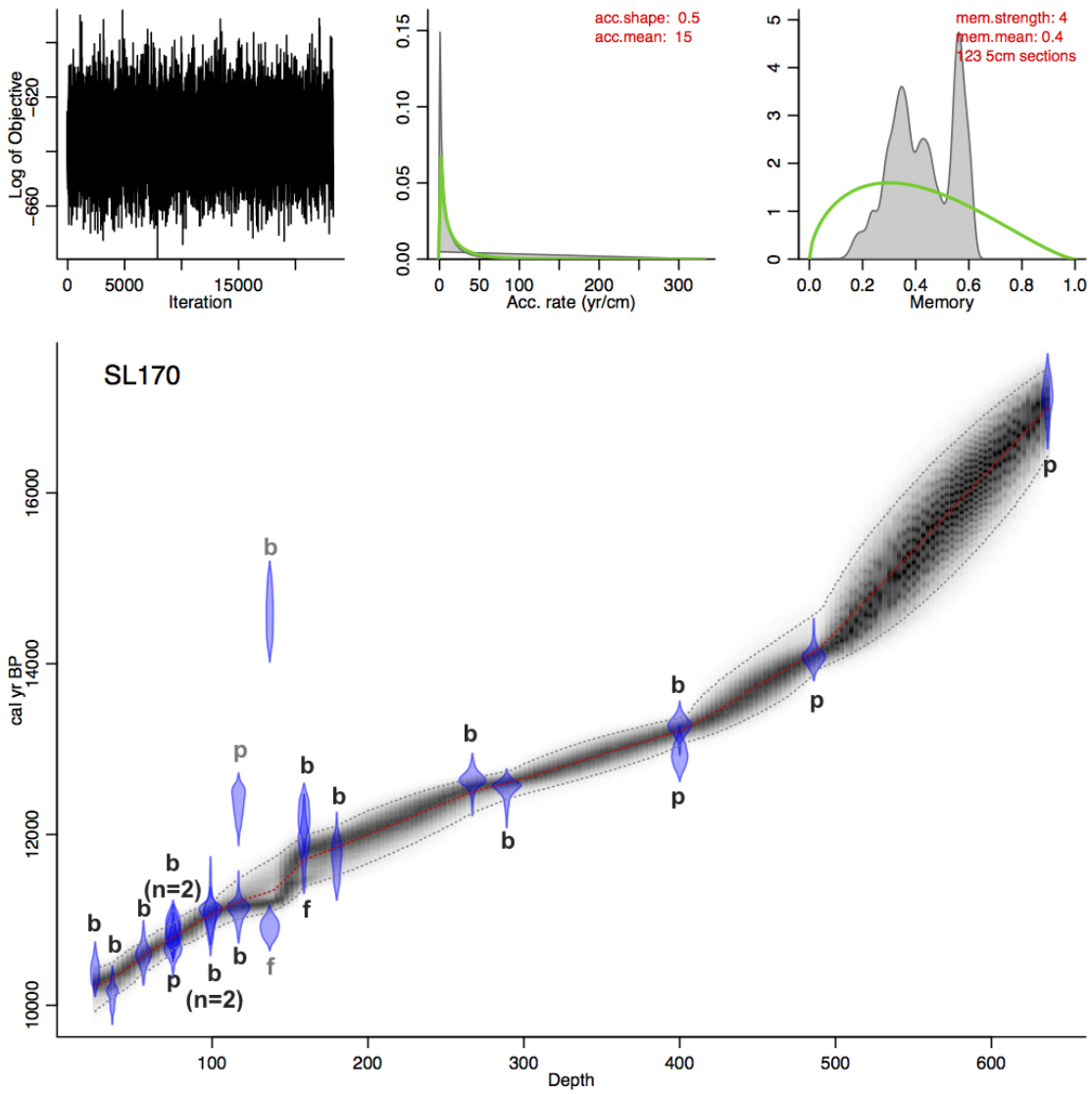

Figure S3.2: Age-depth relationship for core SL170 (output from the Bacon software). Labels indicate type of material dated: b = mixed benthic foraminifera; p = planktic foraminifera; f = shell fragments; n indicates the number of duplicates from the sample interval. Grey labelling indicates samples that were removed from the final age-depth calculation (see Figure 3 in the main article).

dating protocol and a large amount of material was dated (12.22 grams, see Table 2 in main article). The inability of the age model to reach this younger date (mean age, red line in Fig. S3.2) could therefore be due to analytical or methodological differences. This younger age could also be due to bioturbation of younger shell fragment material into a lower layer of sediment. Conversely, the ^{14}C date based on mixed benthic foraminifera at the same depth is considerably older than 8 of the ^{14}C dates below it (with the exception of the last planktonic ^{14}C date at 636-637 cm). This would suggest that this sample was contaminated with older carbon. There are no obvious signs of bioturbation at this point in the core. For the final age model details see Table 2 and Figure 3 in the main text.

3.2.3 Sedimentation rates

Using the Bacon output of age versus depth, sedimentation rates were manually calculated between radiocarbon-dated intervals in cm kyr^{-1} for each core.

3.2.4 Computerised tomography (CT) scanning

CT scanning was conducted using the General Electric CT Prospeed SX scanner at the MARUM, University of Bremen, Germany. Core sections were scanned in the single radiographic plane at 1 cm resolution.

3.2.5 X-ray fluorescence (XRF) analysis

XRF core scanner data were collected every 1 cm down-core over a 1.2 cm^2 area with down-core slit size of 1.2 mm using generator settings of 50 kV, (current of 1.0 mA), 30kV (1.0 mA) and 10kV (0.2mA) with a sampling time of 15 seconds directly at the split core surface of the archive half with XRF Core Scanner II (AVAATECH Serial No. 2) at MARUM, University of Bremen. The split core surface was covered with a 4 micron thin SPEXCerti Prep Ultralene foil to avoid contamination of the XRF measurement unit and desiccation of the sediment. The data were acquired by a Canberra X-PIPS Silicon Drift Detector (SDD; Model SXD 15C-150-500) with 150eV X-ray resolution, the Canberra Digital Spectrum Analyzer DAS 1000, and an Oxford Instruments 50W XTF5011 X-Ray tube with rhodium (Rh) target material. Raw data spectra were processed by the analysis of X-ray spectra by iterative least square software (WIN AXIL) package from Canberra Eurisys. Detector (SDD; Model SXD 15C-150-500) with 150eV X-ray resolution, the Canberra Digital Spectrum Analyzer DAS 1000, and an Oxford Instruments 50W XTF5011 X-Ray tube with rhodium (Rh) target material. Raw data spectra were processed by the analysis of X-ray spectra by Iterative Least square software (WIN AXIL) package from Canberra Eurisys.

We are primarily concerned with intervals of high carbonate content. Fig. S3.3 shows key elemental ratios. The match between the area counts for calcium (Ca) and the calcium/strontium ratio (Ca/Sr) shows that this ratio accurately represents the periods of high detrital carbonate input (BBDC events). The proportion of the >63 µm fraction (as a % of the bulk dry sample) obtained while processing sediments for micropaleontological analysis is also shown, as an approximation of grain size changes down core. High Ti intervals in core SL170 are indicative of input from Greenland.

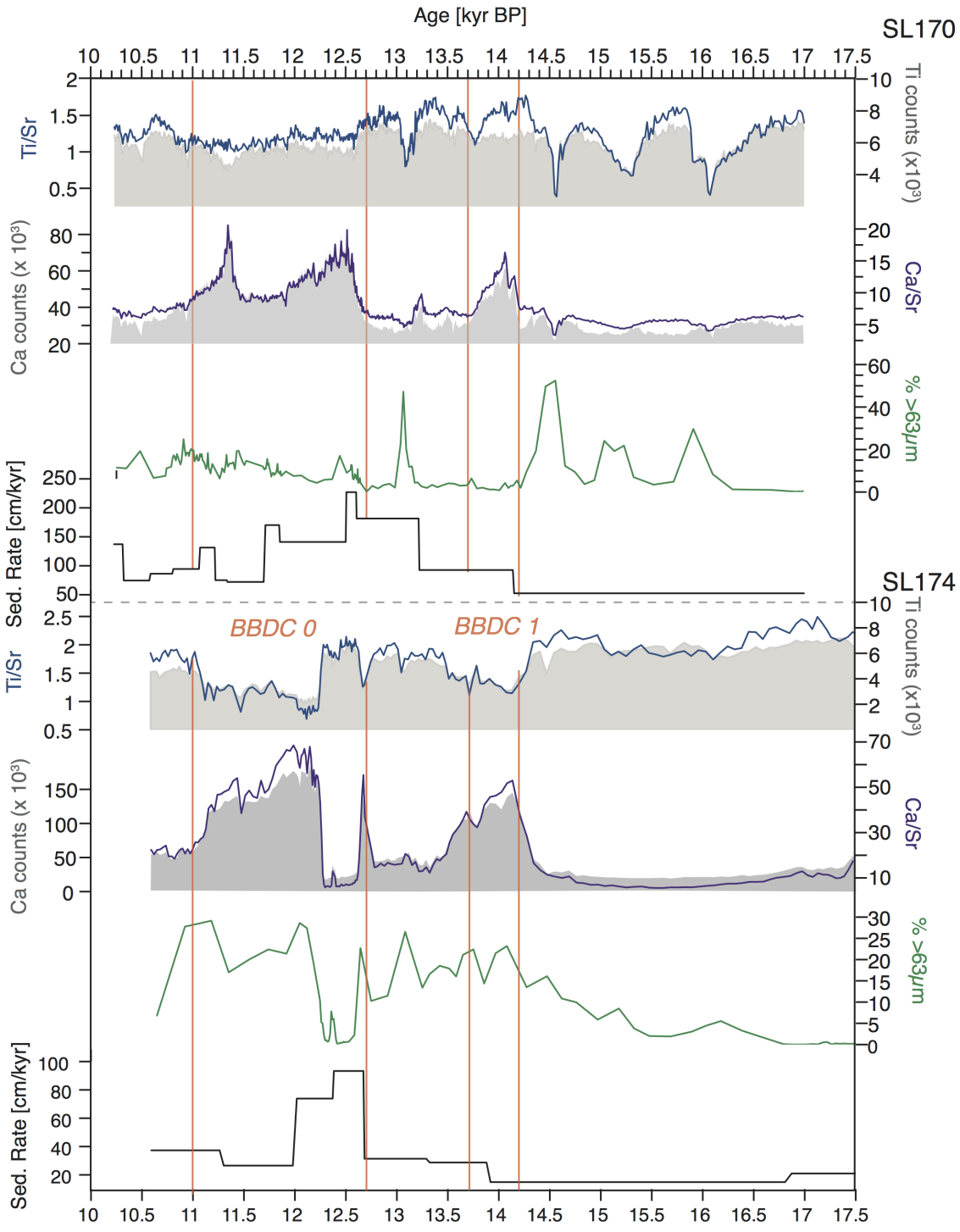

Figure S3.3: Downcore properties of Baffin Bay sediment cores. Sedimentation rates (black), % >63 µm sediment fraction (green), Ca/Sr ratios (purple) and Ca counts (grey shaded area), Ti/Sr ratios (blue) and Ti counts (grey shaded area) against age. BBDC intervals are constrained by orange lines

3.2.6 X-ray diffraction (XRD) analysis

XRD was measured on a Bruker D8 Advance diffractometer equipped with a Cu-tube (Kα_1 1.541, 45 kV, 40 mA), a fixed divergence slit of 0.2 θ, a 8 x 15 samples changer, a receiving slit of 0.1 mm a secondary graphite monochromator and the Lyxneye detector system. The measurements were done as a continuous scan from 3-85°0.2 θ, with a calculated step size of 0.021°2 θ (calculated time per step was 77 seconds).

Mineral identification was carried out by Dr. Christoph Vogt by means of the Philips software X'Pert HighScore™, which, besides mineral identification, gives a semi-quantitative value for each identified mineral on the basis of Relative Intensity Ratio (R.I.R)-values. The R.I.R-values are calculated as the ratio of the intensity of the most intense reflex of a specific mineral phase to the intensity of the most intense reflex of pure corundum (I/Ic) referring to the "matrix-flushing method" [*Chung*, 1974]. Unfortunately R.I.R values are sparse for clay minerals and long chain organic materials hampering the semi-quantification in this case. Additionally, a quantification has been performed using the full-pattern software package QUAX [*Vogt et al.*, 2002].

The comparison of XRD data between core PC16 [*Simon et al.*, 2014] and SL 170/SL 174 (this study) (Fig. 3 in article) concerns the dolomite and calcite content (%) during BBDC events. Only measurements within BBDC events (according each core's respective age model) are presented in Fig 3. Dolomite % presented here is the sum of dolomite and ankerite percentages. This method is still comparable with the method used to obtain % dolomite for PC16 [*Andrews et al.*, 2011].

Chapter 4

Paleoceanographic changes during the last deglaciation and early Holocene in Baffin Bay: links with ice sheet instabilities?

Abstract

There is still on-going debate about the relationship between oceanographic changes, ice-sheet instabilities and wider climatic changes during the last deglaciation and early Holocene. Sediment cores recovered from greater depths in Arctic and sub-arctic regions provide useful archives of ice sheet discharge and thus regional (if not global) climatic changes. Due to poor preservation of biogenic carbonate, not only is the construction of an absolute chronology for such records problematic but also reconstructing oceanographic conditions throughout the water column is challenging. We use a high-resolution sediment core from central Baffin Bay, off the west coast of Greenland, that benefits from a recently constructed radiocarbon chronology and records two periods of detrital input from the surrounding ice sheets (termed BBDC events). The trigger of these events remains fairly unknown as they occur during both stadial and interstadial periods. Good preservation of both planktonic and benthic foraminifera and organic palynomorphs allows for investigation into the changes in surface, sub-surface and deep ocean during the last deglacial and early Holocene (∼17–10 kyr BP). Throughout the deglacial and early Holocene Baffin Bay was subject to near perennial sea ice. Subsurface waters however appear to capture a regional δ^{18}O signal throughout this period. We present evidence of more well-ventilated deep waters in the early deglacial and we note the establishment of a strong connection with the north Atlantic via the West Greenland Current only after ∼14 kyr BP. A first detrital carbonate event (BBDC 1; ∼14.2–13.7 kyr BP does not appear to be lead by changes in oceanographic conditions and we hypothesize that either a large mixing event occurred or the event itself formed a cold meltwater surface layer, capping sub-surface waters. We cannot directly assess the role of oceanic change as a trigger of later event (BBDC 0; 12.7–11 kyr BP), but suggest that the event was a product of continually evolved oceanic and climatic conditions.

4.1 Introduction

The last deglaciation and early Holocene (17–10 kyr BP) was characterised by the landward retreat of some of the major Northern Hemisphere ice sheets, releasing large amounts of meltwater and icebergs into seas and oceans. This was also the case in Baffin Bay; a semi-enclosed basin fed by Atlantic waters from the south via the Davis Strait and later, by Arctic waters from the north via the Canadian Arctic Archipelago. Material from the northern Baffin Bay, rich in detrital carbonate (in comparison to the older Archean Block and Archean Nagssugtoqidian Mobile Belt (NMB) geology of western Greenland), was transported south by the Baffin Island Current (BIC; Fig. 4.1) and dispersed throughout the bay by the anticyclonic gyre. It records the retreat of the northeastern Laurentide (LIS) and Innuitian (IIS) ice sheets as discrete layers, termed Baffin Bay Detrital Carbonate Events (BBDCs) [*Mudie and Aksu*, 1984; *Hiscott et al.*, 1989; *Andrews et al.*, 1998, 2011; *Simon et al.*, 2012, 2014; *Jackson et al.*, 2017]. Off the coast of West Greenland, these layers are accompanied by material from a synchronous local sediment source from the Greenland Ice Sheet (GIS) [*Jackson et al.*, 2017].

The recently revised chronology of these carbonate events places the latest event (BBDC 0) at ∼12.7–11 kyr BP, in line with the Younger Dryas stadial and early Holocene, and an earlier event (BBDC 1) at ∼14.2–13.7 kyr BP during the Bølling/Allerød interstadial [*Jackson et al.*, 2017]. Not only are these events asynchronous with the timing of Heinrich Events recorded in the Atlantic [*Hemming*, 2004; *Carlson and Clark*, 2012; *Jennings et al.*, 2015; *Pearce et al.*, 2015], their occurrence during both stadial and interstadial periods perhaps requires a different mechanism than those initially proposed for Heinrich Events [*Bond et al.*, 1993; *Broecker*, 1994].

Sediment archives from Baffin Bay, where many of these ice sheets terminated at the shelf edge at least during the Last Glacial Maximum (LGM) [*Dyke et al.*, 2002], provide an ideal opportunity to study the possible role of changing oceanographic conditions in ice sheet margin retreat. The modern Baffin Bay is well stratified and the anitcyclonic circulation is driven by the Corilais force and the West Greenland Current (WGC, Fig. 4.1) flowing northwards along the west coast of Greenland and the southward transport of polar-sourced water via the Baffin Island Current (BIC) along the Canadian coast. The WGC is a combination of the sub-surface polar East Greenland Current (EGC) water from the north and advection of the warmer Atlantic water via the Irminger Current (IC), which lies below the EGC when the currents converge off the southern tip of Greenland. As it enters Baffin Bay it forms a warmer 'Intermediate water' layer between ∼150–600 m (Fig. 4.1). This layer caps the Baffin Bay 'Deep water'; a monotonously cool ($\leq 0\,^{\circ}C$) and saline water mass that penetrates waters to a water depth ∼1800 m [*Tang et al.*, 2004]. The surface waters of Baffin Bay are generally cool and fresh and

are thought to originate from the Arctic via the main conduits into northern Baffin Bay, such as the Nares Strait and Lancaster and Jones Sound. However, this connection was blocked during the last glacial period by the confluence of the northern Greenland, Innuitian and northeastern Laurentide ice sheets [*Zreda et al.*, 1999; *England et al.*, 2006].

Changes in the past incursion or strength of the WGC have been implicated as a major driver of melt along the west Greenland margins during the deglaciation [*Sheldon et al.*, 2016; *Jennings et al.*, 2017] and the early Holocene [*Holland et al.*, 2008; *Seidenkrantz et al.*, 2013; *Jennings et al.*, 2014; *Ouellet-Bernier et al.*, 2014] as well as in northern Baffin Bay [*Knudsen et al.*, 2008]. However there are major limitations when investigating the temporal relationship between ice sheets and oceanographic change during the entire deglacial period. Studies based in the fjord areas are influenced by local changes and high-resolution sediments only cover the later part of the Younger Dryas due to the late retreat of the Greenland Ice Sheet from the shelf region [*Perner et al.*, 2013]. Furthermore, pervasive carbonate dissolution in deeper parts of Baffin Bay, where records are lower resolution but cover the entire period, often hinders the establishment of an accurate chronology and material for analysis (i.e. foraminifera) [*Simon et al.*, 2012].

We use a sediment core (SL 170; Fig. 4.1) collected from the central west Greenland margin to try and ascertain the timing of oceanographic changes in Baffin Bay throughout the last deglaciation and early Holocene. It benefits from a robust chronology (chapter 3) [*Jackson et al.*, 2017] and the availability of material facilitates a full multi-proxy reconstruction of changes in surface (palynomorph analysis) and sub-surface water conditions (planktonic foraminiferal abundance and stable isotopes), as well as deeper ocean conditions (benthic foraminifera abundance, assemblages and stable isotope analysis). Using this information, we ascertain the timing of changes throughout the water column and relate this to wider changes in regional circulation. Furthermore, this core clearly documents periods detrital input from the ice sheets surrounding Baffin Bay (BBDC events) [*Jackson et al.*, 2017]. This co-registered record allows us to assess if there was a phase relationship between ice sheet instability and paleoceanographic change in Baffin Bay during the deglaciation and early Holocene.

4.2 Methods and material

4.2.1 Coring and construction of the age model

Gravity core Geo Tü SL 170 (68° 58.15' N 59° 23.58' W, MSM09/02-0455/13)1078 m water depth) was retrieved aboard the RV Maria S. Merian research cruise MSM09/02

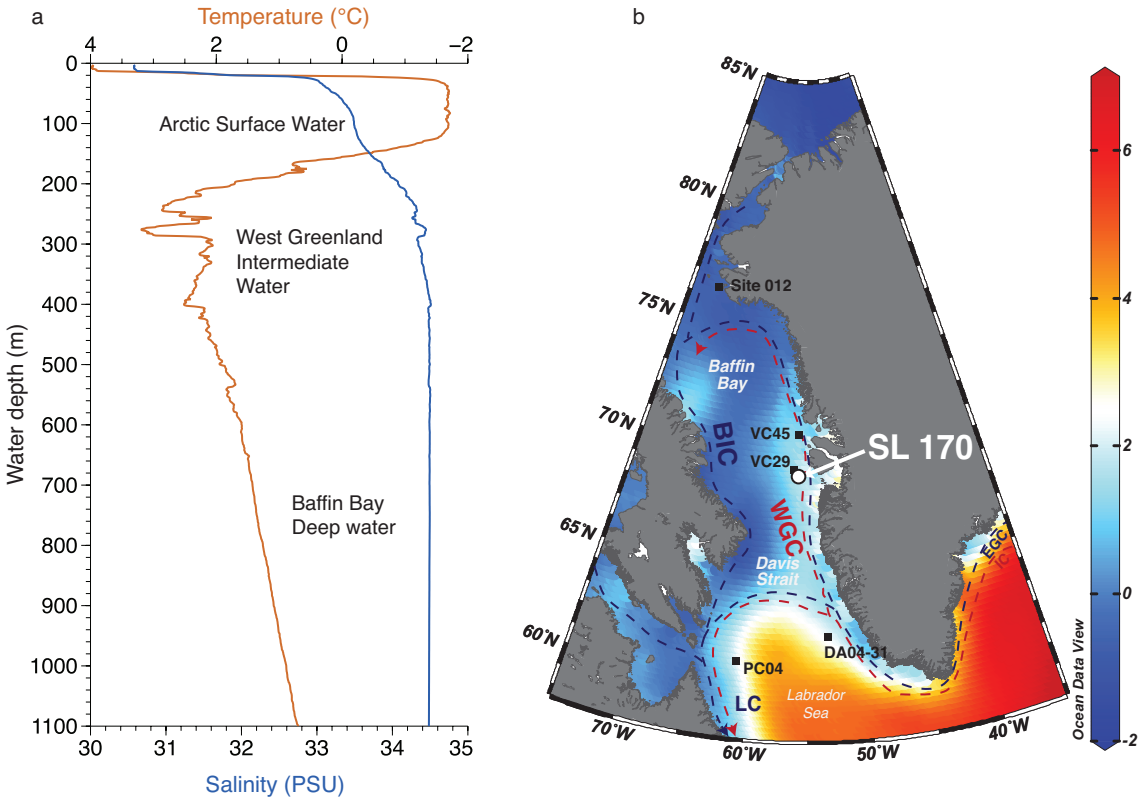

Figure 4.1: Core location of SL 170 and modern oceanography of Baffin Bay. Modern sea surface temperatures and near surface currents in Baffin Bay and surrounding region as well as the core location (b). EGC = East Greenland Current; IC = Irminger Current; WGC = West Greenland Current; BIC = Baffin Island Current; LC = Labrador Current. Temperature (note the inverted scale) and salinity profile from CTD cast (a) at the core site [*Krahmann*, 2013; *Kucera et al.*, 2014], with the three water masses indicated based on [*Tang et al.*, 2004]

[*Kucera et al.*, 2014] in 2008 (Fig. 4.1) and is 683 cm long. The core was split in half lengthwise and the working half fully sampled at in slices of 1 cm thickness for further analysis. The age model for Geo Tü SL 170 (herein referred to as SL 170) is based on 18 ^{14}C dates on planktonic or benthic foraminifera and mollusc fragments. The age model was constructed using the Bayesian age modelling software bacon [*Blaauw and Christen*, 2011], calibrated using the Marine13 ^{14}C calibration curve [*Reimer*, 2013a]. An additional local marine reservoir correction (ΔR) of 140 $\pm$ 35 years, estimated from calibration of modern (post-bomb) samples [*Lloyd et al.*, 2011; *Perner et al.*, 2013; *Jennings et al.*, 2014; *Ouellet-Bernier et al.*, 2014], was added. Sedimentation rates were calculated between dated intervals. A more detailed description of the chronology for SL 170 can be found in *Jackson et al.* [2017].

4.2.2 Physical sediment properties and X-ray florescence (XRF) analysis

Computerised tomography (CT) and high-resolution linescan (LS) images were carried out on the archive half of core SL 170 at the University of Bremen, Germany. To analyse the elemental properties downcore, XRF scanning was performed on the archive half of the core using an XRF Core Scanner II^{TM}(AVAATECH^{TM}serial No. 2) at MARUM, University of Bremen. For full details of the methods used, the reader is referred to *Jackson et al.* [2017].

4.2.3 Palynomorph analysis

The % <63 µm fraction was kept for a subset of samples at 10 cm intervals during the wet sieving process. All material exiting the sieve was collected in beakers and left to settle. Water was then siphoned off and samples dried in a 50 °C oven. Between 2–5 cc ($\sim$ 39 grams) of sediment were processed for dinoflagellate cyst (herein referred to as dinocyst) analysis. The treatment followed the protocol of *de Vernal et al.* [1996]. Due to high quantities of silicate in the samples the second hydrofluoric acid treatment was left overnight. After mounting remaining material on slides, dinocyst assemblages, pollen, spores, foraminiferal linings and reworked palynomorphs were counted. During sample processing, where possible, at least 150 Lycopodium spores were counted per slide to assess palynomorph concentration (specimens per gram sediment).

4.2.4 Foraminiferal analysis

Samples from the working half of the core were immediately frozen and subsequently freeze dried. Between 5–10 grams of sediment was wet sieved over a 63 µm sieve. This fraction was then oven-dried at $\sim$50 °C for 24 hours or until completely dry. Subsequently the <63 µm fraction was dry-sieved over a 150 µm mesh. Planktonic and benthic foraminifera were picked from the >150 µm fraction and counted. In a subset of samples foraminifera in the 63–150 µm fraction were also counted. Foraminifer abundances are presented here as both foraminifera per gram sediment and planktonic (PFAR) or benthic (BFAR) accumulation rates (fluxes). This corrects for the highly variable sedimentation rate down core (Fig. 4.2). Benthic foraminifera species were identified and counted.

4.2.5 Multivariate statistics

Multivariate statistical analysis was performed on the benthic assemblage dataset. Only samples were benthic foraminifera counts were >40 specimens (in both size fractions combined) were included. Correspondence analysis (CA) was used to confirm visual inspection of the benthic foraminifera assemblage data into 'zones'. CA was carried out using the program PAST [*Hammer et al.*, 2001].

4.2.6 Stable isotope analysis

Both planktonic and benthic foraminifera were analysed for oxygen and carbon stable isotopes. The only planktonic foraminifera found were the polar species *Neogloboquadrina pachyderma* (sinistral) and isotope measurements were carried out on samples containing between 11–64 individuals (denoted Npl). A total of 35 planktonic foraminiferal samples were measured. Stable isotope measurements on benthic foraminifera were dependent on the abundance of various species at different intervals. Each sample contained between 11 and 82 specimens of the same species and, where possible, a replicate measurement on a second species was conducted. A total of 32 benthic foraminiferal samples were measured on various species, see Fig. 4.7 for details. Samples were measured on a Finnigan MAT 251 gas isotope ratio mass spectrometer connected to a Kiel 1 automated carbonate preparation device at MARUM, University of Bremen. The instrument was calibrated against the house standard (ground Solnhofen limestone), which in turn was calibrated against the NBS 19 standard reference material. Over the measurement period the standard deviations of the house standard were 0.03 ‰ for δ^{13}Cand 0.06 ‰ for δ^{18}O. Results are presented relative to the Vienna Pee Dee Belemnite (VPDB) using the conventional δ-per-mil notation.

4.3 Results

4.3.1 Chronology

Results of the Bayesian age modelling in the BACON program indicate that the radiocarbon dated interval of core SL 170 (24–636 cm) cover the period ∼10.22–16.99 kyr BP (Fig. 4.2). According to CT and linescan images there are no hiatuses in this core. Sedimentation rates vary between 52.5 to 227 cm kyr^{-1}. The first increase in sedimentation rate is ∼14.2 kyr BP but highest sedimentation rates occur between 13.3 and 11.7 kyr BP. Increases in sedimentation rates are concurrent with increased Ca/Sr ra-

tios, associated with increased detrital input from northern Baffin Bay. These two events (BBDC 1 and 0) occur ∼14.2–13.7 kyr BP and ∼12.7–11 kyr BP respectively.

For more detail about the chronology and age modelling uncertainties, as well as physical sediment properties and geochemical analysis the reader is referred to *Jackson et al.* [2017].

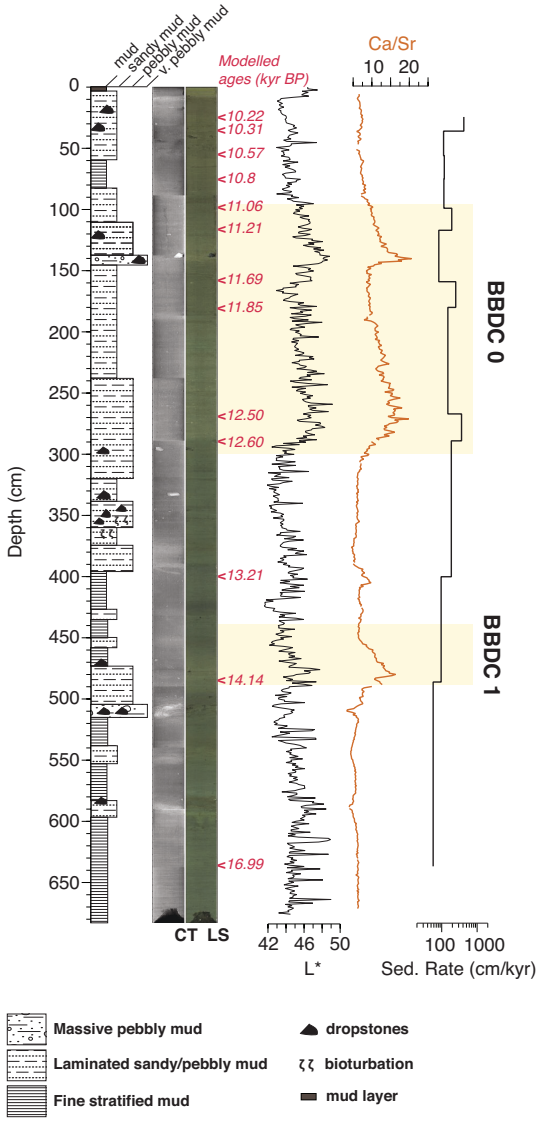

Figure 4.2: Chronology and lithostratigraphy for core SL 170. Computerised tomography (CT) and colour linescan images (LS) are shown as well as sediment lightness (L*) measurements. Lithofacies are defined from CT, LS images and visual inspection of the core. The modelled ages, based on 18 ^{14}C dates are shown in red. Sedimentation rate (shown here on a log scale) was calculated between each dated interval. Computerised tomography (CT) and colour linescan images (LS) are shown as well as sediment lightness (L*) measurements. The Ca/Sr ratio down-core is shown in orange and BBDC events are shown by yellow shading.

4.3.2 Surface ocean conditions: palynomorph analysis

Pollen and spores are rare throughout the core the lower section of the core, but increase sharply at 14.9 kyr BP to concentrations ∼3116 per gram (Fig. 4.3). From then on, pollen and spore abundance remains between 166 and 1655 per gram, but generally decreases up-core. Foraminiferal linings vary between 0 and 1230 per gram. Concentrations are stable and low until ∼10.6kyr BP(early Holocene) when they increase. The concentration of reworked palynomorphs peaks between 15–14.8, 13.9–13.6, ∼13.1 and 10.6–10.3 kyr BP with values >300 per gram.

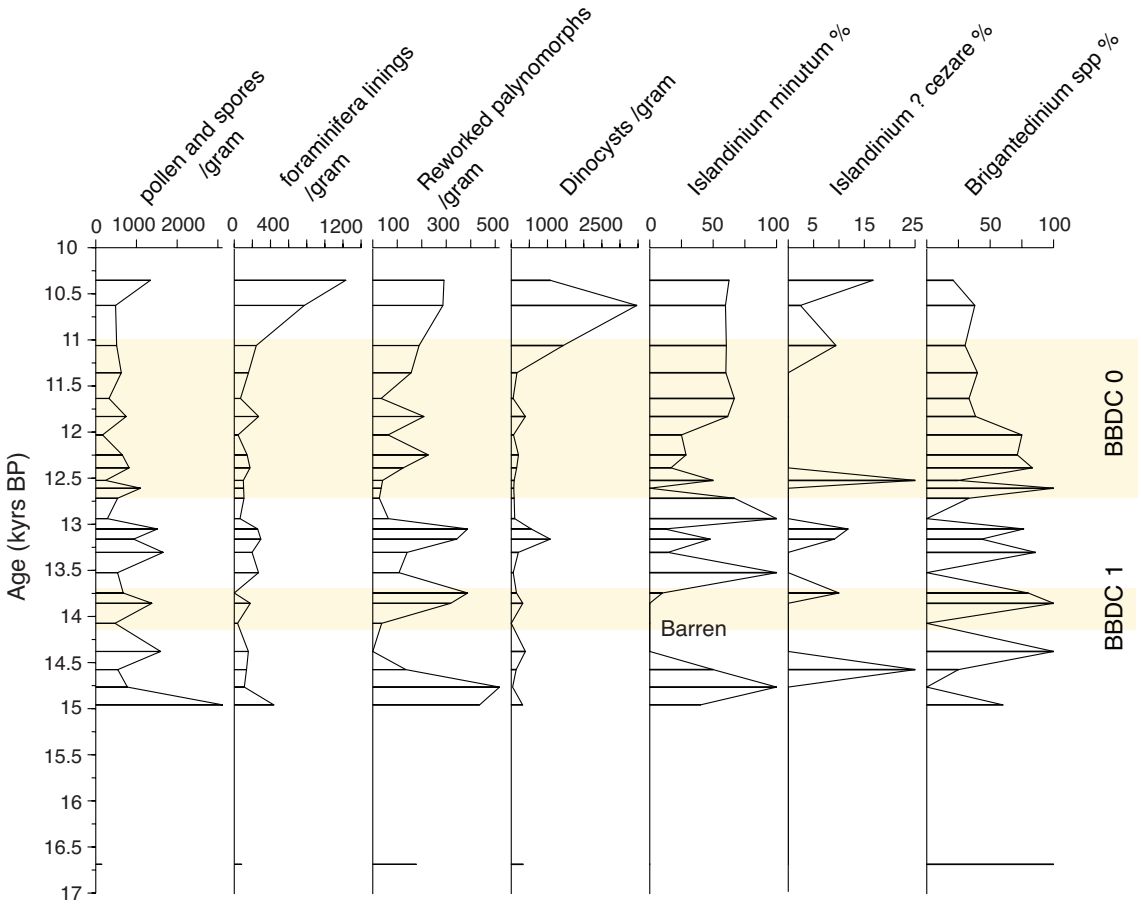

Figure 4.3: Palynomorphs in core SL 170. (From left to right) Pollen, foraminiferal linings, reworked palynomorphs and dinocysts per gram sediment. Dinocyst assemblages contained only 2 main species whose relative abundances are shown (%): *Islandinium minutum*, *Islandinium? cezare* and *Brigantedinium spp*. BBDC intervals are shaded in yellow.

Dinocyst abundance remains low throughout the lower section of the core (<500 per gram), with the exception of a peak ∼13.1 kyr BP of 1077 cyst per gram and increased concentration of up to 3456 cysts/g between 11 and 10.3 kyr BP (early Holocene). In all samples the assemblage was comprised entirely of the heterotrophic species *Islandinium minutum*, *Brigantedinium spp*. and to a lesser extent *Islandinium? cezare* (Fig. 4.3).

4.3.3 Sub-surface ocean conditions: planktonic foraminifer abundance and stable isotopes

Planktonic foraminiferal abundance (per gram sediment) is higher in the lower sections of the core, averaging values of between 0 and 30 foraminifera/gram during the Heinrich 1 stadial and the Bølling interstadial (17–13.7 kyr BP), with the exception of a peak of ∼220 foraminifera/g at ∼16 kyr BP (Fig. 4.4). From 13.7 kyr BP onwards, planktonic foraminifera are less abundant, with values between 0 and 10 foraminifera/g. Abundance is similar in both the finer (63–150 µm) and coarser (>150 µm) fractions. When this abundance is corrected for changes in sedimentation rate (becoming accumulation rate, Fig. 4.4) the whole core average is 319 $cm^2\,kyr^{-1}$ (foraminifera per cm^2 per 1000 yr) in the fraction (>150 µm) and 82 $cm^2\,kyr^{-1}$ in the finer (63–150 µm) fraction. PFAR peaks at ∼16 kyr BP (>150 µm = 6808 $cm^2\,kyr^{-1}$). There is a general decrease in PFAR from∼14–11.5 kyr BP when PFAR increases again during the early Holocene.

4.3.4 Bottom water conditions: benthic foraminifer abundance, assemblages and stable isotopes

A total of 13 calcareous benthic foraminifera species were identified in SL 170, from a total of 41 samples in which both the finer (63–150 µm) and coarser (>150 µm) fraction were counted. These species and a summary of their environmental preferences are shown in Table 4.1. These species are part of common assemblages found in the Baffin Bay [*Lloyd*, 2006; *Perner et al.*, 2011, 2013; *Seidenkrantz et al.*, 2013]. No agglutinated benthic foraminifera were found in the core, with the exception of two specimens in the top 2 cm (undated) of the core.

The total benthic faunal assemblage is dominated by *Cassidulina neoteretis* (0–91%), *Cassidulina reniforme* (0.1–60%), *Elphidium excavatum* (0–57%) and *Islandiella norcrossi* (0–78%), with the additional occurrence of *Melonis barleeanus* (up to 25%) and *Astrononion gallowayi* (up to 29%) (Fig. 4.5). Species that account for less than 5% of the total faunal assemblages are not shown here. The full dataset will be available online via the PANGEA database.

The benthic assemblage record was divided into benthic assemblage zones downcore, based on a combination of visual inspection of the relative abundance of different species (Fig. 4.5). Correspondence analysis confirmed that the 3 different benthic assemblage zones were correctly identified (Fig. 4.6).

The period 17 14kyr BP is defined as Zone FA. The lowest section of the core, representing 17 15 7kyr BP, is characterised by high percentages of *A. gallowayi* (10–30%),

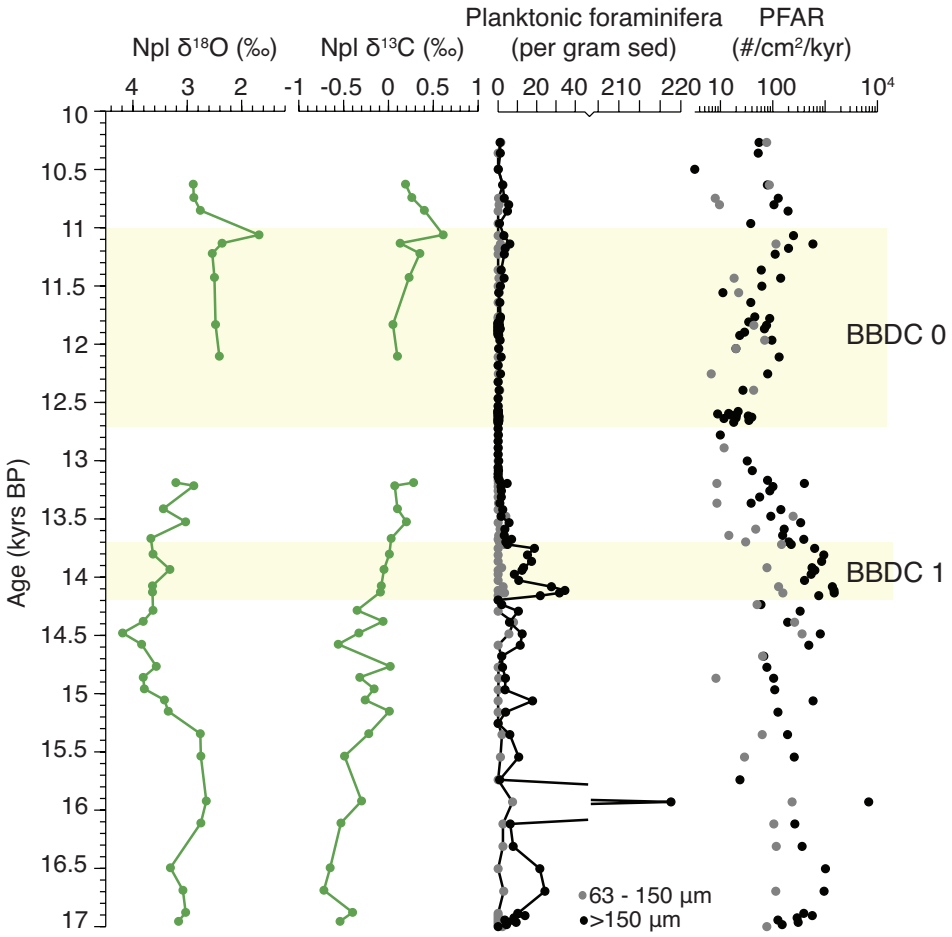

Figure 4.4: Sub-surface ocean conditions indicated by planktonic (Npl) stable isotopes δ^{18}O and δ^{13}C (green). Planktonic foraminifera per gram sediment was calculated at processed intervals throughout the core. Owing to high numbers of foraminifera per gram sediment ~16 kyr BP, data is shown on a broken axis. Planktonic foraminifera accumulation rate (PFAR) was also calculated to account for large changes in sedimentation rate. Planktonic foraminifera per gram sediment and PFAR were calculated in both the finer (63–150 µm) and coarse (>150 µm) sediment fractions. BBDC intervals are shaded in yellow.

M. barleeanus (20–29%) and *C. lobatulus* (9%) (Fig. 4.5). Following this, there is an increasing presence of *E. clavatum* (up to 60%) and constant presence of *C. reniforme* (up to 60%). Zone FA is characterised by CA Axis 1 scores between 1 and -0.3 (Fig. 4.6).

The period from 14 ~11.6kyr BP is defined as Zone FB and is the characterised in the beginning by the dominance of *C. neoteretis*(41–91%) and decreased percentage (<10%) of *E. clavatum* and *I. helenae*. From 12.9 to 11.6 kyr BP the percentage of *C. neoteretis* decreases to <50%, while *E. clavatum* accounts for up to 40%. *S. concava* and *I. helenae* account for a small proportion of these assemblages ≤ 16%. There is a constant presence of *C. reniforme* (10–23%) and near absence of *A. gallowayi*, *N. labradorica*, *M. barleeanus* and *C. lobatulus*. Zone FB is characterised by more strongly negative scores on Axis 1 (-1.6–0.4) and Axis 2 scores between 0.4 and -0.4 (Fig. 4.6).

Table 4.1: Benthic foraminifera species found in core SL 170 (this study) and their environmental preferences.

Species	Environmental Preferences	Reference
Astrononion gallowayi	Epifaunal, high energy environments (strong currents)	Loeblich and Tappan, 1953 [*Rytter et al.*, 2002]
Cassidulina neoteretis	Infaunal, warm, Atlantic waters, seasonal sea ice cover	*Seidenkrantz* [1995], [*Jennings and Helgadottir*, 1994; *Seidenkrantz*, 1995; *Jennings and Weiner*, 1996]
Cassidulina reniforme	Infaunal, Atlantic water, glacial meltwater, seasonal sea ice cover	Nørvang, 1945 [*Vilks*, 1981; *Mackensen et al.*, 1985; *Hald and Korsun*, 1997; *Korsun and Hald*, 2000]
Cibicides lobatulus	Epifaunal/infaunal, warm, low salinity, high energy environments (strong currents)	Walker and Jacob, 1798 [*Hald and Korsun*, 1997; *Polyak and Solheim*, 1994]
Elphidium clavatum	Epifaunal, colder polar waters, meltwater and low salinities, proximal glaciomarine conditions	Cushman, 1930 [*Vilks*, 1981; *Jennings and Helgadottir*, 1994; *Hald and Korsun*, 1997; *Korsun and Hald*, 2000]
Islandiella helenae	Infaunal, cold polar waters, seasonal sea ice and productivity	Feyling-Hanssen and Buzas, 1976 [*Polyak and Solheim*, 1994]
Islandiella norcrossi	Infaunal, chilled Atlantic-type waters	Nørvang, 1945 [*Lloyd*, 2006]
Melonis barleeanus	Intermediate infaunal, warmer waters, productivity	Williamson, 1958 [*Jennings and Helgadottir*, 1994; *Jennings et al.*, 2004]
Nonionellina labradorica	Infaunal, high energy environments, productivity	Dawson, 1860 [*Polyak et al.*, 2002; *Jennings et al.*, 2004]
Pullenia osloensis	warm, Atlantic waters, productivity	Feyling-Hanssen, 1954 [*Lloyd et al.*, 2011]
Stainforthia concava	Infaunal, productivity, cold polar waters	Höglund, 1947 [*Jennings et al.*, 2004]
Stetsonia horvathi	sea ice cover, productivity	Green, 1959 [*Lagoe*, 1977]

From ∼11.6 kyr BP onwards, Zone FC, there is a continuous presence of *C. neoteretis* (3–50%) and *C. reniforme* (1–17%) and a peak in the percentage of *S. concava* at ∼11.4 kyr BP (18%). There is an increasing dominance of *I. norcrossi* (45–79%) and the recurrence of N. labradorica (11.5 kyr BP) and *M. barleeanus* (11 kyr BPonwards) (Fig. 4.5). Zone FC is characterised by CA Axis 1 scores between 0.4 and -0.4 and Axis 2 scores <0.2 (Fig. 4.6).

Benthic foraminifera per gram sediment remains lower than 45 foraminifera/g through-

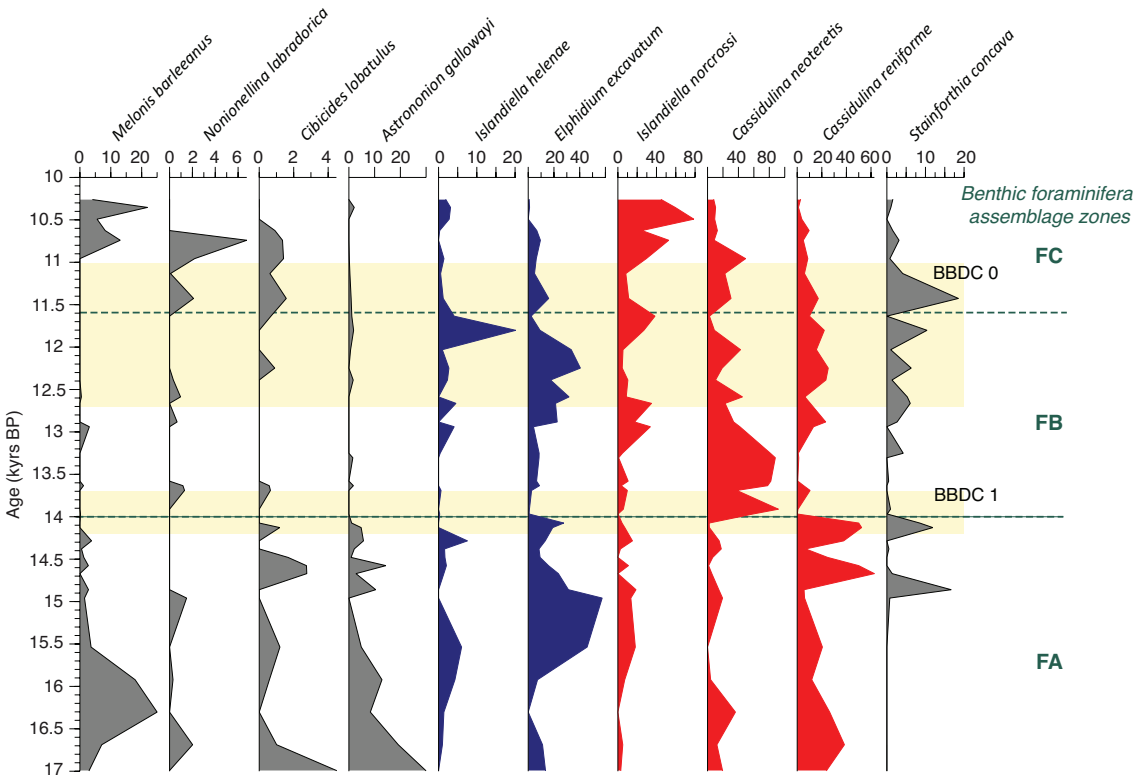

Figure 4.5: Benthic foraminifera assemblages shown against age for core SL 170. Species indicative of warmer and more saline Atlantic-type water are shaded red; those associated with Arctic-type (colder and fresher) water are shaded blue following previous studies in Baffin Bay [*Perner et al.*, 2013; *Seidenkrantz et al.*, 2013]. Benthic assemblage zones (F) are based on visual identification of downcore changes in assemblage characteristics and on correspondence analysis. Species that accounted for less than 5% of the assemblage at all intervals sampled throughout the core are not shown here. BBDC intervals are shaded in yellow.

out most of the core, with the exception of a short ∼200 yr increase to values around 65 foraminifera/g at ∼14 kyr BP (Fig. 4.7). Concentration is also higher (30–40/g) in the later part of the Younger Dryas and early Holocene. Benthic foraminifera accumulation rate (BFAR, Fig. 4.7) is comparable between the different size fractions, with average downcore values of 867 $cm^2\,kyr^{-1}$ (>150 µm) and 968 $cm^2\,kyr^{-1}$ (63–150 µm). BFAR remains low until ∼15.9 kyr BP, when there is a sharp increase to 1175 $cm^2\,kyr^{-1}$ (>150 µm). From 15.9 to ∼14 kyr BP BFAR remains below 1000 $cm^2\,kyr^{-1}$. Subsequently BFAR peaks at the onset of the Younger Dryas (12.7–12.5 kyr BP, ∼3000 $cm^2\,kyr^{-1}$, the end of the Younger Dryas (12–11.8 kyr BP, ∼3000–6470 $cm^2\,kyr^{-1}$) and early Holocene (11.2–10.8 kyr BP, ∼3000–9000 $cm^2\,kyr^{-1}$) in both size fractions. BFAR shows an inverse trend with PFAR.

From 17 to 13.3 kyr BP benthic $\delta^{18}O$ values remain between 4.4 and 3 ‰ (Fig. 4.7). From ∼13.3 kyr BP there is a gradual trend toward lighter values culminating in a period of lighter $\delta^{18}O$ values (3–1.8 ‰) during the Younger Dryas and early Holocene. From ∼11 kyr BP onwards there are constantly heavier values (up to 4.3 ‰). Offset between

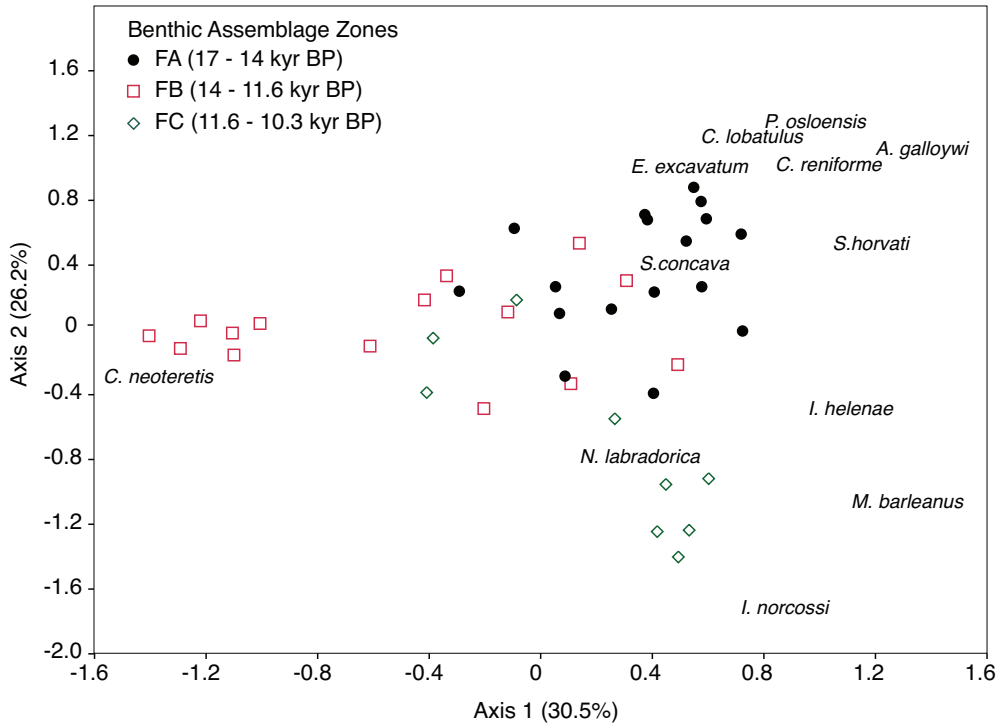

Figure 4.6: Correspondence Analysis cross plot of benthic foraminifera assemblages throughout core SL 170. Data are plotted against Axis 1 (accounting for 30.5% of the variance) and Axis 2 (26.2% of the variance) and where individual species plotted along these axis's is also shown.

replicate δ^{18}O measurements on different species is between -0.67 and 0.97 ‰.

Benthic δ^{13}C values remain $\sim$−1–−2 ‰ during the Heinrich Stadial 1. At $\sim$14.7 kyr BP there is a shift to more enriched δ^{13}C values (−0.01–−0.7 ‰), which continues until $\sim$12.4 kyr BP. From $\sim$12.4–12 kyr BP values are lower ($\sim$−3.5–−2.8 ‰) although we note that these strongly negative values are associated measurements on the species *E. clavatum*. There is currently no correction for stable isotopes measurement on this species. A replicate measurement on shells of *C. neoteretis* at $\sim$12 kyr BP shows less depleted values (−0.75 ‰). From $\sim$11.8 to 10.2 kyr BP, δ^{13}C values vary between -0.22 and 1.37 ‰. The offset between replicate δ^{13}C measurements on different species is lower in sediment of Heinrich Stadial 1 ($<$0.33 ‰) and Holocene ($<$0.6–1.6 ‰) age than during the Younger Dryas (2.7 ‰). Apart from the measurements on *E. clavatum* during the Younger Dryas, benthic δ^{13}C remains roughly stable (0–−1 ‰) from 14.2 kyr BP to 10.3 kyr BP.

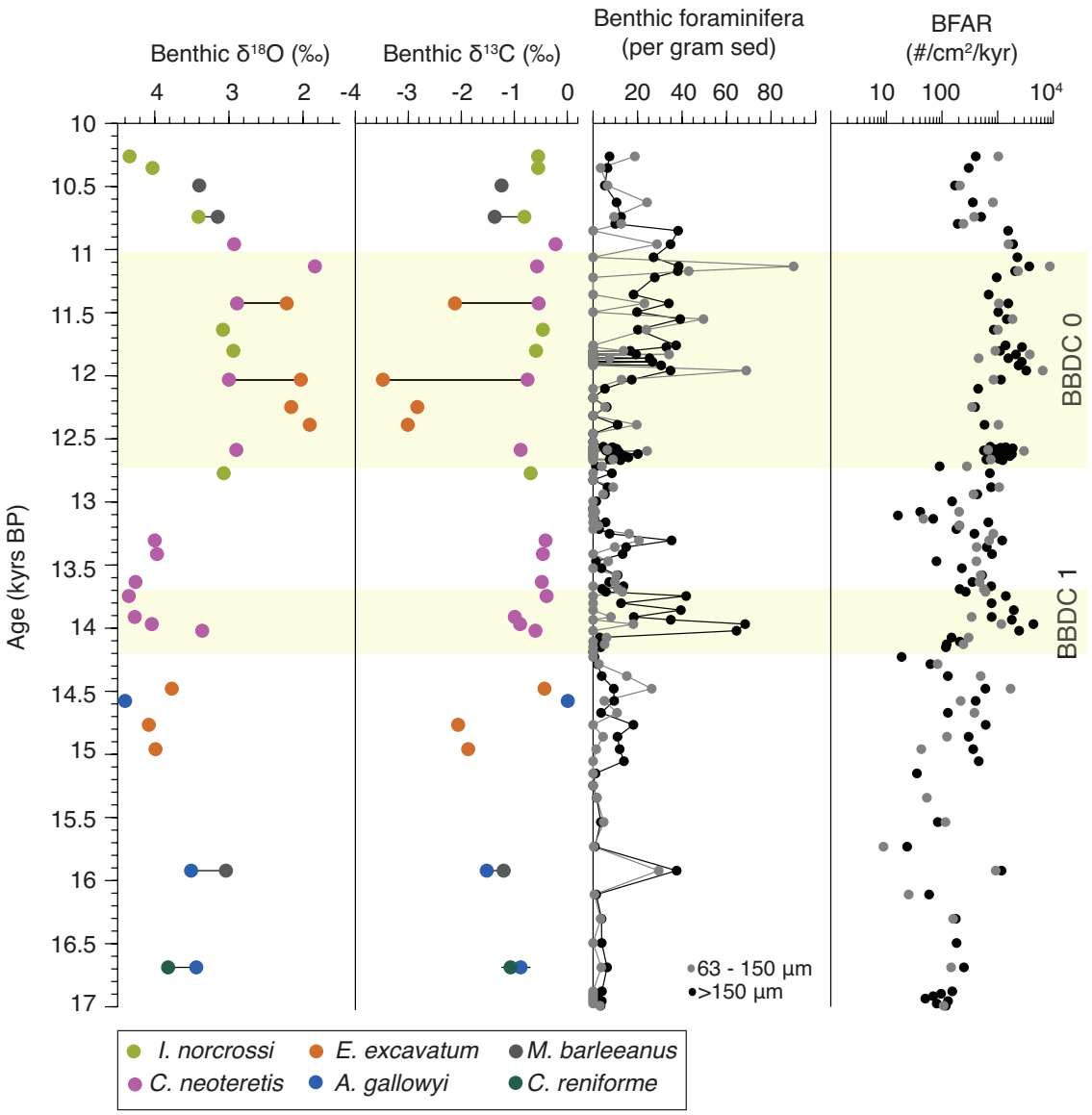

Figure 4.7: Changes in bottom ocean conditions indicated by benthic δ^{18}O and benthic δ^{13}C values from SL 170. Coloured points indicate on which species on stable isotopes analysis was performed. Benthic foraminifera per gram sediment and benthic foraminifera accumulation rate (BFAR) was also calculated to account for large changes in sedimentation rate. Benthic foraminifera per gram sediment and BFAR were calculated in both the finer (63–150 µm) and coarse (>150 µm) sediment fractions. BBDC intervals are shaded in yellow.

4.4 Discussion

4.4.1 Changes in surface conditions during the deglaciation and early Holocene

Dinocyst concentrations and assemblages indicate very little change in surface ocean conditions throughout the deglacial period (~17–11.7 kyr BP). Dinocyst concentrations, with the exception of a peak around 13.5 kyr BP during the Allerød warming (Fig. 4.3),

remain low until ∼11 kyr BP, after the onset of the Holocene. Low concentrations did not permit the use of the modern analogue technique (MAT) [*de Vernal et al.*, 2013a]. However, only two dinocyst taxa were found throughout the core: *Islandinium minutum*, *Brigantedinium spp* and to a lesser extent *Islandinium? cezare*. The quasi exclusive occurrence of these heterotrophic species indicate persistently harsh conditions and dense sea ice cover potentially perennial in nature [*de Vernal et al.*, 1997; *Rochon et al.*, 1999; *de Vernal et al.*, 2001, 2013b] throughout the deglacial and early Holocene in Baffin Bay. Moreover, the taxa present are prone to degradation through oxygenation [*Zonneveld et al.*, 1997]. Hence their presence throughout the core confirms that our assemblage data is not biased by differential preservation and may also suggest a poorly oxygenated environment [*Zonneveld et al.*, 2007].

Records covering longer time scales, i.e. spanning the entire deglaciation, are consistent with our findings. In the north-western Labrador Sea, dinocyst assemblages were composed almost entirely of *Brigantedinium spp*, indicating these dense sea-ice conditions were a regional phenomenon [*Gibb et al.*, 2014]. Furthermore, the section of our record covering the Younger Dryas-Holocene transition is consistent with findings from the nearby Disko Bugt core CC70, where dinocyst concentrations were low and assemblages mostly composed of *Islandinium minutum*, with a reconstructed >50% sea-ice cover for ∼11 months of the year [*Jennings et al.*, 2014] . Increased productivity was documented in this core from ∼11.4 kyr BP based on increasing numbers of dinocysts and foraminiferal linings, a change we also observe in our record (Fig. 4.3). This could indicate a slightly shorter duration a sea-ice cover during the Younger Dryas, allowing a longer time window for increased productivity in the summer months. Dinocyst concentration and foraminiferal linings reach their maximum after between 11 and 10.3 kyr BP in our record and this is perhaps a response to more open and productive conditions in the region, tracing the landward retreat of central west Greenland ice streams [*Kelley et al.*, 2015, 2013; *Young et al.*, 2013]. The breakup of perennial sea ice began only after ∼9.5 kyr BP in Disko Bugt area [*Jennings et al.*, 2014; *Gibb et al.*, 2015] and is thus not captured in the record presented here.

4.4.2 Sub-surface conditions in Baffin Bay: a regional δ^{18}O signal?

The SL 170 Npl δ^{18}O record shows a deglacial trend through to the early Holocene (Fig. 4.4), a trend which compares with other records in the region such as those from the Labrador Sea [*Gibb et al.*, 2014] and SW Greenland [*Knutz et al.*, 2011] (Fig. 4.8). The light Npl δ^{18}O values recorded during the latter part of Heinrich stadial 1 suggests either subsurface dilution by meltwater or the formation of sea ice and expulsion of

isotopically light brines [*Hillaire-Marcel and de Vernal*, 2008]. The near-continuous sea ice cover suggested by the dinocyst assemblages [*de Vernal et al.*, 1997, 2013b, 2001; *Rochon et al.*, 1999] as well as the generally cold conditions recorded during the stadial period supports the latter. The scarcity of planktonic foraminifera between 13.2 and 12.2 kyr BP is a feature also seen nearby Disko Bugt trough mouth core [*Jennings et al.*, 2017] and northwest Labrador Sea [*Gibb et al.*, 2014], which we attribute here to a dilution of by a large input of detrital material (Fig. 4.2). A trend toward lightest values at 11 kyr BP does not indicate any major meltwater and/or sea ice formation events but rather the continued presence, to some extent of one or the other. A shift to Npl δ^{18}O values of $\sim$1 ‰ at 11 kyr BP is although more likely related to meltwater from the Greenland Ice Sheet as it retreated into nearby Disko Bugt following the onset of warmer Holocene conditions [*Ò Cofaigh et al.*, 2013; *Ó Cofaigh et al.*, 2013; *Jennings et al.*, 2014]. As this is one data point however, we treat its interpretation with caution.

The sub-surface conditions are problematic to reconstruct from the Npl δ^{18}O signal. Consistently light values in high latitude records could be a response to either subsurface dilution by (fresh) meltwater or by the production of sea ice and associated expulsion of isotopically light brines to the subsurface living habitat of *N. pachyderma* sinistral [*Hillaire-Marcel and de Vernal*, 2008]. Both of these mechanisms could shift the depth at which *N. pachyderma* live and calcify. Preferring salinities $>$34 PSU [*Hilbrecht*, 1996], meltwater release could effectively drive the prefered living habitat of *N. pachyderma* (sin) deeper, once again complicating the interpretation of the δ^{18}O signal. Furthermore, we lack an independent proxy for temperature of sub-surface waters. If the habitat of *N. pachyderma* (sin) remains between $\sim$150–300m, the Npl δ^{18}O should capture changes in the influx of sub-surface water from the Atlantic. To evaluate if this water mass is the same as that along the path of the EGC/IC, WGC and BIC/LC (Fig. 4.1) we compare our record with that from other sites to see if the Npl δ^{18}O signal is a regional or local signal.

Comparing the Npl δ^{18}O signal here with the regional signal it appears that there is very little modification of this water mass along its path from east to western Greenland, throughout Baffin Bay and subsequently into the Labrador Sea. Early deglacial (17–15 kyr BP) values from the Kangerlussuaq Trough on the south east coast of Greenland *Jennings et al.* [2006] and off the south coast of Greenland [*Knutz et al.*, 2011] vary between 2 and 3 ‰ (Fig. 4.8). In SL 170 values are similar, although we do not capture the depletion of 0.5 ‰ seen in nearby core VC 29 [*Jennings et al.*, 2017]. From then on the general trend toward isotopically lighter values is seen in all records. After 13.5 kyr BP and into the Younger Dryas, two further depletion 'spikes' are seen in the Kangerlussuaq Trough records ($\sim$13.4 kyr BP and $\sim$12.2 kyr BP) and Npl δ^{18}O values $\sim$2 ‰ at $\sim$13–12.5 ‰ off southern Greenland were attributed to meltwater input from the retreating

GIS under the influence of increased Irminger Current influence [*Jennings et al.*, 2006; *Knutz et al.*, 2011]. The absence of these peaks in both the Baffin Bay records (SL 170 and VC29) are likely due to a lack of data for this interval; but we also note that these event are not seen in the Labrador Sea (Fig. 4.8) [*Gibb et al.*, 2014].

Npl δ^{18}O values in the latter part of the Younger Dryas are consistent in all Baffin Bay records, even northernmost Baffin Bay (Fig. 4.8) [*Knudsen et al.*, 2008]. This supports the incursion of a similar sub-surface or intermediate water mass, by the end of the Younger Dryas and values ∼2 ‰ suggest either some meltwater input or the formation of sea ice along the entire coast of West Greenland. All other cores where data is available (Kangerlussuaq Trough, northern Baffin Bay and Labrador Sea) Npl δ^{18}O remain ∼3 ‰. The somewhat delayed signal of lighter isotopic values seen in central Baffin Bay (vs. East and south Greenland) is supported by evidence that the GIS was retreating earlier along its eastern and southern margins than along the west coast [*Sinclair et al.*, 2016]. The isotopically light signal in SL 170 and VC 29 is most likely due to the retreat continued retreat of the nearby Jakobshaven Isbrae into the early Holocene [*Ò Cofaigh et al.*, 2013; *Jennings et al.*, 2014]

From this comparison we suggest that the water masses forming the WGC remained relatively stable throughout the deglacial and the signal of this water mass is seen not only throughout Baffin Bay but is also highly comparable with that from the Labrador Sea.

4.4.3 Changes in deeper waters throughout the deglaciation and early Holocene

Early deglacial period (17 to ∼14.1 kyr BP)

Benthic foraminifera assemblages (Zone FA) are composed of the species *M. barleeanus*, *A. gallowyi* and *E. clavatum* suggest that deep waters in Baffin Bay were cool, somewhat productive and there was potentially strong currents (Table 4.1). The continual presence of *C. neoteretis* suggests some influx of Atlantic source water reached the depth of the study site. From 14.6–14.1 kyr BP the dominance of *C. reniforme* suggests an increasingly glaciomarine (and potentially saline) environment, most likely the influence of enhanced break-up of the marine terminating GIS in the nearby Disko Bugt. Similar assemblages were found in nearby core VC 29 [*Jennings et al.*, 2017]. During this stadial and the early Bølling warming benthic δ^{18}O values remain between ∼2–3.5 ‰ (Fig. 4.9), indicating relatively cool bottom ocean conditions in Baffin Bay. There is a small shift at ∼14.7 kyr BP to lighter isotopic values which could indicate a freshening of bottom waters.

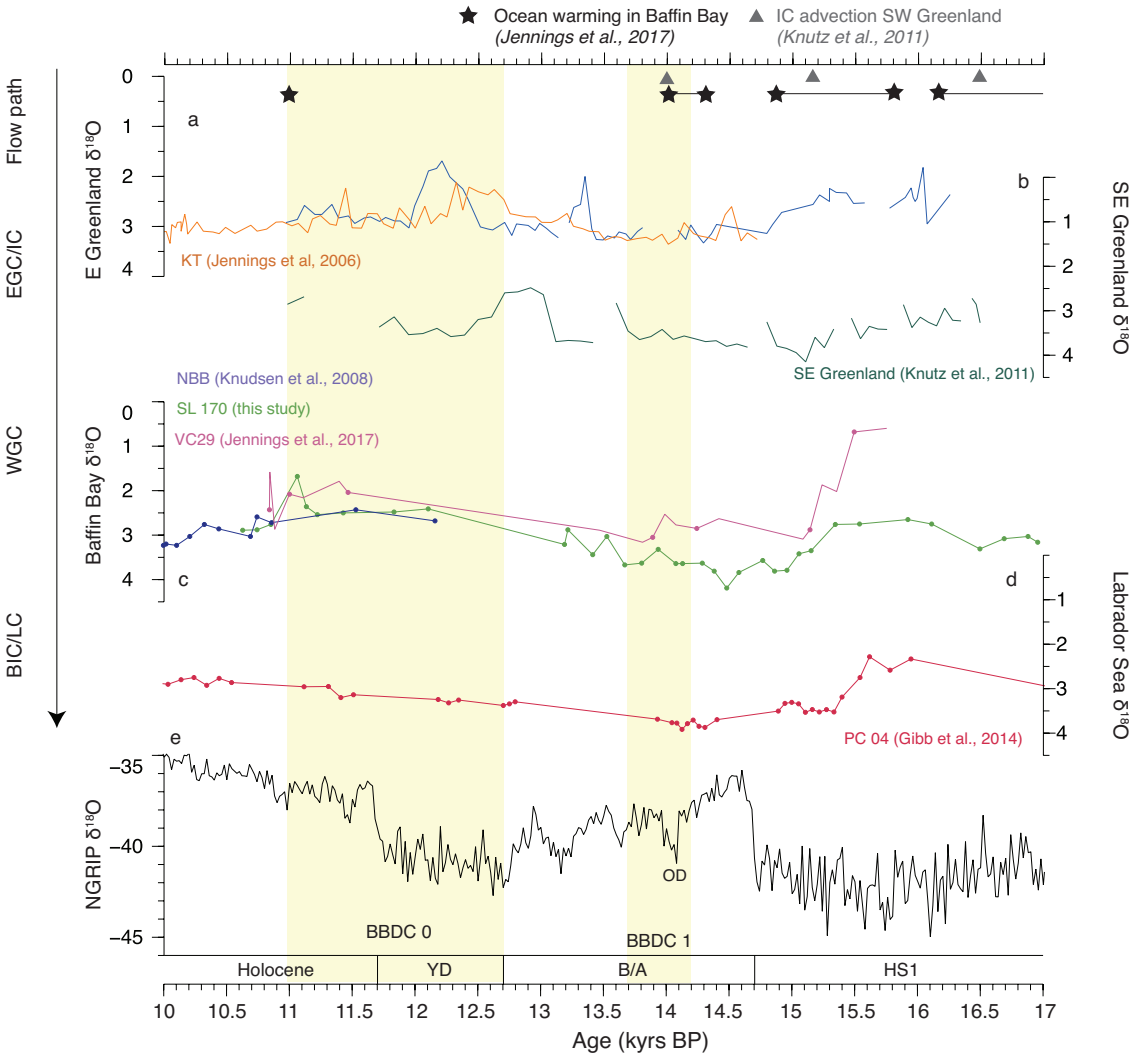

Figure 4.8: Compilation of Npl δ^{18}O from the Greenland margins and Labrador Sea. The Npl δ^{18}O record from core SL 170 (this study, c) is compared with records along the path of the East Greenland Current (EGC) and Irminger Current (IC) from the Kangerlussuaq Trough (a) [*Jennings et al.*, 2006] and off the southeast coast of Greenland (b) [*Knutz et al.*, 2011]. The record from SL 170 is compared directly with a shorter record from northern Baffin Bay (c) [*Knudsen et al.*, 2008], further downstream of the West Greenland Current (WGC). The Npl δ^{18}O from core PC04 in the Labrador Sea captures the outflowing Baffin Island Current (BIC) and Labrador Current (LC) (d) [*Gibb et al.*, 2014]. For comparison, all Npl δ^{18}O records are shown on the same scale. Deglacial and early Holocene climatic changes are depicted by the NGRIP δ^{18}O record (e) *Rasmussen et al.* [2006] with stadial and interstadial periods shown. Symbols (top) indicate periods of warming noted in the Disko Bugt area [*Jennings et al.*, 2017] and periods of Irminger current (IC) advection noted from south Greenland [*Knutz et al.*, 2011]. BBDC intervals are shaded in yellow.

Benthic foraminifera accumulation rates (BFAR) are often used as a proxy for productivity. However, we interpret this signal with caution in the earlier part of the record (∼17–14.1 kyr BP). The high planktonic/benthic ratio (Fig. 4.9) and high planktonic foraminifera accumaultion rate (PFAR) during this period suggests that instead of BFAR

being limited by productivity (i.e food availability), it is instead a key indication of preservation and thus bottom water ventilation. The modern ratio of benthic to planktonic foraminifera in Baffin Bay is 10 or lower (or planktonic/benthic ratio of 0.1 or lower) [*Aksu*, 1983], owing to preferential dissolution of planktonic foraminifera [*Berger*, 1970] as well as organic matter availability at depth. The period 17–14.2 kyr BP, where planktonic/benthic ratios are between ∼0.6 and ∼9, is therefore anomalous. This could suggest the presence of relatively well-ventilated bottom waters that, depleted in carbon, prompted widespread carbonate dissolution at the water/sediment interface. We do not observe high abundances of formainiferal linings that would support this [*de Vernal et al.*, 1992]. However the presence of the benthic species *A. gallowayi* and *C. lobatulus* is indicative of strong bottom currents. These assemblages coupled a) the presence of *M. barleeanus*, indicative of a good food supply and b) relatively high planktonic foraminifer accumulation rate (PFAR; Fig. 4.4) support better ventilation and thus preservation of planktonic foraminifera during the Heinrich 1 stadial.

Bølling /Allerød–Younger Dryas transition to the onset of the Holocene (∼14–11.6 kyr BP)

The transition to benthic foraminifera assemblage zone FB indicates a major change in deep-water conditions at ∼14 kyr BP (Fig. 4.5 and Fig. 4.9). During this period the assemblage is almost entirely dominated by *C. neotertis*, a species associated with Atlantic-type water [*Seidenkrantz*, 1995]. The dominance of this species at ∼14 kyr is also noted in nearby cores VC29 and 12PC in the northern Disko Trough Mouth Fan [*Jennings et al.*, 2017], as well as further north in the Uummannaq Trough area [*Sheldon et al.*, 2016; *Jennings et al.*, 2017]. Although this species is present throughout core SL 170, its dominance here indicates that by this time there was a stronger influx of warmer Atlantic water via the WGC off the central west Greenland margin. The shift toward planktonic/benthic ratios consistently <1 for the remainder of the record is concomitant with the major change in benthic assemblage at the boundary of zones FA and FB. This points to a major reorganisation or change in bottom water conditions around this time in Baffin Bay, representing the point at which the water column becomes more stratified and thus sub-surface and deeper waters are no longer well connected, similar to the current state of the water column in Baffin Bay [*Tang et al.*, 2004]. The latter part of this zone (∼13–11.6 kyr BP) is characterised by CA Axis 1 scores ∼0, a diminished presence of *C. neotertis* and increase in *E. clavatum* indicating a cooling and more glacio-marine conditions into and over the early part of the Younger Dryas stadial.

The Younger Dryas stadial (12.7–11.7 kyr BP) is characterised by a persistent trend to isotopically lighter benthic δ^{18}O values, although we treat extremely lighter values of

$\sim$1.7 ‰ at the beginning of the Younger Dryas with caution; there seems to be a persistent offset during this time between the epifaunal species *E. clavatum* and measurements from the infaunal species *I. norcrossi* and *C. neotertis* around the same time (Fig. 4.7 and Fig. S4.2). Planktonic/benthic ratio decreases throughout the Allerød interstadial and by the onset of the Younger Dryas are very low, indicating poor preservation. However it appears that productivity was not limited during the Younger Dryas; increased benthic foraminifera abundance and accumulation rates and the appearance of the productivity indicator *S. concava* suggest food availability. If the Younger Dryas was characterised by increased ice rafting, as seen in the sediment record [*Jackson et al.*, 2017], this would allow for more frequently 'open' or ice margin setting and higher seasonal productivity, allowing the benthic community to thrive.

The early Holocene ($\sim$11.6–10 kyr BP)

Following the onset of the Holocene, 11.6 kyr BP marks the boundary of benthic foraminifera assemblage zone FC and more diverse benthic assemblages. Deeper waters in Baffin Bay appear to become more productive, with further increases in the presence of *S. concava* and *N. labradorica*. This change is possibly linked to changes in the subsurface ocean; there is a more or less concurrent increase in dinocyst concentrations and in the PFAR. Lower percentages of cold polar water species *E. clavatum* and *I. helenae* and increased proportion of the Atlantic water species *C. neoteretis* indicate a continual presence of the warmer WGC. From 11 kyr BP onwards, CA Axis 1 and Axis 2 scores diverge with strong negative scores on Axis 2 (-1.3). The dominance of *I. norcrossi* in these early stages of the Holocene could indicate a strong influx of the WGC. Similar benthic assemblages found in the early Holocene in northernmost Baffin Bay [*Knudsen et al.*, 2008] support a well-established and strong WGC that could penetrate far north by this time. However the dominance of *I. norcrossi* in the early Holocene, in contrast with the dominance of *C. neotertis* in the Bølling /Allerød, might suggest that the WGC was somewhat more chilled in the early Holocene, in contrast to the characteristics of WGC inflow during the Bølling /Allerød. A change in the characteristics of this water mass is supported by a shift toward heavier benthic δ^{18}O values. We also note exceptionally poor preservation of both planktonic and benthic foraminifera from this interval (25 cm downcore) to the core top, which prevented radiocarbon dating. We tentatively interpret this as the onset of water mass characteristics that lead to extensive carbonate dissolution in deeper Baffin Bay [*Aksu*, 1983]. Although the Nares Strait was not fully open by this time [*Knudsen et al.*, 2008], the presence of the detrital carbonate at our core site indicates a retreat of the ice sheets surrounding northern Baffin Bay (i.e north eastern Laurentide and Innuitian ice sheets). It is through these Canadian Arctic Archipelago conduits that low saturation state water reaches Baffin Bay, leading

to extensive carbonate dissolution in the present day [*Azetsu-Scott et al.*, 2010]. The increasing concentration of foraminifera linings (vs. decreasing foraminifera abundance) certainly supports increased carbonate dissolution from ∼11 kyr BP onward at the study site [*de Vernal et al.*, 1992].

4.4.4 Relationship between ice sheet instabilities (BBDCs) and paleoceonographic changes

Combining the radiocarbon-dated sedimentological record of detrital delivery from ice sheets with a suite of micropaleontological proxies allows us to evaluate the interactions and phase relationships between ice sheet instabilities and oceanic conditions during the last deglaciation and early Holocene. There is still on-going debate as to whether such ice sheet discharge events were a trigger [*Broecker*, 1994] or product [*Bond et al.*, 1993] of abrupt climate change. Baffin Bay Detrital Carbonate Event (BBDC) layers already identified in this core [*Jackson et al.*, 2017], others in the Disko Bugt area [*Jennings et al.*, 2014, 2017] and as far south as the Labrador Sea [*Andrews et al.*, 2014] record ice-rafting and melting events from both the nearby Greenland Ice Sheet and northern Baffin Bay, the latter from where carbonate- (dolomite-) rich material is transported south via the Baffin Island Current. Previous work summarised that the disintegration of the marine terminating portions of these ice sheets was likely triggered by an increasingly strong and warm WGC [*Aksu and Piper*, 1987; *Hiscott et al.*, 1989; *Andrews et al.*, 1998; *Jennings et al.*, 2014, 2017]. We focus on the onset these two radiocarbon-dated events with our co-registered record of both surface/sub-surface and deeper water conditions to in order to evaluate the possible role of changing oceanographic conditions as a trigger for these events.

BBDC 1 (14.2–13.7 kyr BP)

The onset of Baffin Bay Detrital Carbonate Event 1 (BBDC 1) at ∼14.2 kyr BP is marked by two-fold increase in sedimentation rate (Fig. 4.2) and contains detrital carbonate originating from northern Baffin Bay (North American-Arctic ice sheets) and a synchronous sediment input from the nearby Greenland Ice Sheet [*Jackson et al.*, 2017]. Its timing is consistent with other layers with similar characteristics in the area [*Sheldon et al.*, 2016; *Jennings et al.*, 2017]. However, its occurrence is seemingly anomalous, in that it a) post-dates Heinrich Event 1 as seen in the North Atlantic and b) occurs during the Bølling warming, unlike 'classic' ice-rafting events that occurs during stadial periods [*Jackson et al.*, 2017].

Our Npl δ^{18}O shows little change at the onset of this event and records from further

down-stream of the WGC off the southern tip of Greenland do not indicate increasing Irminger Current advection until ∼14 kyr BP [*Knutz et al.*, 2011]. We argue therefore, that this event is not caused by a dramatic change in sub-surface conditions. According to our record, there is also no change in the benthic realm until after the onset of this event. The major change in species assemblage, namely to transition from benthic foraminifera zone FA to FB, representing the dominance of *C. neoteretis* and increasing influx of Atlantic-type water, occurs ∼200 yrs later than the onset of BBDC 1. Similarly, the change in the planktonic/benthic ratio to values an order of magnitude lower, which we argue indicates a change in bottom water ventilation, occurs at ∼14 kyr BP. This is more than likely related to the advection of Irminger Current noted in off the coast of south-east Greenland [*Knutz et al.*, 2011] and is in keeping with the beginning of a stong influx of the WGC between ∼14.5–14 kyr BP [*Jennings et al.*, 2017].

Prior to the onset of this event, we note an almost coeval shift in benthic δ^{13}C values at ∼14.6 kyr BP from our record with the resumption/increased strength of the Atlantic Meridional Circulation (AMOC), represented by the Pa/Th record in the north Atlantic [*McManus et al.*, 2004] (Fig. 4.9). Many argue that the resumption of the AMOC was coupled with a large release of warmer, deep water [*Thiagarajan et al.*, 2014]. If this increasingly active deep water entered into Baffin Bay over the Davis Strait, it could potentially mix the water column at depth and decrease stratification. A mixing of the water column could prompt melting at the ice-sheet margin as the cold sub-surface water was displaced and cycled through the water column and deeper, warmer waters were released upward. Although we interpret the benthic δ^{18}O records here with caution, we note that the offset between Npl and benthic δ^{18}O values ($\Delta\delta^{18}$O; benthic δ^{18}O–Npl δ^{18}O) during the period ∼14.5–14 kyr BP are slightly negative or very close to 0 (Fig. S4.3), which tentatively supports a more mixed water column. Following this, glacial meltwater from the ice sheet margins during the later part of BBDC 1 would establish the cold and fresh surface layer, providing a layer under which the Atlantic Intermediate water brought in by the WGC could flow, thus capping deeper water layers and slowly decreasing ventilation/ increasing stratification in the water column. A more stratified water column would subsequently lead to less well-ventilated deeper water and thus better preservation of benthic foraminifera, as indicated by both increasing BFAR and decreasing planktonic/benthic ratios to values consistent with the current day situation in Baffin Bay. Correspondence analysis scores (Fig. 4.9) after this point is also more clearly driven by somewhat warmer species often associated with the input of Atlantic water. In this scenario, the destabilisation of the Greenland Ice Sheet margins was not prompted by an increasing WGC, but rather by a large mixing event prompted by the strengthening of the AMOC following the Bølling warming. It is also possible that the release of icebergs and meltwater at the onset of BBDC 1 triggered the changing

oceanic conditions. Baffin Bay was consistently covered with fast sea-ice during the early deglacial, as is shown by the lack of an increased sedimentation rate or change in sediment composition prior to the event (Fig. 4.2) [*Jackson et al.*, 2017] and the dinocyst assemblages presented here. There is evidence for an ever-present but perhaps weaker WGC during the early deglacial from benthic foraminifera assemblages. One scenario could be that the meltwater created from the retreat of the nearby Greenland ice margins, following atmospheric warming during the Bølling interstadial, as well as more distal northern Baffin Bay margins, pushed the warmer and potentially more saline WGC deeper. Following this and the strengthening and greater influx of the WGC ∼14 kyr BP, a thicker Intermediate Atlantic Water layer could have been established in Baffin Bay. However, the plausibility of either of these scenarios would require further investigation.

BBDC 0 (12.7–11 kyr BP)

Baffin Bay Detrital Carbonate Event 0 (BBDC 0) began with the onset of the Younger Dryas stadial. This event was decidedly longer than BBDC 1, lasting until the early Holocene (∼11 kyr BP) [*Jackson et al.*, 2017]. It could be that this event was in fact a response to the colder climatic conditions of the Younger Dryas, as has been suggested for Heinrich events [*Bond et al.*, 1993; *Pearce et al.*, 2013, 2015].

Due to low abundance of planktonic foraminifera, we have no information on the sub-surface conditions at the onset of this event. Recent diatom-based reconstructions of August sea surface temperature do point to warmer than previously thought surface ocean conditions and increased seasonality during the early part of the Younger Dryas stadial [*Oksman et al.*, 2017] the could prompt basal melting and subsequent weakening of the ice-sheet margins. There is strong evidence for rapid advance and retreat of the nearby Jakobshavn Isbrae ice stream during this stadial, mostly via ice calving [*Ò Cofaigh et al.*, 2013; *Ó Cofaigh et al.*, 2013; *Jennings et al.*, 2014; *Jackson et al.*, 2017].

Planktonic/benthic ratios remain low; indicting that poorly ventilated deeper waters were a persistent feature of this event. Deeper waters show general trend toward lighter benthic δ^{18}O, if we disregard the large shift seen in the epifaunal species E. clavatum. Although we note that the increased presence of this species and *C. reniforme* in the lead up to this event could indicate the presence of meltwater and a more glacio-marine setting, replacing the strong WGC signal (dominance of *C. neoteretis*). This is supported by a shift from Correspondence Analysis scores from ∼-1 to 0. Analysis of benthic assemblages from the nearby core VC29 also indicate general trend to cooling deeper ocean conditions in the run up to a detrital carbonate event of similar timing to the BBDC 0 event represented in our core [*Jennings et al.*, 2017]. It appears therefore from

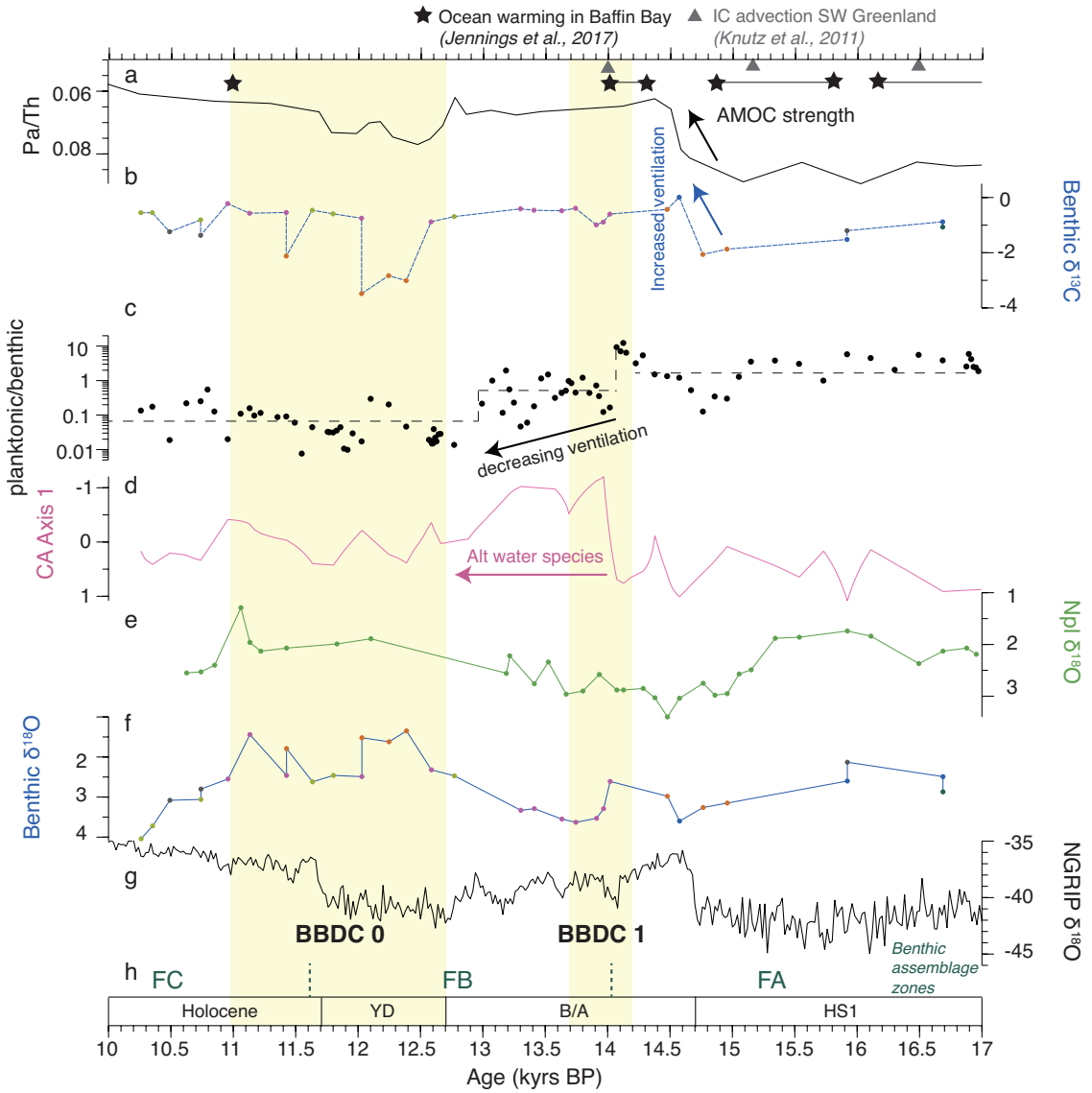

Figure 4.9: BBDC events and the timing of paleoceanographic change in Baffin Bay and wider region. Deglacial and early Holocene climatic temperatures from the North Greenland ice core (NGRIP δ^{18}O, g) from *Rasmussen et al.* [2006] are shown for context. Changes in Npl δ^{18}O show an expected deglacial to Holocene trend (e, this study), while benthic δ^{18}O appears to show a warming during the Younger Dryas stadial (f, this study). Benthic δ^{13}C (b, this study) appears to respond to the strength of the AMOC (a) indicated by the Pa/Th record [*McManus et al.*, 2004]. Planktonic/benthic ratio (c, this study) indicates decreasing ventilation following this and at the same time as the major change influx of benthic species associated with Atlantic water, indicated by Axis 1 of the Correspondence Analysis (d, this study) and the onset of benthic foraminifera zone FB (h). Symbols (top) indicate periods of warming noted in the Disko Bugt area [*Jennings et al.*, 2017] and periods of Irminger current (IC) advection noted from south Greenland [*Knutz et al.*, 2011]. BBDC intervals are shaded in yellow.

our data that BBDC 0 was forced by a combination of evolving (not direct) changes in sub-surface and deep ocean conditions and general climatic conditions. We cannot verify if changing oceanic conditions are a trigger or a response to this period of ice

sheet instability.

4.5 Conclusions

We use a high-resolution, radiocarbon-dated marine sediment core from the margin of west Greenland to reconstruct paleoceanographic conditions in central eastern Baffin Bay throughout the last deglaciation and early Holocene (∼17–10 kyr BP). We assess the timing of changes in surface and sub-surface characteristics, deepwater conditions and ventilation using a range of micropaleontological proxies.

Throughout the deglacial and early Holocene, dinocyst assemblages indicate central eastern Baffin Bay was covered by perennial sea ice. This is in keeping with other Baffin Bay studies and further afield in the Labrador Sea [*Gibb et al.*, 2014; *Jennings et al.*, 2014]. Dinocyst concentrations and the abundance of foraminiferal linings increase only after the onset of the Holocene, perhaps indicting a shift toward higher productivity and more frequently 'open' conditions observed elsewhere in Baffin Bay during the early Holocene.

Npl δ^{18}O records indicate, where available, that sub-surface waters in Baffin Bay contain a region signal, with values similar to other records along the flow path of the EGC/IC and WGC and subsequently the BIC/LC as it flows into the Labrador Sea over the Davis Strait. This indicates that the region was likely under the same conditions for much of the early deglacial and Younger Dryas/Holocene transition. Subsurface δ^{18}O values indicate the presence of either meltwater or the formation of sea-ice. Further work is needed to establish which of these mechanisms is responsible for the isotopically light sub-surface water signal.

Decidedly more variability was observed in the proxies for deeper ocean conditions. Prior ∼14 kyr BP benthic assemblages and planktonic/benthic ratios indicate a cooler and well-ventilated basin. At ∼14 kyr BP a sudden shift toward lower planktonic/benthic ratios and dramatic change in the benthic assemblage, dominated by the Atlantic water indicator species *C. neoteretis*, suggests a stronger (and potentially warmer) WGC, that acted to 'cap' deeper waters. This WGC incursion is consistent with other records and could represent the first establishment of this water mass in Baffin Bay following the LGM. Poorly ventilated deep water persisted for the remainder of the record. Evidence of cooler water in the early part of the Younger Dryas is superseded by a more cosmopolitan fauna at the onset of the Holocene and a more stratified water column, as in the present day.

Previous work on core SL 170 identified the two periods of instability of the ice sheets surrounding Baffin Bay, termed Baffin Bay Detrital Carbonate Events (BBDCs). This

co-registered record allows us to determine if there is a temporal, possibly even causal, relationship between changes in paleoceanographic conditions and discharge of meltwater and detrital material from the marine-terminating portions of these ice sheets.

BBDC 1 (14.2–13.7 kyr BP) was not preceded by a major change in any of the ocean proxies. A strengthening of the WGC, changing bottom water conditions and shift toward a more stratified water column post-date the onset of this event. From our results here and comparison with AMOC behaviour in the North Atlantic, we propose two scenarios for this phase relationship; firstly, that a large influx of Atlantic water entered the Baffin Bay prior to the event, causing a mixing and the release of warmer water to the subsurface. Following this, a cold meltwater layer was formed, forcing Atlantic water deeper which formed a cap over deeper waters and lead to a more stratified water column. Secondly, we propose that the BBDC 1 event and associated meltwater caused the change in bottom ocean conditions: following the same mechanism the first scenario.

The onset of BBDC 0 was concurrent with the onset of the Younger Dryas ($\sim$12.7kyr BP); this period of ice sheet instability could have been forced by colder general conditions, a mechanism previously proposed for Heinrich Events [*Bond et al.*, 1993]. Benthic assemblages indicate cooler glacio-marine conditions and weakened WGC prior to this event. However, there is evidence for warmer surface waters at the onset of the Younger Dryas than previously found [*Oksman et al.*, 2017] and this could have triggered the retreat of the ice margins. From our data we cannot confirm that this event was a direct product of oceanographic change and it more likely represents a response to a combination of the evolution toward 'modern' Baffin Bay conditions and wider climatic changes. By the onset of the BBDC 0 event it appears that there was a strong but variable connection between the Atlantic Ocean and Baffin Bay and increased influence of Arctic water via the Baffin Island Current.

4.6 Supplementary Figures

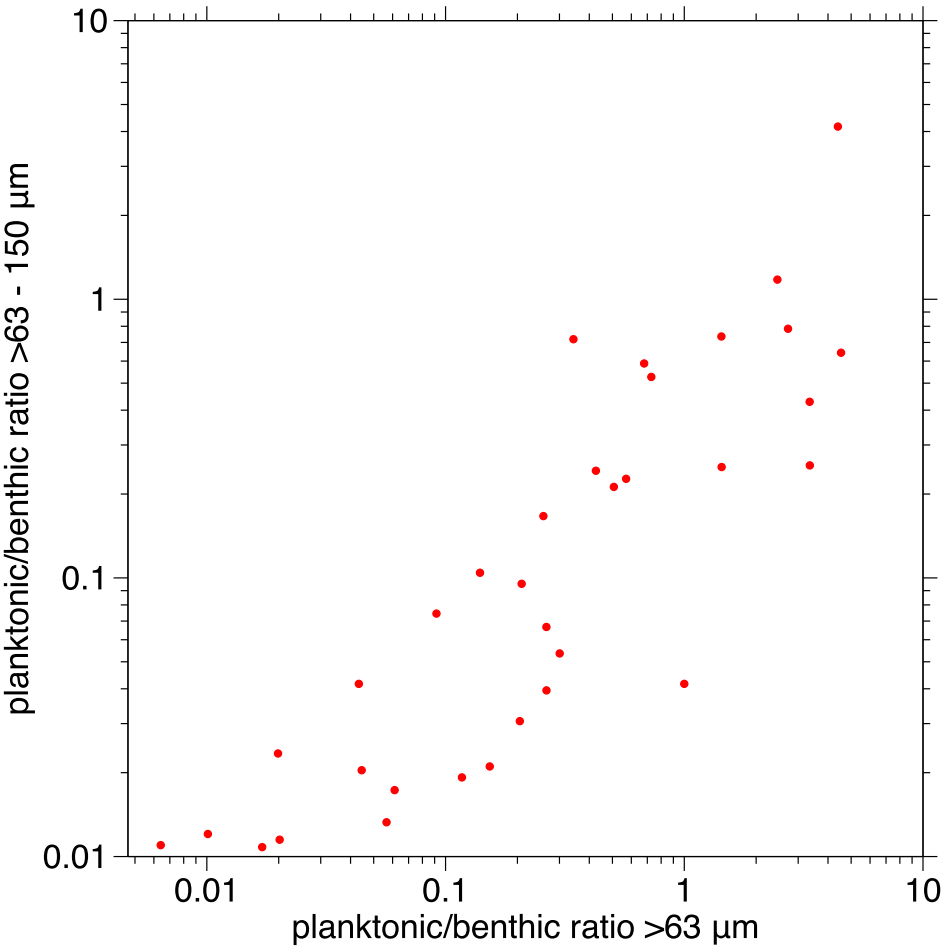

Figure S4.1: Ratio of planktonic to benthic foraminifera in the different size fractions. There is a positive correlation between the planktonic/benthic ratio in both size fractions (>63 µm) and coarser fraction (>63–150 µm) indicates that ratios are representative for both fractions.

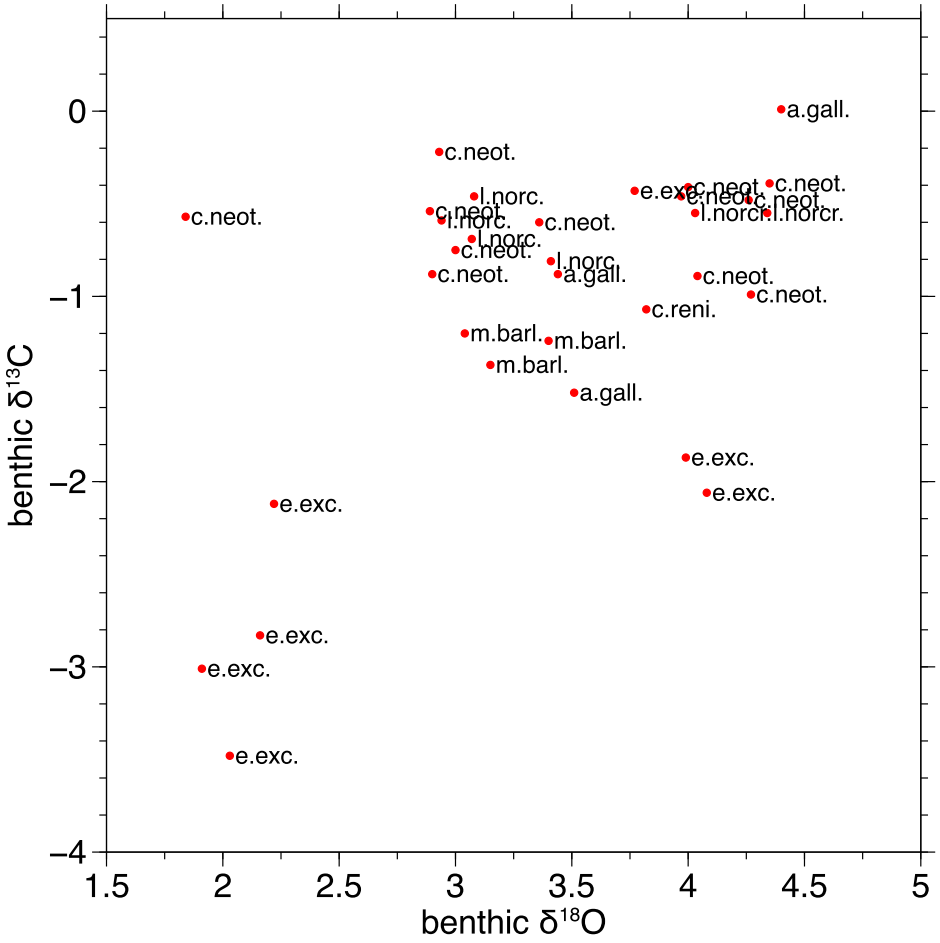

Figure S4.2: Cross plot of benthic δ^{18}O and benthic δ^{13}C with the species on which the measurements were carried out labelled. The isotopically lighter δ^{18}O values in the 4 *E. clavatum* samples suggest a consistent offset between these and the other species. These samples correspond to the samples at 12.4–12 kyr BP and 11.4 kyr BP. We interpret these parts of the benthic δ^{18}O and δ^{13}C record with caution.

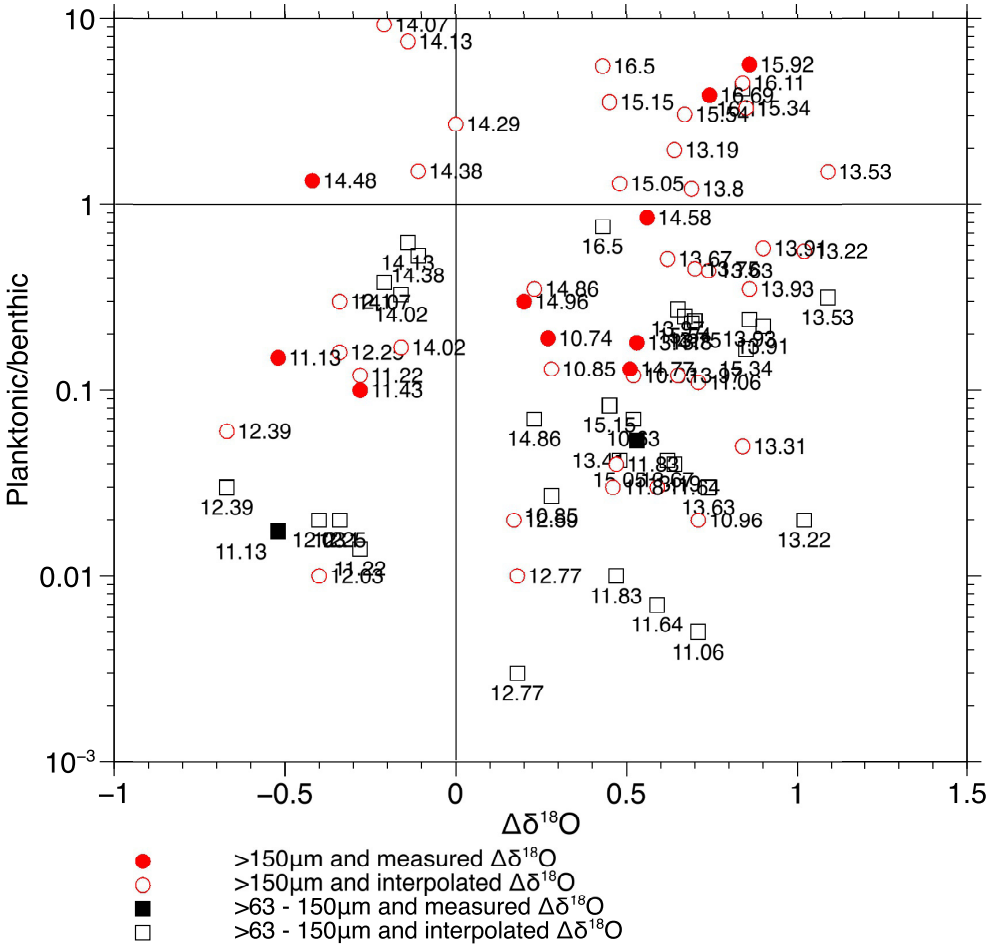

Figure S4.3: Cross plot of $\Delta\delta^{18}$O (benthic δ^{18}O–planktonic δ^{18}O) and planktonic to benthic ratio. Measured $\Delta\delta^{18}$O is where both planktonic and benthic δ^{18}O were measured at this same interval. Interpolated refers to where only a benthic or planktonic δ^{18}O measurement was taken and $\Delta\delta^{18}$O calculated from the interpolated curve of the unavailable measurement. The label indicates the date interval. Between 14.5 and 14 kyr BP $\Delta\delta^{18}$O values are minus or close to zero and planktonic/benthic ratios around 1, supporting a more ventilated water column around this time.

Chapter 5

A new chronology of ice sheet retreat in Baffin Bay since Marine Isotope Stage 3

Abstract

Understanding the complex nature and timing of discharge from the ice sheets surrounding Baffin Bay is vital to the construction of accurate meltwater chronologies. Studies largely focus on the west Greenland margins where absolute dating is possible but records are largely constrained to the deglaciation and more the Holocene. While efforts have been made to compile records of iceberg and meltwater discharge in the central west Baffin Bay region for longer periods of time, they are hampered by the lack of material for absolute dating methods. In this study, we utilise a sediment core recovered from central western Baffin Bay, with good preservation of biogenic carbonate, to characterise and define the timing of Baffin Bay Detrital Carbonate Events (BBDCs), representing discharge from the ice sheets surrounding northern Baffin Bay (north-eastern Laurentide and Innuitian ice sheets) from Marine Isotope Stage 3 to the early Holocene (~52–0.9 kyr BP). We combine radiocarbon and Relative Paleointensity dating to construct a new age model and within this context asses the timing and characteristics of these events using physical, geochemical and multivariate analysis. Results indicate the presence of 7 BBDC events throughout Marine Isotope Stage 3 to the early Holocene, occurring between ~45–43.6 kyr BP, ~38.5–35 kyr BP, ~33–31.6 kyr BP, ~26–24.6 kyr BP, ~17.7–16.2 kyr BP, ~14.5–13.3 kyr BP and ~12.8–10.9 kyr BP. This chronology confirms previous findings that retreat of the ice sheets surrounding northern Baffin Bay were out of phase Heinrich events. Furthermore, rock magnetic properties are used to gain insight into the timing of changes in background sedimentation and from the Greenland Ice Sheet. There were three main phases of change in background sedimentation at 52–44 kyr BP, 44–10.6 kyr BP and 10.6 kyr BP onwards, reflecting a change in source area or delivery mechanism. The chronology and data presented here offer a solid basis for further work on such events in Baffin Bay and the quality of the Relative Paleointensity

record could be used as a correlative tool for future records in the region.

5.1 Introduction

5.1.1 Regional setting and glacial history

Baffin Bay is a semi-enclosed oceanic basin lying between Greenland and the Canadian Arctic Archipelago (Fig. 5.1), formed by the North Atlantic-Labrador Shelf Rift System [*Maclean et al.*, 1990]. In the present day, Baffin Bay is supplied by cool and fresh Arctic Waters, which enter from the north through the various conduits of the Canadian Arctic Archipelago and largely through Nares Strait/Smith Sound, Lancaster and Jones Sounds. Water sourced from the North Atlantic enter the southern part of the basin; polar waters of the East Greenland Current (EGC) and warmer north Atlantic Irminger Current (IC) converge at the southern tip of Greenland and form the West Greenland Current (WGC), which flows northward along the west Greenland margin. It is met by arctic water inflow in the northwest of the basin and then travels south via the Baffin Island Current (BIC) [*Tang et al.*, 2004]. This anti-cyclonic gyre circulation then exits Baffin Bay via the Davis Strait once more, reaching its terminus in the Labrador Sea.

Three large ice sheets previously surrounded Baffin Bay; the Greenland Ice Sheet (GIS; still present today), and the northeastern sector of the Laurentide Ice Sheet (NE LIS). Recent studies have highlighted the presence of the Innuitian Ice Sheet, bridging the NE LIS and GIS in the north (Fig. 5.1). These ice sheets extended seaward onto the shelf areas along the Greenland coast such the Disko Bugt and Uummannaq Trough regions during the Last Glacial Maximum (LGM) [*Ò Cofaigh et al.*, 2013; *Ó Cofaigh et al.*, 2013; *Funder et al.*, 2011]. Along the eastern Baffin Bay margins, the LIS extended out through Lancaster Sound [*Li et al.*, 2011] and possibly laterally across northern Baffin Bay [*Marcott et al.*, 2011] and the shelf areas flanking Baffin Island [*Briner et al.*, 2007]. The subsequent retreat of the different ice sheets is traceable in Baffin Bay sediments due to the varying geology that underlay them. The geology of the west Greenland margin is dominated by Proterzoic Nagssugtoqidian Mobile Belt (NMB) and Archean Block (AB), whereas the northwestern section of Baffin Bay, namely Ellesmere Island and the area surrounding Lancaster Sound, is surrounded by areas of Palaeozoic limestones and dolostones (Fig. 5.1). The carbonate- and dolomite-rich signature of the latter in Baffin Bay marine sediments has been a key area of interest to constrain the timing of retreat and thus discharge from these ice sheets, termed Baffin Bay Detrital Carbonate events (BBDCs).

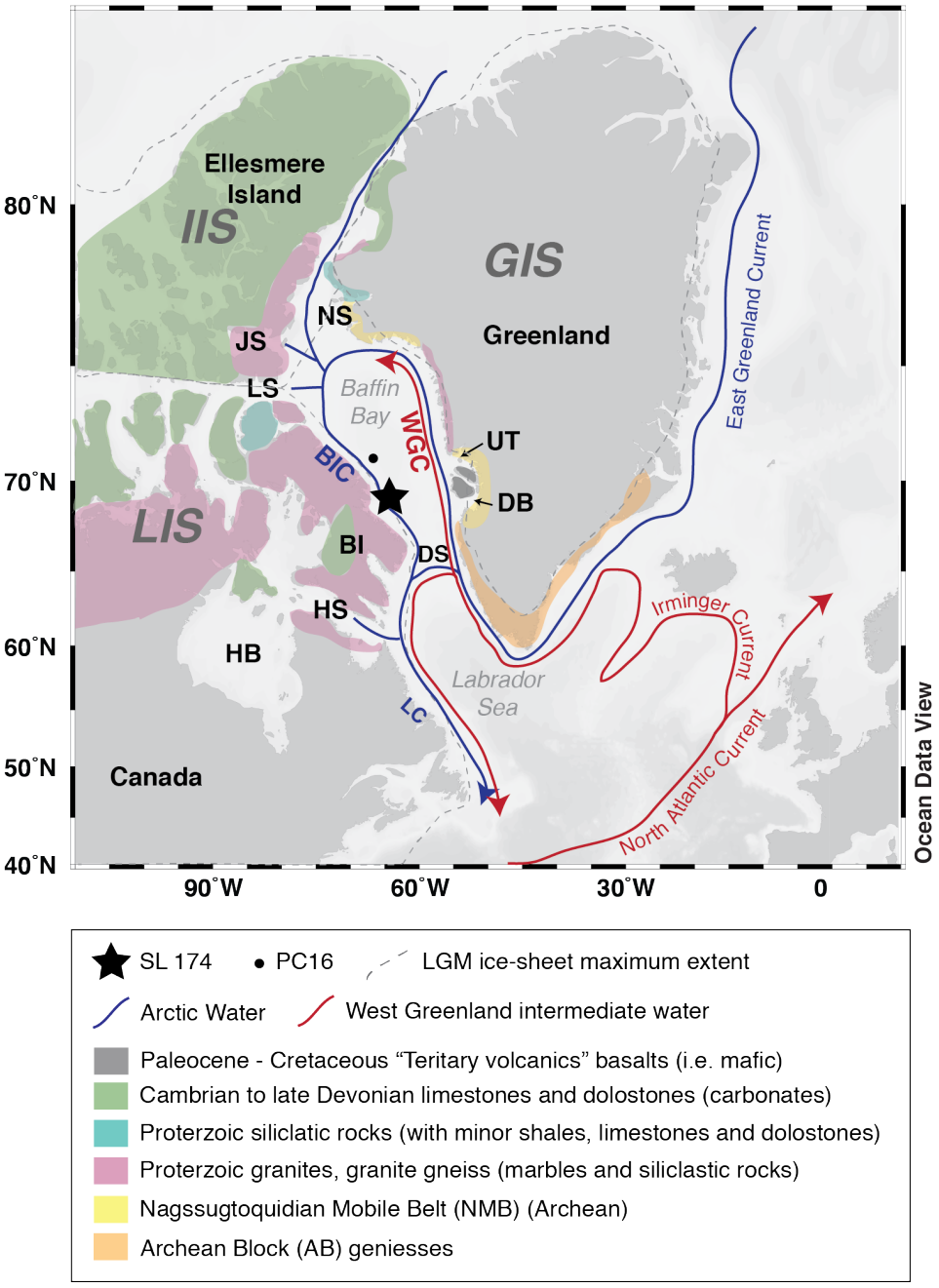

Figure 5.1: Location of Baffin Bay, surrounding landmasses, simplified geology and core location. The location of SL 174 and nearby core PC 16 are shown [*Simon et al.*, 2012, 2014] is also shown. Simplified geology is adapted from *Simon et al.* [2014] and references therein. Approximate maximum LGM ice sheet extent of the Greenland (GIS), Innuititan (IIS) and Laurentide (LIS) ice sheets from *Dyke et al.* [2002] and *England et al.* [2006]. Warm currents originating in the North Atlantic are shown: WGC = West Greenland Current. Cooler currents of Arctic origin are shown: BIC = Baffin Island Current, LC = Labrador Current. Modern inlets into the Baffin Bay are indicated: DS = Davis Strait, DB = Disko Bugt, UT = Uummannaq Trough, NS = Nares Strait, JS = Jones Sound; LS = Lancaster Sound, BI = Baffin Island, HB = Hudson Bay, HS = Hudson Strait.

5.1.2 Previous work

BBDC layers are not a newly identified phenomena in Baffin Bay and their presence has been identified by a number of previous studies [*Aksu et al.*, 1988; *Andrews et al.*, 1998; *Hiscott et al.*, 1989; *Jennings et al.*, 2017, 2014; *Jackson et al.*, 2017; *Simon et al.*, 2012, 2014] to name but a few. These characteristic carbonate- and dolomite-rich layers are found throughout Baffin Bay [*Andrews et al.*, 2011], as far south and eastward as the Disko Bugt area (Jackson et al., 2017; Jennings et al., 2017, 2014) and in some cases, as far south as the Labrador Sea [*Andrews et al.*, 2011]. To date, the consensus is that they did not occur at the same as drainage from the LIS via the Hudson Strait (i.e. Heinrich Events) suggesting a asynchronous retreat of the Laurentide Ice Sheet and so-called North-American Arctic ice sheets [*Jackson et al.*, 2017]. A further contribution of meltwater and detrital material from the GIS is observed in the western part of the bay [*Simon et al.*, 2014] and retreat of even the major paleo-ice streams in central west GIS was asynchronous [*Kelley et al.*, 2013; *Sinclair et al.*, 2016], creating an even more complex glacial retreat and meltwater history.

Constraining the timing of these events is important; large-scale meltwater discharge flowing from these ice sheets via Baffin Bay could have had an impact on deepwater formation in the Labrador Sea, something which is not normally considered in modelling studies. Timing of such ice sheet retreat has actually constrained in many of the shallower fjord regions of Baffin Bay, but records often only extend back to the Younger Dryas [*Ouellet-Bernier et al.*, 2014; *Perner et al.*, 2013; *Seidenkrantz et al.*, 2013]. In central Baffin Bay, marine records capture longer time intervals [*Hiscott et al.*, 1989; *de Vernal et al.*, 1987] but pervasive carbonate dissolution often hinders the construction of an absolute chronology.

We use a sediment core recovered off the coast of Baffin Island, to try to bridge this gap between longer records of lower resolution and those in the fjord areas. The core has good preservation of biogenic carbonate and we combine radiocarbon dating using a new method and a relative paleointensity age model from palemagnetic measurements to create a chronology. We apply this newly constructed chronology to physical, elemental and mineral magnetic properties and apply multivariate analysis to try and constrain a) the timing of BBDC events and possible differences between them and b) changes in sedimentary input from elsewhere in the Baffin Bay since Marine Isotope Stage 3 (MIS 3) to present.

5.2 Methods and Materials

5.2.1 Core GeoTü SL 174

Gravity core GeoTü SL 174 (68° 31.88' N 63° 19.82' W, MSM09/02-0467/3) was retrieved aboard the RV Maria S. Merian research cruise MSM09/02 [*Kucera et al.*, 2014] in 2008 (Fig. 5.1). The core is herein referred to as SL 174. SL 174 is 777.5 cm in length was retrieved from 1559 m water depth off the coast of Baffin Island. PARASOUND surveys at the core site and the initial on-board magnetic susceptibility profiles, carried out at 1 cm intervals, show no evidence of turbidites or hiatuses in sediment deposition (Fig. S3.1). The core was stored at <4 °C and split lengthways into archive and working halves.

5.2.2 Physical and elemental properties

Computerised tomography (CT) scanning was conducted on the archive half of core SL 174 using the General Electric CT Prospeed SX scanner at the MARUM, University of Bremen, Germany. Core sections were scanned in the single radiographic plane at 1 cm resolution. The archive half was also scanned by a line-scan camera (3 CCD device using 3 x 2048 pixel CCD arrays and a beam-splitter), mounted on the Super-Slit XRF core scanner at MARUM. The linescan software produced visual colour images (BMP, TIF and JPG) and colour data.

We use the colour data obtained in the CIE-L*,a*,b* colour space format. Of particular interest was the L* parameter, a unit-less value that represents lightness (in this case of sediment) on a scale from darkest black (L*= 0) to brightest white (L* = 100). L* values are often used as a proxy for relative carbonate content in marine sediment cores; high L* values indicting higher carbonate content [*Balsam et al.*, 1999].

To determine grain size distribution and obtain samples for radiocarbon dating, the working half was continuously sampled in slices of 1 cm thickness. All slices were weighed directly after sampling (wet weight) and frozen. A selection of samples were freeze-dried to obtain the dry weight. Sampling effort was focussed on the upper part of the core (0–530 cm), in part to compare with data from core SL 170 used for a previous study [*Jackson et al.*, 2017]. Part of the sediment sample ($\sim$10 grams dry weight) was then washed over a 63 µm mesh until the entire fine fraction was removed. The proportion of the sediment in the fraction $>$63 µm was calculated as the ratio between the dry weight of the residue ($>$63 µm) and dry weight of the bulk sample.

XRF scanning was used to determine elemental properties in the cores. XRF core scanner

data were collected every 1 cm down-core over a 1.2 cm^2 area with down-core slit size of 12 mm using generator settings of 50 kV (current of 1.0 mA), 30 kV (current of 1.0 mA) and 10 kV (current of 0.2 mA) with a sampling time of 15 seconds directly at the split core surface of the archive half with XRF Core Scanner II (AVAATECH^{TM} Serial No. 2) at MARUM, University of Bremen.

Sediment intervals containing large amounts of calcium (Ca) were noted, as in previous studies, as an indication of detrital input from source areas surrounding northern Baffin Bay [*Aksu and Piper*, 1987; *Andrews et al.*, 1998, 1995; *Andrews and Eberl*, 2012; *Andrews and Tedesco*, 1992; *Mudie and Aksu*, 1984; *Simon et al.*, 2012, 2014]. We use the ratio of calcium (Ca) to strontium (Sr) counts to define these layers, as used in studies of North Atlantic sedimentary sequences with detrital carbonate layers *Channell et al.* [2012]; *Hodell et al.* [2008]; *Pearce et al.* [2013]; *Winsor et al.* [2012]. Previous studies on Baffin Bay sediment records also highlight the importance of titanium (Ti) as an indicator of differing terrestrial source and associated with clay-rich layers [*Simon et al.*, 2012, 2014]. We also present this here as Ti/Sr ratio in order to a) compare with the Ca/Sr ratio and b) in both cases, correcting for Sr as a proxy for increased terrigenous (vs. biogenic) input. Intervals with high iron (Fe) counts were also noted, as this gives some indication and background on the likely magnetic properties of sediment (see section below).

Lithofacies were determined from CT, LS and >63 µm (where available), along with visual analysis, with particular interest in areas of coarser, potentially ice-rafted sediment.

5.2.3 Magnetic Susceptibility measurements

Magnetic susceptibility was measured at 1cm intervals on the surface of the archive half of core SL 174 using a Bartington MS2 susceptibility meter connected to a MS2F spot sensor. Each measurement on the sediment surface was completed by a respective reference measurement 'in air' in order to correct for an instrumental drift during post-processing. Magnetic susceptibility (MS) measurements are reported in the standard SI units (-10^6 SI).

5.2.4 Rock and Paleomagnetic measurements

Rock and paleomagnetic samples were analyzed at the paleomagnetic laboratory at the Faculty of Geosciences, University of Bremen. Paleomagnetic directions and intensities of natural remanent magnetization (NRM), anhysteretic remanent magnetization (ARM),

generated in a peak alternating field of 100 mT and a biasing DC field of 50 µT, as well as isothermal remanent magnetization (IRM), imparted by applying 23 steps in DC fields from 0 to 700 mT using the internal pulse coil, were measured on an automated cryogenic magnetometer (model 2G Enterprises 755HR).

NRM was measured on each sample before it was subjected to a systematic demagnetization treatment involving 16 steps for each sample with increments of 5 mT up to an alternating field (AF) of 50 mT and 10 mT increments up to the maximum AF intensity of 100 mT. A detailed vector analysis was applied to the results [*Kirschvink*, 1980] in order to determine the characteristic remanent magnetization (ChRM). Demagnetization of ARM and IRM was performed using the same field increments as for NRM.

5.2.5 Relative Paleointensity (RPI) dating

Relative paleointensity (RPI) were calculated using the so-called 'slope-method' or pseudo Thellier method [*Tauxe et al.*, 1995; *Channell et al.*, 2002]. RPI was computed as the slope of the regression line of NRM intensities plotted versus the intensities of ARM and IRM for AF demagnetization levels 10 to 50 mT and 25 to 50 mT, respectively, $NRM_{10\text{-}50mT}$/ $ARM_{10\text{-}50mT}$ (RPI_{ARM}) and $NRM_{25\text{-}50mT}$ / $IRM_{25\text{-}50mT}$ (RPI_{IRM}). The results were standardized as zero mean with standard deviation 1. RPI results shown here rely on RPI_{IRM}.

The relative paleointensity (RPI) record from SL 174 was correlated with several stacked records, and best correlation was found with the Global Paleointensity Stack GLOPIS-75 [*Laj et al.*, 2004]. 26 tie-points between the records were assigned and the resulting ages are shown in Table 5.1).

5.2.6 Radiocarbon dating

Accelerator Mass Spectrometry (AMS) ^{14}C dating was carried out on biogenic carbonate from core SL 174. From the >150 µm fraction of processed sediment samples, foraminifera were picked. Either planktonic (*Neogloboquadrina pachyderma* sinistral) or mixed benthic foraminifera were dated, depending on the availability of sufficient material at intervals of interest. The absence of biogenic carbonate in the top 97 cm of the core did not permit dating and the top two dates required a combination of planktonic and benthic foraminifera for a date (97–100 cm and 122–125 cm). Nonetheless, a total of 15 ^{14}C dates were acquired (Table 5.2), including one planktonic replicate (384–385 cm) and one sample interval where replicate planktonic and benthic dates were obtained (196–199 cm).

Table 5.1: Depth and age of tie points produced from correlation between the SL 174 RPI and GLOPIS-75 curve. **Paleomagnetic tie points based on the beginning and end of the Laschamp geomagnetic excursion.

Depth (cm)	Age (kyr BP)
4.1	0.9
32.3	4.35
45.2	5.55
48.2	5.775
53.6	6.15
89.3	8.475
94.6	8.775
151.6	11.55
241.4	15.075
274.8	16.2
276.3	16.275
280.1	16.5
335.6	19.8
338.7	20.025
342.5	20.325
354.6	21.3
397.2	25.575
489.2	36.9
493	37.2
496	37.425
498.3	37.575
502.1	37.8
**556.9	41.025
**560.7	41.175
612.4	43.2
723.4	46.875

Two methods were used for the radiocarbon dating; traditional ^{14}C measurements with AMS on samples converted to graphite and a new method, where CO^2 from ultra-small amounts ($\sim$0.5 mg) of carbonate [*Wacker et al.*, 2013] were directly analysed with a compact AMS facility equipped with a gas ion source was employed at the Laboratory for Ion Beam Physics, ETH Zurich (Table 2). Some of these samples were also leached before measurement [*Bard et al.*, 2015]. There is good agreement between the methods, suggesting the dating procedure is robust.

5.2.7 Age Modelling

Radiocarbon dated intervals and paleomagnetic dated intervals were combined to produce the combined age model for core SL 174. The chronology was constructed with

Table 5.2: Radiocarbon dates, paleomagnetic ages (RPI tie points) and resultant modelled ages for core SL 174. All ^{14}C radiocarbon dates with the ETH lab code were measured as gas samples for this study at the Laboratory for Ion Beam Physics, ETH; other codes are for existing ^{14}C dates for this core. All ^{14}C ages were calibrated using the Marine13 dataset [*Reimer*, 2013b] and a $\Delta R$of either 140 $\pm$ 35 years or 200 $\pm$ 100 years was applied in the age modelling software BACON (see text for details). RPI date tie points used are also shown. An error of 200 $\pm$ 100 years was applied to all RPI tie points. Maximum and minimum ages represent the 95% uncertainty in the age model. Dates in grey are those that feel outside of this uncertainty and were removed from the final age model calculation (see Section 3.1 for details). *Dates that feel outside the 95% uncertainty of the age model and were thus removed from the final combined age model. **Paleomagnetic tie points at the beginning and end of the Laschamp geomagnetic excursion.

Lab code	Depth interval (cm)	Material (foraminifera)	Weight (mg)	^{14}C/RPI tie point age (yrs)	Error $\pm$ (years)	Min (kyr BP)	Max (kyr BP)	Mean (kyr BP)
ETH-55690	97-100	planktonic(*N. pachyderma*) and mixed benthic	0.32	9793	120	10.178	10.832	10.491
*P-mag 1	120			10350	200			
Beta-344508	122-125	planktonic (*N. pachyderma*) and mixed benthic	4.16	10390	40	11.117	11.551	11.268
ETH-55691	142-145	mixed benthic	0.565	10997	110	11.583	12.278	11.996
ETH-58356	169-170	mixed benthic	0.914	11010	85	12.099	12.514	12.333
P-mag 2	171			12375	200	12.132	12.529	12.354
Beta-344505	196-199	planktonic (*N. pachyderma*)	8.54	11410	50	12.585	12.777	12.674
Beta-344506	196-199	mixed benthic	12.72	11150	50			
KIA 40767	215-219	planktonic (*N. pachyderma*)	1.1	12000	80	13.11	13.487	13.299
Beta-344507	233-236	planktonic (*N. pachyderma*)	3.42	12580	60	13.719	14.122	13.922
ETH-58357	278-279	planktonic (*N. pachyderma*)	0.906	14510	120	16.44	17.151	16.765
ETH-58358	294-295	planktonic (*N. pachyderma*)	0.975	15060	110	17.474	18.071	17.765
P-mag 3	308			20625	200	19.958	20.907	20.451
ETH-58360	384-385	planktonic (*N. pachyderma*)	0.5678	22380	289	25.65	26.44	26.006
ETH-58360	384-385	planktonic (*N. pachyderma*) replicate	0.732	22640	190			
ETH-64602	400-401	planktonic (*N. pachyderma*)	0.59	24010	310	26.699	27.882	27.356
P-mag 4	429			30225	200	29.703	30.629	30.172
*ETH-64603	455-456	planktonic (*N. pachyderma*)	0.325	24970	360			
P-mag 5	499			37050	200	36.521	37.485	37.011
**P-mag 6	551			40875	200	40.418	41.324	40.882
**P-mag 7	570			42000	200	41.538	42.38	41.956
P-mag 8	670			45975	200	45.581	46.507	46.045
P-mag 9	761			51375	200	50.937	52.911	51.441
*ETH-58362	756-766	mixed benthic		46370	3370	Date out of range		

the Bayesian age modelling software BACON [*Blaauw and Christen*, 2011], an open source code run in the program 'R'. Within the program the ^{14}C ages were calibrated using the Marine13 calibration curve [*Reimer*, 2013b]. An additional local reservoir correction(ΔR) of 140 $\pm$ 35 years was applied to all radiocarbon dates representing the deglacial period, up to and including the radiocarbon date at 294–295 cm depth (^{14}C age = 15060 years). This local reservoir correction has been applied in many Baffin Bay sediment studies [*Jennings et al.*, 2014; *Lloyd et al.*, 2011; *Ouellet-Bernier et al.*, 2014; *Perner et al.*, 2011, 2013]. For a full discussion of local reservoir correction in Baffin Bay during the last deglacial period the reader is referred to *Jackson et al.* [2017]. Beyond this depth, (uncalibrated) ^{14}C ages suggest the core is of last glacial maximum age and beyond. Due to the uncertainty with regards to local reservoir in Baffin Bay

during this period, we applied a higher correction of ΔR of 400 $\pm$ 100 years to ^{14}C dates from 384–385 cm and deeper. While no calibration is required for paleomagnetic ages, to provide the age model with some flexibility we applied an uncertainty of 200 years to all paleomagnetic age tie points.

5.2.8 Multivariate Analysis

Taking advantage of the high-resolution and continuous measurements collected (XRF and mineral magnetic properties), we performed Principal Component Analysis (PCA) and Linear Discriminate Analysis (LDA). Linear interpolation was performed on the magnetic remanence data so as to have 1 cm resolution in all measured parameters and all data were normalised before multivariate analysis. We do not include the >63 µm data due to a lack of data between 500 and 740 cm downcore. All multivariate analysis was performed within the software package PAST [*Hammer et al.*, 2001].

5.3 Results

5.3.1 Lithology, physical and geochemical properties

The lower section of core SL 174 (777.5–655 cm) is characterised by fine stratified muds (Fig. 5.2). Although we lack grain size information for this section of the core, CT and linescan images show fine lamination with some evidence of recognisable bioturbation. Sediment composition is uniform in this interval; Ca/Sr values fluctuate ~10, Ti/Sr ratios ~2 and Fe content remains stable. The section above this (665–595 cm) it interrupted by thin coarser layers and is associated with a peak in Ca/Sr ratios (~60) between 650 and 610 cm, a coeval decrease in Ti/Sr ratios and lighter sediment (L* ~55). Above this layer is an extended interval (610–480 cm) of coarser material, containing pebbles we deem likely to be dropstones but relatively uniform sediment composition according to elemental ratios. From 480 to 270 cm depth downcore two layers (460–445 cm and 400–375 cm) containing between 15 and 27% of sediment in the >63 µm fraction correspond to increases in Ca/Sr ratio and decreases in the Ti/Sr ratio and Fe counts. From 270 cm upwards the sediment is coarser and two intervals of coarse material containing dropstones, average 20% >63 µm fraction and Ca/Sr ratios between 50 and 60. The top of the core is topped by a ~4 cm brown mud layer.

We note 8 intervals of increased Ca/Sr ratio (greater than the background average of ~7–9) throughout the core at 646–608cm, 518–482cm, 455–446cm, 384–368cm, 286–272cm, 242–217cm, 201–191cm and 161–103cm (Fig. 5.2). L* values are consistently

higher in these intervals (∼45–57), where measurements are available the percentage of sediment in the >63 µm is higher, and Ti/Sr ratios and Fe counts are consistently lower.

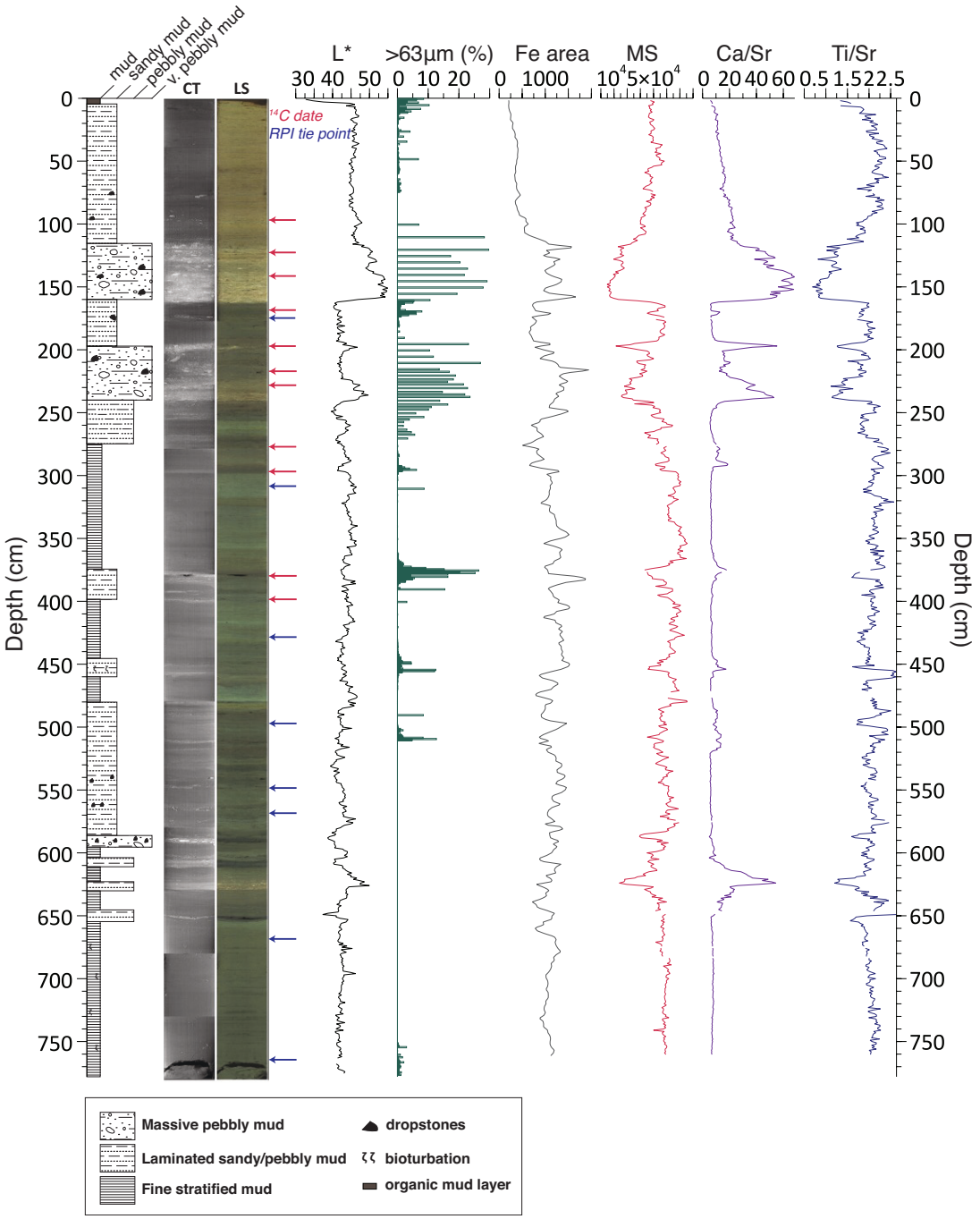

Figure 5.2: Summary of lithostratigraphy, some sediment physical properties, magnetic susceptibility measurements and elemental data for core SL 174. From right to left: core lithology, computerised tomography (CT) and high-resolution linescan images (LS). Dated intervals are also shown (Table 5.2). Sediment lightness (L*) is shown in grey, and grain size in green (% >63 µm). XRF scanning counts are shown for iron (Fe) in grey, calcium/strontium (Ca/Sr) ratio in purple and titanium/strontium (Ti/Sr ratio) in blue. Magnetic susceptibility (MS) is shown in red.

5.3.2 Magnetic Susceptibility and magnetic remanence properties

Magnetic susceptibility (MS, Fig. 5.2) is highly variable down core and measures between 244×10^{-6} SI and 3000×10^{-6} SI. The MS signal is less variable in the bottom (777.5–650 cm) and top (115–0 cm) sections of the core. Lower MS roughly coincides with intervals of high Ca/Sr ratios, especially visible ∼625 cm, 217-242 cm and 103-161 cm. Measurements of the acquisition of anhysteretic and isothermal remanent magnetization (ARM and IRM), as well as the 'hard' isothermal remanent magnetization (HIRM; IRM_{700mT}/IRM_{300mT}) can be used to indicate the presence and concentration of high-coercivity minerals such as magnetite and hematite (for a thorough review of parameters see *Liu et al.* [2012]). In core SL 174 the overall concentration of magnetic minerals, indicated by the IRM acquired at 700mT (IRM_{700mT}) is lower in the bottom ∼70 cm of the core and top ∼150 cm (Fig. 5.3). Towards the middle section of the core (∼650–350 cm) there is an increase in the overall magnetic mineral concentration (IRM_{700mT} = 26000 mA/m) and a subsequent decrease from then on. The concentration of fine magnetite and fine hematite, indicated by ARM_{100mT} and HIRM respectively, show a similar trend. Maximum concentrations of fine magnetite (ARM_{700mT} = ∼600 mA/m) and fine hematite (HIRM = ∼240 mA/m) occur between 400 and 300 cm downcore. Hematite and goethite, antiferrimagnetic minerals, exhibit a wide range of coercivities, often as a reflection of changing source area, and as such using HIRM as a measure of absolute concentration can be ambiguous. *Liu et al.* [2007] proposed a new parameter, the L-ratio, calculated as the ratio of two remanences after alternating field (AF) demagnetization of an IRM imparted in a 1 T field with a peak AF of 100 mT and 300 mT, as a test for the reliability of the HIRM. The L-ratio calculated for SL 174 is relatively constant (Fig. S5.1) thus suggesting that the HIRM reflects concentration.

The ratio of ARM_{100mT}/IRM_{100mT} and ARM susceptibility to magnetic susceptibility (KARM/Sus) indicate changes in the magnetic grain size of magnetite. Throughout the core grain size appears to be quite uniform, with KARM/Sus values ∼10 mA/m and ARM_{100mT}/IRM_{100mT} ratios of ∼0.3, with the exception of smaller values (larger grain sizes) found ∼670 cm and ∼590 cm. Magnetite grain size is becomes increasing smaller from ∼120 cm to the top of the core, with the exception of the top ∼4 cm (we note in Section 5.3.1 that this is a layer of brown mud distinct from the layer below it).

Information on the relative concentration of magnetic minerals is indicated by saturation isothermal remanence, termed the S-ratio. The S ratio (IRM_{300mT}/IRM_{700mT}) is the ratio of 'soft' to 'hard' IRM acquisition. When this ratio reaches toward unity (value = 1) it indicates a ferromagnetic, magnetite dominated magnetic mineral assemblage. In SL 174 this appears to be the case for the majority of the core from the bottom to around

200 cm depth. From here to the top of the core S ratio values ~0.980–0.975 indicate the increasing presence of antiferrimagnetic minerals (e.g. hematite). As with HIRM, the reliability of the S ratio as a representation of relative abundance of antiferrimagnetic minerals can be tested with the L-ratio (Fig. S5.1).

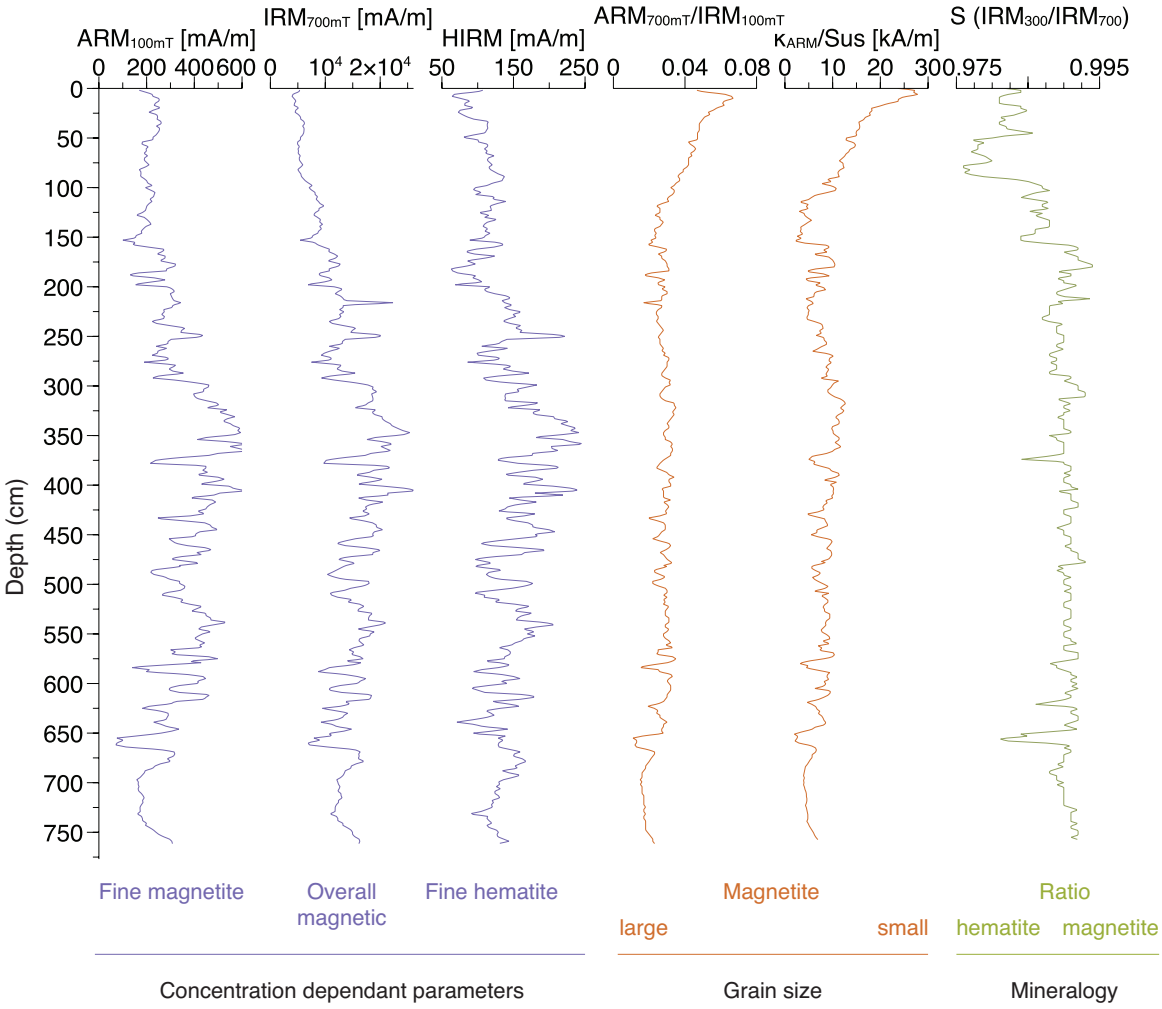

Figure 5.3: Mineral magnetic parameters indicting concentration, grain size and mineralogy down core.

5.3.3 Multivariate analysis

Principal component analysis: entire core

Principal Component Analysis (PCA) on data sets throughout the whole core indicate that nearly 70% of the total variance is accounted for by Axis 1 and 2 (Table 5.3). A bi-plot (Fig. 5.4) indicates that Ca/Sr and L* have strongly negative loading scores on both Axis 1 and 2 and account for one direction of variation, while Ti/Sr and magnetic susceptibility account plot in the opposite directly. Clustering of most samples is asso-

ciated with positive scores on Axis 1 and Axis 2 scores between -2 and 2. MDFarm and $ARM_{100mT}/_{100mT}$ scores are strongly negative on Axis 1 but positive on Axis 2.

Table 5.3: PCA scores and variable scores for the whole core dataset

Loading	PC 1	PC 2	PC 3	PC 4	PC 5	PC 6	PC 7	PC 8	PC 9	PC 10	PC 11
Eigenvalues	4.53	3.07	1.29	0.71	0.5	0.39	0.21	0.15	0.09	0.05	0.01
% Variance	41.17	27.89	11.77	6.41	4.52	3.58	1.92	1.36	0.78	0.47	0.12
Variance (cumulative %)	41.17	69.06	80.83	87.24	91.76	95.34	97.27	98.63	99.41	99.88	100
L*	-0.27	-0.3	0.32	0.28	0.01	0.71	-0.14	0.2	-0.1	-0.3	0.02
Ca/Sr	-0.27	-0.44	0.05	0.11	0.02	0.08	0.46	-0.15	0.45	0.54	0
Magnetic sus.	0.3	-0.35	0.27	-0.14	0.17	-0.24	0.14	0.72	-0.22	0.15	0.06
Fe counts	0.32	0.36	0.1	0	-0.04	0.38	-0.42	0.17	0.25	0.58	0.07
Sratio	0.37	-0.11	-0.19	-0.15	0.68	0.24	0.11	-0.23	0.11	-0.17	0.41
ARM_{100mT}/IRM_{100mT}	0.28	0.33	0.36	0.15	0.43	-0.05	0.13	-0.21	-0.54	0.34	0.01
HIRM	0.31	-0.06	0.58	0.2	-0.35	-0.2	0.01	-0.32	0.06	-0.1	0.49
Ti/Sr	0.17	0.47	-0.02	0.02	-0.23	0.31	0.74	0.2	0	-0.14	0.02
MDFarm	-0.3	0.34	0.22	0.23	0.34	-0.29	-0.05	0.31	0.57	-0.26	0.09
IRM_{700mT}	0.42	-0.05	0.34	0.09	0.19	0.01	0.06	-0.22	0.16	-0.13	-0.75
NRM	0.24	-0.06	-0.39	0.86	0.04	-0.11	0	0.08	-0.13	0.08	0.01

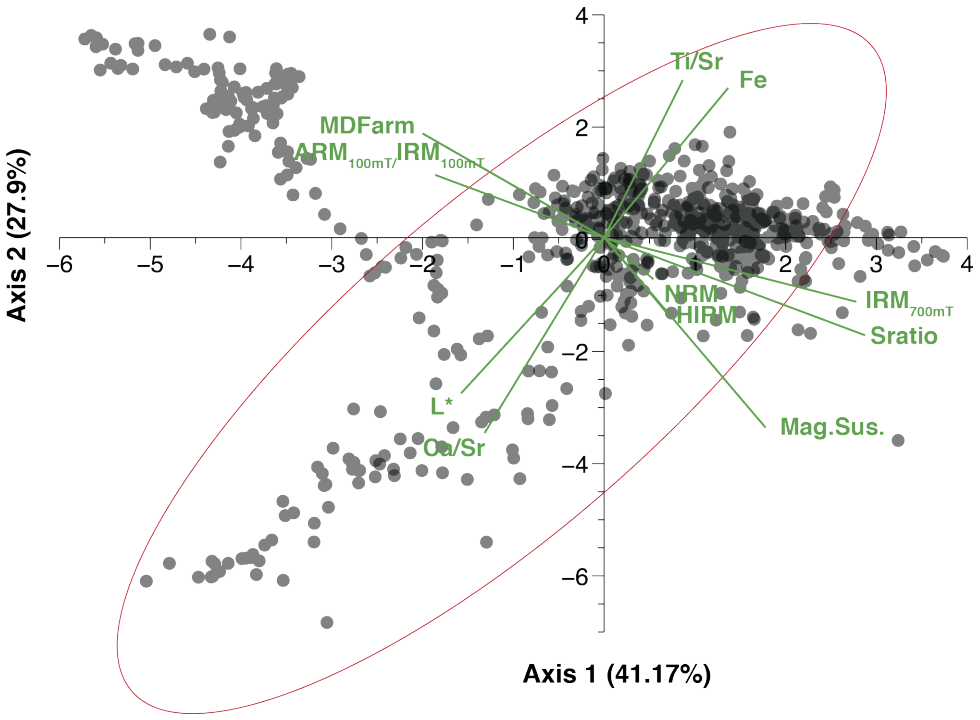

Figure 5.4: PCA analysis of core SL 174. 41% of the variance is explained by PCA Axis 1 and 28% by Axis 2. Biplot (green) shows where the variables plotted. The red ellipse shows the how the high Ca/Sr ratio and L* values layers plotted on the axes.

'Event' layers vs. 'non-event' layers

PCA on the whole core with all parameters included indicated that Ca/Sr ratios and L* values had highly negative loadings on both Axis 1 and 2 (Fig. 5.4). To check that the Ca/Sr ratio, that reflects the Ca area counts in this core (Fig. S3.3) is an useful proxy for, or definition of, detrital carbonate events, we performed Linear Discriminant Analysis (LDA) using all parameters but based on 2 groups: 'event' layers (suspected BBDC layers) and non-layers. 'Event' layers were defined as having a Ca/Sr ratio grater

than the background signal of ~7-9 (Fig. 5.2). 87.4% (jack-knifed) of the 1 cm core intervals were correctly classified by the LDA.

Detrital carbonate-rich 'event' layers

Linear Discriminant Analysis (LDA) was performed on sample intervals deemed detrital carbonate rich (see previous section). These sample intervals were grouped by depth presenting 'event' layers (e.g. 103–161 cm, Fig. 5.2). According to the test 93% of samples were grouped correctly. Moreover, a MANOVA test, performed to test if variance was explained by the parameters, returned a Wilks' Lambda score of 0 and associated p value of 0, confirming that the groups are statistically significantly different. A bi-plot (Fig. 5.5) indicates that the event layer 103–161 cm is different from that of the interval 482–518 cm, for example. A PCA analysis (covariance between groups) of this same data subset indicates that 85% of the variance is accounted for by the first two axes (65 and 16% respectively).

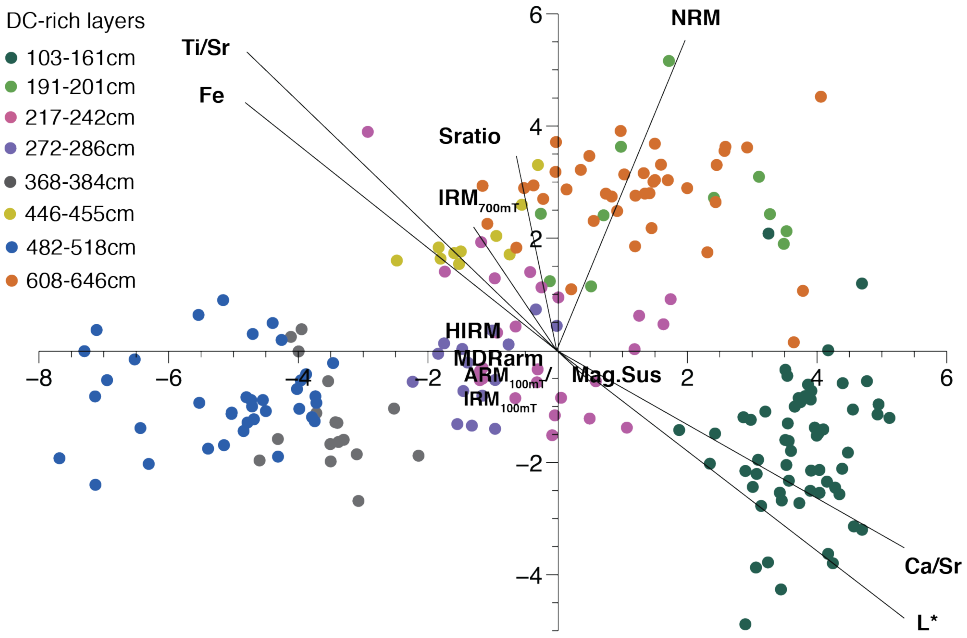

Figure 5.5: Linear Discriminant Analysis (LDA) of Detrital carbonate-rich (DC-rich) layers only.

'Non-event' layers

The entire core variance is clearly dominated by two parameters and we deemed the Ca/Sr and L* value to be discriminating the 'event' layers. These event layers are rich in detrital carbonate and have a low magnetic susceptibility (Fig. 5.2). In order to see if the non-layers were different in their mineral magnetic characteristics or elemental

composition, we ran LDA excluded not only event layers but also Ca/Sr and L*. Non-event layers were grouped by interval (depth) and 75% of non-layers were correctly classified. MANOVA tests confirm that these layers are significantly different (Wilks' Lambada score of 0 and associated p value of 0). The bi-plot of these results (Fig. 5.6) clearly shows that the top of the core (non-layer 0–102 cm) is different to that of the other 'non-event' layers. The plotting of layers in the middle section of the core (287–367 cm, 385–445 cm and 519–607 cm) seems to drive by magnetic susceptibility (and Fe), HIRM and IRM_{700mT}. Theses layers also plot somewhat differently to the remaining layer at the bottom of the core (647–777 cm) and other layers in the upper section of the core (162–190 cm, 202–216 cm and 243–271 cm). There thus appears to be a change in the downcore mineral magnetic signal.

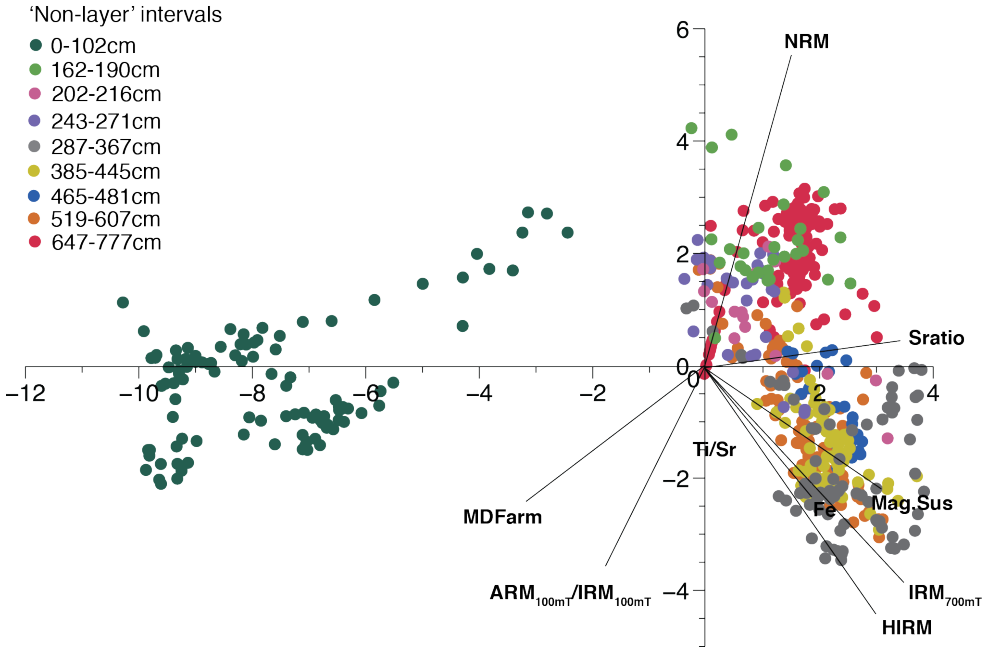

Figure 5.6: Bi-plot of Linear Discriminant Analysis (LDA) results of 'non-event' layers only.

5.3.4 Chronology

We produced two age models for core SL 174: one based solely on correlating the SL 174 relative paleointensity (RPI) curve with the GLOPIS-75 (Table 5.1) stack and the other combining the radiocarbon dating with RPI-GLOPIS stack correlations; considering the ^{14}C dates before correlating the RPI records (Table 5.2). Based on the combined age model, the chronology of SL 174 (4-761cm) captures the period 0.99-52.1kyr BP.

A combined age model was required as a) a radiocarbon measurement at the base of the course returned a 'blank' ^{14}C (i.e. out of the range of radiocarbon dating, Table 5.2) and b) as no radiocarbon dating in the top 98 cm of the core was possible. The top section of the core contained only very small amounts of biogenic carbonate, insufficient

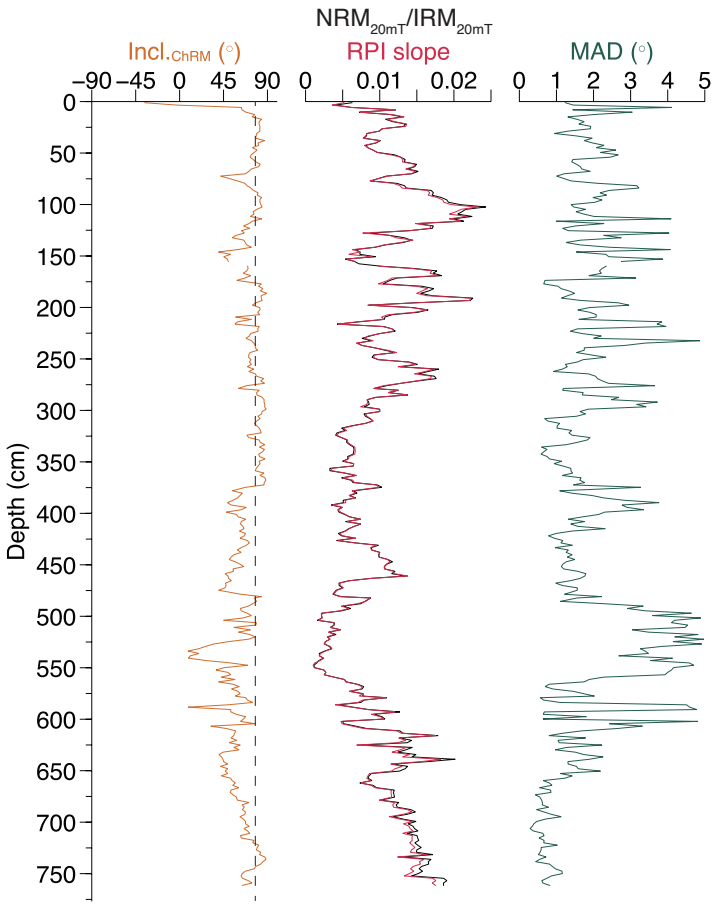

Figure 5.7: Directional magnetic measurements for core SL 174. Relative paleointensity (RPI) was normalised by the ARM and shows good correlation with the NRM_{20mT}/IRM_{20mT}T

for even the new method used here [*Wacker et al.*, 2013]. Furthermore the RPI curve for SL 174, despite downcore changes in lithology (Fig. 5.2), appears to be robust. Following established procedure and normalising for the isothermal remanence (IRM), the RPI curve is consistent with the NRM_{20mT}/IRM_{20mT}. Furthermore, the maximum angular deviation (MAD; *Kirschvink* [1980]) only varies between 0.5 and 4.5° (Fig. 5.7) which, in the context of Quaternary marine sediments and times of stable polarity when MAD values $\geq 5°$ are suspect [*Stoner and St-Onge*, 2007], supports the reliability of the RPI curve. The RPI curve presented here is also of higher resolution than other RPI curves obtained from Baffin Bay cores (e.g. *Simon et al.* [2012]) and as such a combined chronology including RPI tie points and radiocarbon dating was advantageous to utilise the whole core record. We note that the bottom ∼8cm of the core were disturbed and thus are not included this in either age model.

Sedimentation rates produced by the two age models are in good agreement; excluding the very high sedimentation rate in the combined age model between ∼13–11 kyr BP of up to 98 cm kyr^{-1}, which we attribute to closely spaced radiocarbon dating and interpret actual values with caution (Fig. 5.8). Both models indicate a period of high sedimentation rate (25–30 cm kyr^{-1}) between ∼45 and 43 kyr BP. A period of stable sedimentation

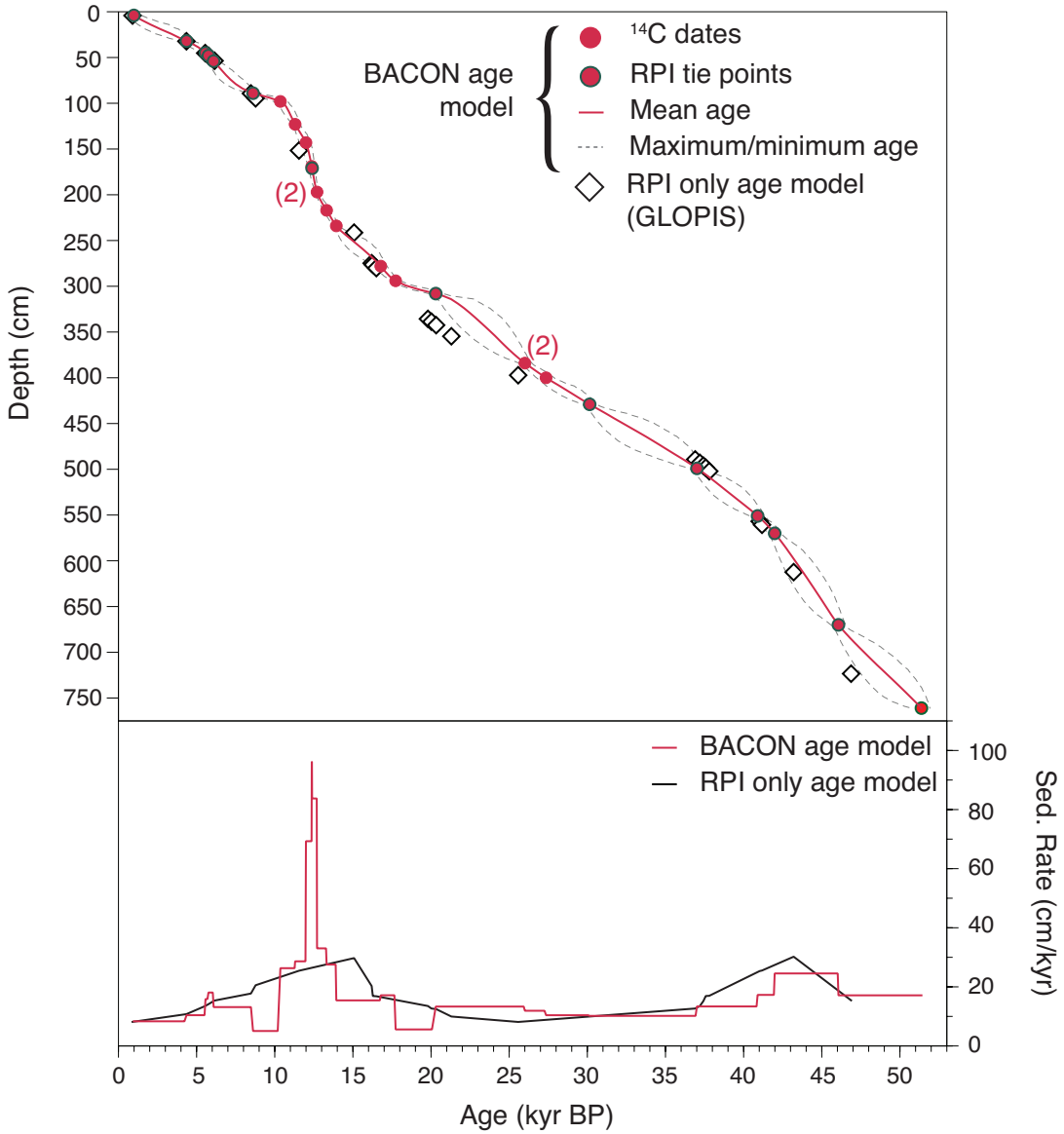

Figure 5.8: Chronology of core SL 174. Age-depth relationships (top panel) for both the combined ^{14}C and relative paleointensity (RPI) tie point age model (red) and that solely based on RPI tie points (black). For the combined age model, the mean age is shown according to output from BACON and grey-dashed lines indicate maximum and minimum ages produced by the age model (95% uncertainty). Intervals where more than one ^{14}C was obtained are indicated by brackets. Resulting sedimentation rates (bottom panel) produced for the two age models are relatively consistent, with the exception of the peak in sedimentation rate at ∼12.5 kyr BP produced by the combined age model (red).

rate (∼15 cm kyr^{-1}) in both age models characterises the period ∼37–21 kyr BP. Despite an offset of ∼10 cm kyr^{-1} around 21–18 kyr BP, both age models demonstrate increased sedimentation rate between 15–10 kyr BP and a subsequent decrease from then on to 10 cm kyr^{-1} in the top few centimetres of the core.

We present the data based on this combined age model from here on. Despite the reliability of the RPI curve and similarity in resulting sedimentation rates produced by

both models, combining these two dating protocols requires discussion surrounding uncertainties and implicit assumptions. In some sections of the core where have both ^{14}C dates and independent RPI tie points at the same interval (e.g. ∼145, ∼233, ∼280 cm) there is good agreement between the two age models, with the RPI tie points falling within the 95% uncertainty produced by the combined age model. We note that these dates correspond to post-LGM and early Holocene age (Fig. 5.8). We treat the 'late-Holocene' (∼10.5–0.9 kyr BP, 98–0 cm) period with caution; the combined age model relies solely on RPI tie-points during this interval and we note a) sedimentation rate during this period is very low and b) that the dominance of antiferromagnetic, potentially low-coercivity minerals may not record the directional measurements as consistently as other intervals. Thus we only refer to interval in general terms (∼10.5 kyr BP onwards) and avoid defining a specific age to small variations in the proxies.

Comparison between the combined age model and RPI only age model from ∼400–300 cm (corresponding to 26–20 kyr BP) shows a larger discrepancy, with RPI only age model predicting older ages. This could be explained by uncertainties surrounding both dating methods, but we argue that it is likely due to the 'lock-in' depth of paleomagnetic signal. This refers to depth below which magnetisation is fixed; i.e. when the magnetic grains can no longer be remobilised and thus the depth at which the directional signal is captured (e.g. *Teanby and Gubbins* [2000]). Estimates of lock-in depth vary between 2 and 30 cm (e.g. *Boudreau* [1998]) and we do not have a way to quantify this here.

On the other hand, it could be the combined age model, dependant upon ^{14}C, where the error lies. We note that this is a stadial period and thus the local reservoir correction we have prescribed for the upper part of this interval ($\Delta R = 140 \pm 35$ years) is, if anything, too small [*Bard et al.*, 1994]. However, increasing ΔR would make ^{14}C ages younger and thus increase the offset between the age models. The other option would be that the sediment was reworked but we see little evidence for this in the CT and linsecan images (Fig. 5.2).

5.4 Discussion

5.4.1 BBDC events: identification and timing

Investigation of downcore changes in lithology and elemental composition indicate the presence of several intervals with increased detrital carbonate content in central Baffin Bay from ∼52–10 kyr BP. That the presence of layer with increases detrital carbonate content represents a BBDC event is, however, an assumption. To test if these are in fact BBDC events (described by other authors), PCA and LDA analysis on XRF,

mineral magnetic characteristics and colour data were used to see if these layers could be statistically classified by the Ca/Sr ratio.

PCA analysis clearly points to the overriding importance of Ca/Sr (and L*) in determining if a layer is an 'event' layer. Downcore peaks in Ca/Sr are consistent with more negative PCA Axis 1 scores (Fig. 5.9). To further test if this was meaningful, LDA analysis between 'event' layers and 'non-event layers proved that these layers are statistically different. We can therefore have confidence in assigning the peaks in our Ca/Sr record as BBDC layers and thus refer to 'event' layers as BBDC events from here on in.

Previous work on core PC 16, north of our site (Fig. 5.1) identified 6 BBDC layers between ∼52 and 10 kyr BP [*Simon et al.*, 2012, 2014], defined as periods of high % carbonate (Fig. 5.9). These BBDC layers were seen to represent the discharge of icebergs and meltwater from the ice sheet surrounding northern Baffin Bay. This core, PC 16, is upstream from core SL 174 and thus we expect these layers will also be present at our study site.

According to our record, which is of higher resolution during this period than PC 16 and benefits from extensive radiocarbon dating in the combined age model, there were in fact 7 BBDC events occurring during this time period. Five of these events occur between ∼44-43, ∼38-35.5, ∼33-31.5, ∼25.5-24.4, ∼17.5-16.5 kyr BP and are labelled BBDC events 6-2, respectively (Fig. 5.9). The two BBDC events, occurring during latter part of the deglaciation and early Holocene, were previously defined as occurring at 14.2–13.7 kyr BP (BBDC 1) and 12.7–11 kyr BP (BBDC 0) by *Jackson et al.* [2017]. As the age-depth relationship in upper part of the core has been somewhat adjusted by the inclusion of additional RPI tie points, these events are redefined here as 14.5–13.3 kyr BP (BBDC 1) and 12.8–10.9 kyr BP. All BBDC events appear to be of relatively short duration; each event recorded here lasted between 1.2 and 1.4 kyrs, with the exception of the longer BBDC 5 event (3.5 kyrs). With the exception of BBDC 3, all events are associated with an increase in sedimentation rate (Fig. 5.9).

Comparing our record of detrital carbonate with the nearby core PC 16 requires caution. The resolution is much coarser than that found in our core. We present the data by the authors' original age model for that core, where only 3 radiocarbon dates were obtained and yielded dates between 16.4–13 kyr BP and note that they used a slightly higher and more variable local reservoir correction (ΔR) of 200 $\pm$ 200 years than we do for this same period (ΔR) of 140 $\pm$ 35 years. As there is no real 'error' estimate produced when correlating RPI records and the resultant age models, it is also difficult to compare the older sections of these records.

We also note that our BBDC 2 event coincides with a hiatus in core PC 16; as such we cannot evaluate whether or not this event was a regional phenomena or found only at the

core site here. Despite this the general structure of the two records appears comparable: BBDC 5 in PC 16 could present BBDC 6 in SL 170 and the structure of BBDC 4 (PC 16) is very similar to that of BBDC 5 in SL 174 (Fig. 5.9). The events taking place during the deglaciation and early Holocene (BBDC 1 and 0) are of similar timing in both records, although more well constrained in SL 174 [*Jackson et al.*, 2017]. Despite these differences in the timing of BBDC events, the similar structure in the carbonate record of PC 16 upstream from the study site with that presented here and clear evidence that these BBDC layers are statistically significant from their 'non-event' layer equivalents suggest that discharge from the ice-sheets surrounding northern Baffin Bay is recorded in central west Baffin Bay.

5.4.2 BBDC events: a link with climatic variation?

The asynchronous discharge from the ice sheets surrounding northern Baffin Bay (BBDC events) and detrital carbonate events originating from the Laurentide Ice Sheet via the Hudson Strait (Heinrich layers) is well established [*Andrews et al.*, 1998, 2014; *Jackson et al.*, 2017; *Simon et al.*, 2012, 2014]. Our new chronology confirms this: BBDC events 6-3 and 1 are asynchronous with Heinrich Events recorded in the North Atlantic (Fig. 5.9).

There appears to be no consistent phase relationship between BBDC and Heinrich Events. In the earlier part of the record ($\sim$52–10 kyr BP) BBDC events appear to lag Heinrich Events recorded in the north Atlantic (Fig. 5.9, *Channell et al.* [2012]) by between $\sim$0.5-2 kyr. *Simon et al.* [2014] noted that the timing of deposition of dolomite- and IRD-rich layers originating from iceberg discharge from the ice sheets surrounding northern Baffin Bay and Baffin Island (North-American Arctic) were more likely linked to Dansgaard-Oeschger (DO) events, Greenland interstadial events recorded in the Greenland δ^{18}O record. These BBDC layers were found to be coeval with increases in the proportion of sediment sourced from east Baffin Island [*Simon et al.*, 2014] (Fig. 5.9) suggesting that both the north eastern Laurentide and southern Innuitian ice sheets were discharging icebergs and meltwater around the same time. Certainly the earlier part of our record would support this; BBDC 6 occurs following the major DO event 12, BBDC 5 round the time of DO 8. Warmer climatic conditions and a stronger inflow of Atlantic water via the West Greenland Current have been proposed as triggers of ice-sheet margin retreat (e.g. *Hiscott et al.* [1989]), destabilising and melting the base of marine terminating glaciers. Initial δ^{18}O stratigraphy and marine palynomorph analysis suggests cooler and lower salinities during MIS 3, possibly caused by the release of meltwater from melting sea ice and icebergs into the surface and subsurface waters of Baffin Bay [*de Vernal et al.*, 1987]. Evidence of dolomite-rich, northern Baffin Bay sourced detrital

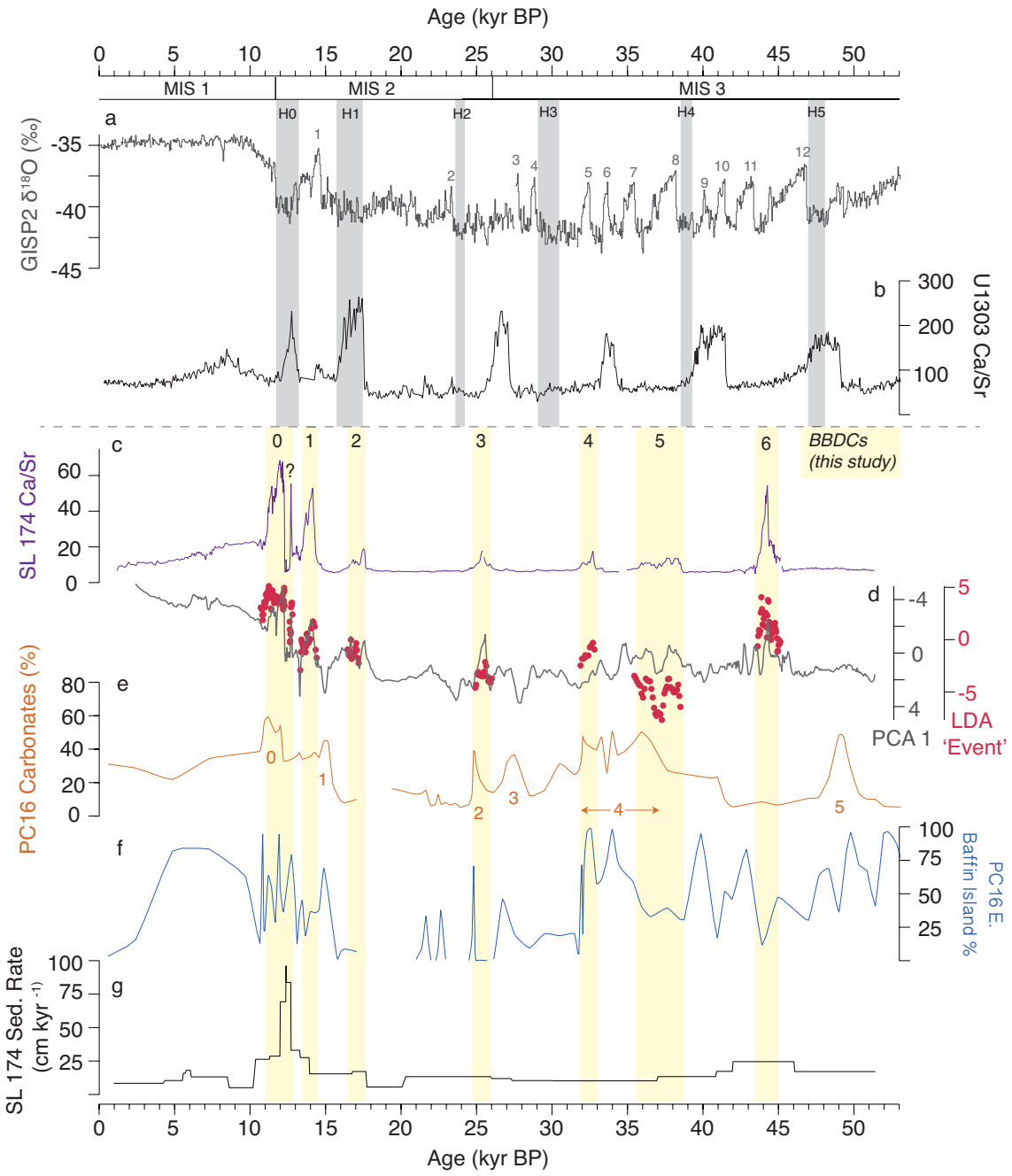

Figure 5.9: Timing of BBDC events in core SL 174 and comparison with other records. Ca/Sr ratio from core SL 174 (c, this study) indicates the timing of 7 BBDC events between ∼53 and 10kyr BP(yellow shading). PCA Axis 1 scores through time of the whole core with all parameters (d, grey) represents these BBDC events and LDA Axis 1 of the 'event' layers shows how the different layers plot (d, red). For comparison, % carbonate from the more northern core PC 16 [*Simon et al.*, 2014] is shown (e), along with the BBDC events prescribed for that core. The % weight of sediments derived from East Baffin Island in PC 16, from SedUnmix analysis [*Simon et al.*, 2014] is correlated with BBDC events in that core (f). The GISP2 δ^{18}O ice core record (a) [*Rasmussen et al.*, 2006] is shown for context. Grey numbers refer to Dansgaard-Oeschger events and 'H'to Heinrich stadials [*Hemming*, 2004]. The Ca/Sr (detrital carbonate) record from core U1303 (b), representing the timing of Heinrich (H) events seen in the North Atlantic [*Channell et al.*, 2012] is also shown.

carbonate layers south of the Davis Strait ∼47–43 kyr BP [*Andrews et al.*, 2014] support strong circulation in Baffin Bay during MIS 3.

BBDC events 6, 5, and 4 reflect the retreat of marine terminating portions of the Innuitian and northeastern Laurentide ice sheets from shelf areas, driven by increasing circulatory strength and temperatures of the West Greenland and subsequently Baffin Island Current. One could tentatively speculate that this is the mechanism behind the asynchronous nature of discharge from the Laurentide Ice Sheet via the Hudson Strait (Heinrich events) and the ice sheets draining into northern Baffin Bay. It is commonly accepted that the large amounts of freshwater driven into the Labrador Sea as a result of Heinrich events reduced deepwater formation and thus slowed the Atlantic Meridional Overturning Circulation (AMOC) (e.g.*McManus et al.* [2004]). Baffin Bay is intrinsically linked to the North Atlantic by the northward flowing Irminger Current and a reduction in this current would mean a weaker flow of warm subsurface water into Baffin Bay, thus allowing the marine terminating portions of the ice-sheet margins to stabilise. Investigation into the paleoceaongraphic conditions at this core site would be required to test this hypothesis.

The presence of three detrital carbonate events during stadial periods, however, likely requires a different mechanism than warm water advection. BBDC 3 in our record is coeval with the onset of MIS 2 and the Last Glacial Maximum (LGM) (Fig. 5.9). This layer is also coarser than the previous layers where data is available (Fig. 5.2). Such layers have been described as 'ice-distal'; the retreat of the IIS and LIS behind their maximum extent increasing the marine surface area of Baffin Bay and thus allowing for the transport of detrital carbonate via ice-rafting [*Simon et al.*, 2014]. The timing of BBDC 3 in our record would therefore suggest that the north-eastern LIS and IIS had not reached their maximum MIS 2 extent earlier than ∼25 kyr BP and were still discharging meltwater and icebergs into Baffin Bay at this point. An LGM grounding line 270 km off the coast of Lancaster Sound *Li et al.* [2011] was ascribed an age of ∼24 kyr BP and the IIS maximum extent was not thought to have been reached until ∼19 kyr BP [*Dyke et al.*, 2002; *England et al.*, 2006]. The BBDC 3 even could represent the last in a string of ice-sheet retreat events draining into Baffin Bay before these margins extended laterally across Baffin Bay [*Marcott et al.*, 2011] and stabilised under cold MIS 2 conditions. This implies that the maximum extent of the LIS and IIS were short-lived and had already begun to retreat, possibly in stages, in the early deglacial.

The extended chronology places a further event (BBDC 2) between ∼17 and 16.2 kyr BP, not seen in the previous deglacial chronology [*Jackson et al.*, 2017] or in nearby core PC 16, possibly due to a hiatus in the sediment record (*Simon et al.* [2012, 2014]; Fig. 5.9).This implies that the maximum extent of the LIS and IIS were short-lived and had already begun to retreat, possibly in stages, in the early deglacial. Evidence of ice

rafting from the northern IIS into the Fram Strait ~16.5 kyr BP [*Darby et al.*, 2002] is concurrent with this layer in Baffin Bay (considering dating uncertainties) however the retreat/ice-rafting hypothesis is disputed by no on-land evidence for retreat of the IIS this early [*Young et al.*, 2013]. What has been postulated is a thinning, rather than retreat, of the IIS via ice-streams. What is more likely is that this layer corresponded to iceberg calving from the Lancaster Sound region, where detrital carbonate layers roughly coeval with Heinrich Events, were found [*Li et al.*, 2011].

The last two BBDC events, 1 and 0, representing major retreat of the ice sheets surrounding northern Baffin Bay are more thoroughly discussed in *Jackson et al.* [2017]. However the revised chronology in this part of the core places BBDC 1 concomitant with DO 1. From the revised timing of all BBDC events spanning MIS 3 through to the early Holocene, it appears that the northeastern LIS and IIS retreat that lead to the deposition of BBDC layers was climatically forced; events during 'warm' marine isotope stages (3 and 1) appear to have a stronger detrtial carbonate signal (Fig. 5.9).

5.4.3 'Non-event' layers and background sedimentation in Baffin Bay

Central eastern Baffin Bay did not only receive detrital material from the ice sheets flanking it's northern margins. By removing the BBDC layers and the proxies that characterise them (Ca/Sr and L*) from multivariate analysis, elemental and rock magnetic measurement gives clues to the process of continuous sedimentation in Baffin Bay.

Linear discriminant analysis (LDA) highlighted how these intervals differ from each other (Fig. 5.6) . When plotted against age, LDA scores on the first and second axes indicate that the sediment record could be roughly spilt into three sections (Fig. 5.10).

The first, between 52 and 44 kyr BP has higher Axis 2 (vs. Axis 1) scores. There is little variation in either geochemical and rock magnetic proxies throughout this period. This interval is characterised by the dominence of ferrimagnetic minerals (e.g. magnetite), with ARM_{100mT}/IRM_{100mT} values close to 1 and a larger magnetic grain size compared to the rest of the core indicted by the measure of IRM_{700mT} (Fig. 5.6). This interval corresponds to finely stratified muds and clays in the core and as such appears to be 'background' sedimentation. A lack of coarser material and average Ti/Sr values suggest transport of this material was most likely via basal melting of ice-sheets protruding into the basin or the transport of fine material by bottom currents. It is comparable with the 'low detrital carbonate' facies found in PC 16 in [*Simon et al.*, 2012] and the Ti-bearing fine material was likely transported from the Uummannaq Trough region [*Simon et al.*, 2014].

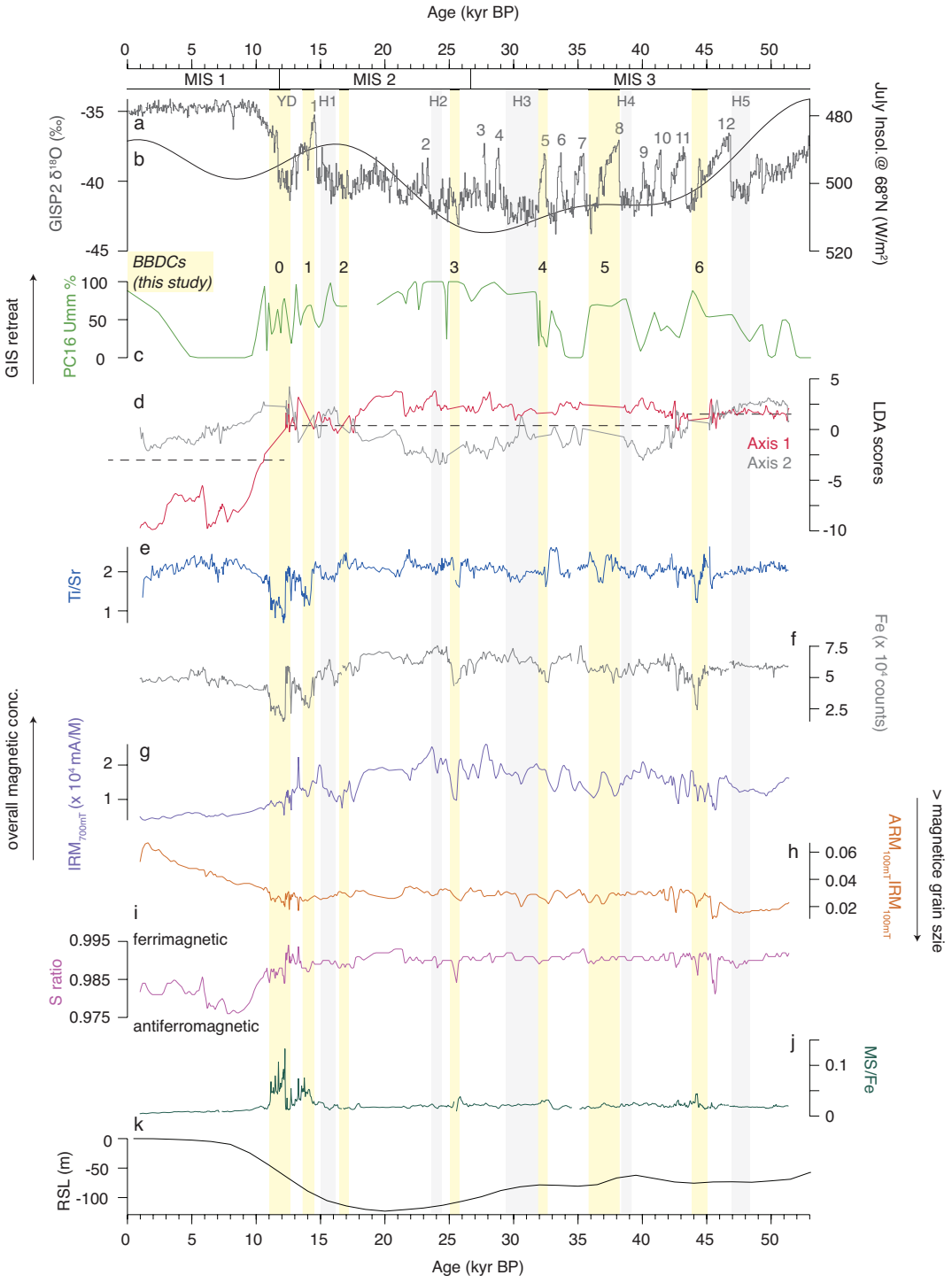

Figure 5.10: 'Non-event' layers and background sedimentation in core SL 174 through time. LDA scores Axis 1 and 2 scores for 'non-event' layers (d) indicate three main periods of changing magnetic properties. Ti/Sr and Fe counts (e and f) are higher in 'non-event layers'. Parameters for overall magnetic concentration (g), magnetic grain size (h) and mineralogy (i) are shown. Increases in the magnetic susceptibility to iron ratio (j) coincide with BBDCs (yellow shading). % weight of sediments assigned to the Uummannaq (West Greenland) in PC 16 track the retreat of the GIS (c) [*Simon et al.*, 2014]. The GISP2 δ^{18}O ice core record is shown and annotated as in Fig. 5.9. July insolation for the core latitude (68°N) is shown (b) [*Laskar et al.*, 2004] as well as relative sea level, (k) [*Waelbroeck et al.*, 2002].

From ∼44–11.7 kyr BP (the onset of the Holocene, MIS 1), LDA Axis 1 and 2 scores deviate and there is much more variability in the Ti/Sr record, the closely matched Fe record and the overall magnetic mineral concentration (IRM_{700mT}). This is reflected in the more variable lithology of core SL 174. Interestingly, peaks in the overall concentration of magnetic minerals in this interval appear to be roughly coincident with DO events. A warmer period when the ice was retreating in more locations could make available more sources of terrestrial magnetic minerals, but this is a very tentative link and would require more investigation. The magnetic mineral assemblage appears to be consistent with the previous interval and dominated by ferrimagnetic minerals and the grain size remains stable. The latter would suggest a stable and continuous supply from the same region (possibly the Uummannaq Trough region). During latter part of this interval, corresponding to the deglacial and Younger Dryas stadial (17–11.7 kyr BP), LDA axes scores converge once more and Fe counts, Ti/Sr ratio and magnetic mineral concentration begin to decrease. Sedimentation rates are high during this interval, so in terms of mineral magnetic concentration, this does not reflect a decrease in the volume of material delivered to the basin. The signal could of course be diluted by the BBDC signal; but even if measurements during BBDC intervals 2, 1 and 0 are excluded there is still a notable decrease in all parameters. According to 'SedUnMix' provenance model of PC 16 (*Simon et al.* [2014]; Fig. 5.10) during this period a majority of sediment is still sourced from the Uummannaq Trough region but as the ice sheets surrounding Baffin Bay retreated during the deglacial there could be a contribution from another sediment source but this is something we cannot substantiate with the current dataset. However, we do note that on the LDA cross plot of 'non-layers' (Fig. 5.6) that this section (corresponding to intervals 243–271 cm, 202–216 cm and 162–190 cm) plots similarly to the very bottom section of the core.

The major change in background sedimentation in Baffin Bay occurs around ∼10.6 kyr BP. From here on LDA Axis 1 scores become negative. There is a steady trend to lower overall magnetic mineral concentration (IRM_{700mT}), less coarse magnetic mineral grain size (ARM_{100mT}/IRM_{100mT}) and smaller S-ratio, all indicating that the mineral magnetic assemblage was dominated by antiferromagnetic minerals (e.g. hematite and goethite). The Ti/Sr ratio, however, remains high. This marks the period following the retreat of the some of the major ice sheets surrounding Baffin Bay. On the western margin of the GIS, exposure dates of ∼11 kyr BP in the Assiat Sill (south of Disko Bugt) and Vagait Sill (northern Disko Bugt) place the landward retreat of the GIS between ∼11 and ∼10 kyr BP [*Kelley et al.*, 2015, 2013] and to north in the Uummannaq Trough, retreat behind a mid-shelf grounding wedge zone occurred ∼11.5 kyr BP [*Sheldon et al.*, 2016]. Retreat of the GIS via some of it's major paleo ice-streams would have depleted the source of material to central west Baffin Bay. Furthermore, the LIS was already

retreating at this point; glaciers that had previously reached the Baffin Island shelf retreated to from fjord mouth positions ∼11.7 kyr BP and had reached the inner fjords of Clyde Inlet by ∼9.3 kyr BP [*Briner et al.*, 2007]. However, it is likely that during the last ∼10.6 kyr BP that there were re-advances of the LIS through Baffin Island channels [*Briner et al.*, 2007], fuelling what appears to be continued deposition of the fine Ti-rich material from the siliclastic rocks of Baffin Island, rather than Uummannaq Trough, during the Holocene period [*Simon et al.*, 2014].

5.5 Conclusions

We used a combined, radiocarbon and Relative Paleointensity (RPI) dating approach to construct an age model for core SL 174 in central western Baffin Bay. The chronology reveals that the core spans the last ∼52 kyr BP. Based on physical, geochemical and rock magnetic proprieties and multivariate analysis of these parameters, we define 7 BBDC events occurring between ∼45–43.6 kyr BP (BBDC 6), ∼38.5–35 kyr BP (BBDC 5), ∼33–31.6 kyr BP (BBDC 4), ∼26–24.6 kyr BP (BBDC 3), ∼17.7–16.2 kyr BP (BBDC 2), ∼14.5–13.3 kyr BP (BBDC 1) and ∼12.8–10.9 kyr BP (BBDC 0). This challenges the prior timing and frequency of these events proposed in a lower resolution core nearby, that did not benefit from extensive radiocarbon dating [*Simon et al.*, 2012, 2014]. These BBDC events represent the retreat of the north-eastern Laurentide and Innuitian ice sheets behind their maximum extent and are asynchronous with discharge from the Laurentide Ice Sheet via the Hudson Strait (Heinrich Events). They appear, in the case of BBDC events 5, 4 and 1 (and possibly 6) to be linked to Dansgaard-Oeschger oscillations and the likely impact of the incursion of Atlantic-sourced waters into northern Baffin Bay. BBDC 3 appeared to be the last in the sequence of events before the north-eastern Laurentide and Innuitian ice sheets grew to their maximum extent between ∼24–20 kyr BP and 19 kyr BP respectively. A thinning of the Innuitian Ice Sheet may have been responsible for BBDC 2.

Removing these layers and the parameters that define them allowed for investigation other changes in the depositional history of Baffin Bay. There were three main phases of change in background sedimentation at 52–44 kyr BP, 44–10.6 kyr BP and 10.6 kyr BP onwards, reflecting a change in source area or delivery mechanism. Further work would be needed to assess the exact processes behind these changes. Nevertheless, the chronology and data presented here offer a solid basis for further work on such events in Baffin Bay and their impact on the wider climate system. Furthermore, the quality and detail of the combined age model could in itself provide a reference curve for future work in the region.

5.6 Supplementary figures

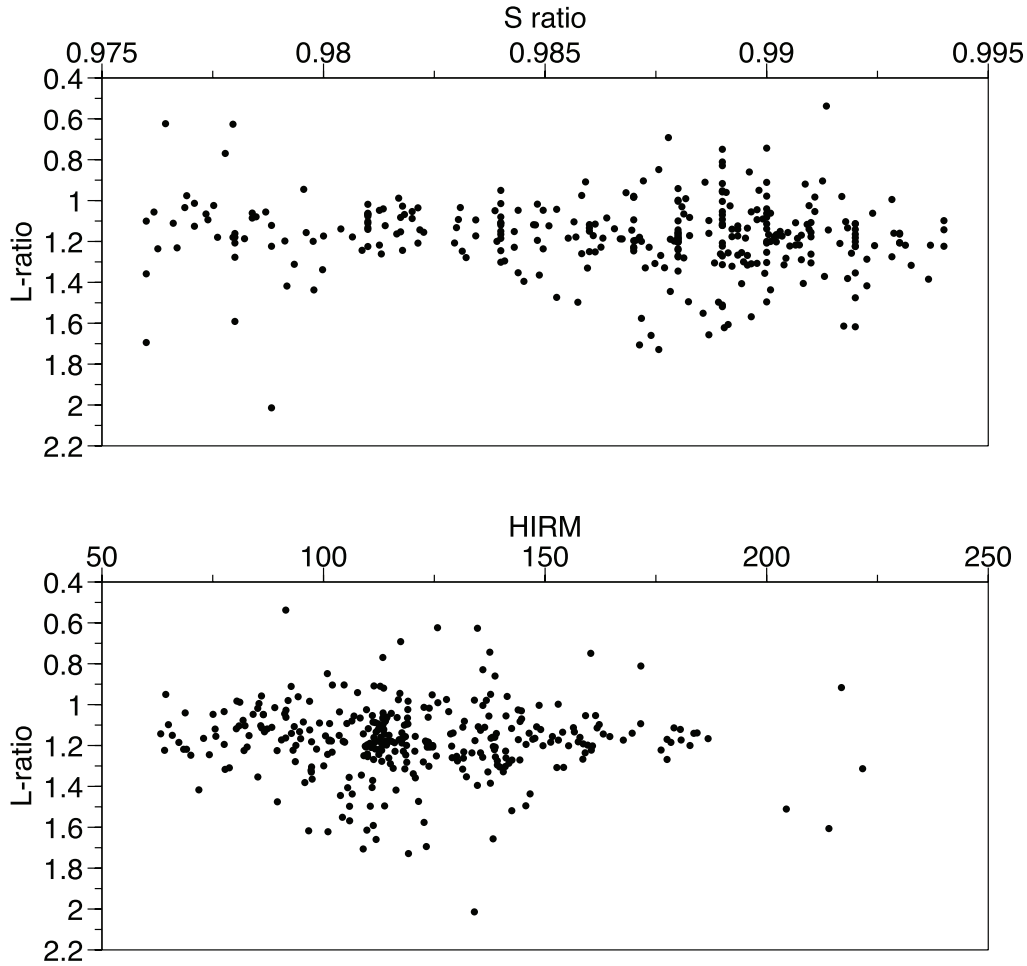

Figure S5.1: Cross plots of L-ratio/S-ratio and L-ratio/HIRM. The L-ratio [*Liu et al.*, 2007], calculated as the ratio of two remanences after alternating field (AF) demagnetization of an IRM imparted in a 1 T field with a peak AF of 100 mT and 300 mT, as a test for the reliability of the S ratio (top) and HIRM (bottom). The L-ratio calculated for SL 174 is relatively constant thus suggesting that the S-ratio is an accurate meausre of relative abundance of antiferrimagnetic minerals downcore and HIRM is a reliable proxy for fine hematite concentration.

Chapter 6

Conclusions and outlook

6.1 Conclusions

The ice sheets surrounding Baffin Bay were influenced by, and likely had an influence on, abrupt climatic changes during the last ∼52 kyr BP. Evidence of Baffin Bay Detrital Carbonate Events (BBDCs), reflecting the instabilities of the north-eastern Laurentide and Innuitian ice sheets, was far-reaching; evidence of these events as far south as the Davis Strait elucidates to the scale of these events. Coupled with discharge from the Greenland Ice Sheet, the release of ice-bergs and meltwater had the potential to influence climatic and oceanic conditions in important regions for climate modulation, such as the Labrador Sea. However, constraining the timing of these events and the paleoceanographic conditions surrounding them has so far been problematic in the deeper sectors of Baffin Bay.

In this study, two sediment cores from central Baffin Bay were analysed. Extensive radiocarbon and paleomagnetic dating were performed to provide the basis for an absolute chronology of BBDC events. Combined lithological, physical, elemental, mineralogical and rock magnetic analysis provided information on sedimentary setting, transport processes and the potential provenance of the sediment contained in the cores. Extensive analysis of foraminifera and palynomorphs complemented this record of ice sheet instability by providing a paleoceanographic context.

This large data set was used for three main research objectives. The first was to establish the timing of BBDC events throughout Baffin Bay by constructing a radiocarbon-dated chronology for last deglacial and early Holocene (17–10 kyr BP), using sediment cores from both east and west Baffin Bay. Results indicated that there were two main detrital carbonate events during the last deglaciation and early Holocene. The first ice sheet instability, BBDC 1, post-dated Heinrich Event 1 and occurred during the Bølling/Allerød warm period at ∼14.2–13.7 kyr BP. The onset of BBDC 0, on the other hand, was

concomitant with the onset of the Younger Dryas stadial and persisted until the early Holocene (∼12.7–11 kyr BP).These two events were synchronous across Baffin Bay, but asynchronous with meltwater and iceberg discharge from the Laurentide Ice Sheet and thus, the North Atlantic climate mode. The study adds to the complexity of understanding of abrupt climate change and highlights the importance of considering the regional response of ice sheets to/with abrupt climate change.

The second objective was to establish a record of paleoceanographic conditions during the last deglaciation and early Holocene (17–10 kyr BP) on the high resolution core SL 170 off the coast of western Greenland, within the framework of the new age model. Analysis of palynomorphs, planktonic and benthic foraminifera stable isotopes and fluxes, as well as benthic foraminifera assemblages, were used to assess changes in surface, sub-surface and deeper ocean conditions. Results indicted that Baffin Bay was subject to extensive sea-ice throughout the last deglacial. Comparison with other records up- and downstream of the cores site indicate that sub-surface waters appear to contain the regional δ^{18}O signal of North Atlantic water, carried into Baffin Bay as the Irminger Current component of the West Greenland Current. No evidence was found for a strengthened inflow of Atlantic water into Baffin Bay via the West Greenland Current prior to ∼14 kyr BP and it was found that Baffin Bay was more well ventilated prior to this. It appears that paleoceanographic changes were not the trigger of ice-sheet instabilities in this region or northern Baffin Bay, contrary to previous studies. The major changes in circulation and ventilation post-date the onset of BBDC 1. The later event, BBDC 0, was not pre-dated by any major changes in the oceanic conditions and was likely linked to climatic conditions and the ongoing evolution of oceanic conditions toward their present state as well as increased influence of polar-sourced waters, the latter likely due to the opening of the Nares Strait. These results highlight the complexity of ocean/ice sheet interactions in the region and the importance of multi-proxy paleoceanographic reconstructions in order to fully understand the influence of region oceanographic change in Baffin Bay and its impact on the marine-terminating ice sheets and glaciers that surrounded it.

The third objective was to produce an age model for the longer record in the west Baffin Bay and refine the chronology of BBDC events in the region. A combined age model was produced for SL 174, using both additional radiocarbon dating and a high quality Relative Paleoinetnsity curve. The core was found to span ∼52–0.9 kyr BP and contain a much better temporal resolution than other cores in the area. Testing the assignment of BBDC events with multivariate analysis of elemental, mineral magnetic and magnetic remanence properties, this core was found to contain 7 BBDC layers during the latter part of MIS 3 through to the Holocene. Some of these events appear to be coeval with Dansgaard-Oeschger warm oscillations and represent the retreat of the ice sheets surrounding northern Baffin Bay away from their maximum extent under increased influence

of 'warmer' Atlantic water inflow. BBDC events appear to be stronger during interstadial periods and their asynchronicity with Heinrich Events is confirmed. By removing these layers and their characteristics from analysis, the hemipelagic sedimentation in Baffin Bay appears to have followed three stages; changes likely linked to source area, transport mechanism and/or differing ice sheet configuration around Baffin Bay. This new chronology provides a good base for further work on this core or in the wider region. The detail of the age model and quality of the paleomagnetic data may provide a useful correlative tool for future sediment records in Baffin Bay.

6.2 Outlook

Despite the contributions of this study to research in Baffin Bay, it remains a challenging area to work and there are many avenues of potential further research.

The first and most common obstacle to paleoclimatic reconstruction in the deeper sections of the Baffin Bay is construction of reliable age models. A large source of uncertainty is that surrounding a local marine reservoir correction (ΔR) and in particular its variation through time. More extensive radiocarbon dating of planktonic and benthic foraminifera than completed here (chapter 3) and comparison between the returned dates could be utilised to test if there is some pattern in this offset through time. Comparison with other dating methods independent of a marine reservoir correction such as pollen stratigraphy and tephra (e.g. Vedde Ash layers) would significantly improve age model reliability but was not possible in core SL 170 studied here. Comparison between paleomagnetic and radiocarbon based age models was completed in core SL 174 (chapter 5), but even small offsets between such models brings both into question. Ascertaining the 'uncertainty' surrounding paleomagnetic tie points, besides that assumed and applied in the age modelling process itself, would be beneficial but would require an investigation of the 'lock-in depth' of the magnetic signal.

Further proxy investigation could significantly improve paleoclimatic reconstruction. Sea-ice reconstruction could have been verified with the addition of biomarker analysis (e.g. IP_{25}) which could have added another level of detail to the dinoflagellate cyst analysis, where concentrations were too low to apply the modern analogue technique (MAT). The presence of sea ice in the high latitudes also complicates interpretation of the planktonic $\delta^{18}O$ record; isotopically light values could related to either the formation of sea-ice or presence of meltwater (chapter 4). This is further complicated by the potential changes in living depth of *N. pachyderma* sin. Combining a temperature/salinity proxy with depth habitat modelling efforts could aid the correct interpretation of the $\delta^{18}O$ record. Furthermore, the stable isotope composition of the benthic foraminifera record

could be better interpreted if species-specific offsets were investigated and accounted for. Applying an independent temperature proxy (such as Mg/Ca) would also be beneficial for understanding paleoceanographic changes in the benthic realm.

Although we have made an attempt here to constrain the timing of BBDC events and other changes in sedimentation here, further work on the provenance of different sediment layers could substantially improve the reconstruction of ice-sheet margin behaviour, though either the quantification of mineral assemblages with extensive down-core XRD analysis and/or the application of provenance models such as the SedUnMix model, particularly relevant at the site of core SL 174. Core SL 174 also provides a promising record for paleoceanographic reconstruction; good preservation of biogenic carbonate was observed in some intervals of the core when sampling for radiocarbon dating. Analysis of foraminifera (and dinoflagellate cysts, if found) could yield information on the sea-ice conditions, possible periods of Arctic Water incursion during MIS 3 and the varying strength of the West Greenland Current as it travels though Baffin Bay. How this might have been related to paleoclimatic and paleoceanographic changes in the Arctic Ocean and its impact downstream in the Labrador Sea remains an open question.

References

Aksu, A. (1983), Holocene and Pleistocene dissolution cycles in deep-sea cores of Baffin Bay and Davis Strait: Palaeoceano-graphic implications, *Marine Geology*, *53*(4), 331–348.

Aksu, A. E., and D. J. W. Piper (1987), Late Quaternary sedimentation in Baffin Bay, *Canadian Journal of Earth Sciences*, *24*(9), 1833–1846, doi:10.1139/e87-174.

Aksu, A. E., P. J. Mudie, S. A. Macko, and A. de Vernal (1988), Upper Cenozoic history of the Labrador Sea, Baffin Bay, and the Arctic Ocean: A paleoclimatic and paleoceanographic summary, *Paleoceanography*, *3*(5), 519–538, doi:10.1029/PA003i005p00519.

Andrews, J., and D. Eberl (2012), Determination of sediment provenance by unmixing the mineralogy of source-area sediments: The "SedUnMix" program, *Marine Geology*, *291-294*, 24–33, doi:10.1016/j.margeo.2011.10.007.

Andrews, J., M. Kirby, A. Aksu, D. Barber, and D. Messe (1998), Late Quaternary Detrital Carbonate (DC-) layers in Baffin Bay marine sediments (67°N-74°N): Correlation with Heinrich Events in the North Atlantic?, *Quaternary Science Reviews*, *17*(12), 1125–1137.

Andrews, J. T., and K. Tedesco (1992), Detrital carbonate-rich sediments, northwestern Labrador Sea: Implications for ice-sheet dynamics and iceberg rafting (Heinrich) events in the North Atlantic, *Geology*, *20*(12), 1087, doi:10.1130/0091-7613(1992)020<1087:DCRSNL>2.3.CO;2.

Andrews, J. T., A. E. Jennings, M. Kerwin, M. Kirby, W. Manley, G. H. Miller, G. Bond, and B. MacLean (1995), A Heinrich-like event, H-0 (DC-0): Source(s) for detrital carbonate in the North Atlantic during the Younger Dryas Chronozone, *Paleoceanography*, *10*(5), 943–952, doi:10.1029/95PA01426.

Andrews, J. T., D. Eberl, and D. Scott (2011), Surface (sea floor) and near-surface (box cores) sediment mineralogy in Baffin Bay as a key to sediment provenance and ice sheet variations, *Canadian Journal of Earth Sciences*, *48*(9), 1307–1328, doi:10.1139/e11-021.

Andrews, J. T., D. C. Barber, A. E. Jennings, D. D. Eberl, B. Maclean, M. E. Kirby, and J. S. Stoner (2012), Varying sediment sources (Hudson Strait, Cumberland Sound, Baffin Bay) to the NW Labrador Sea slope between and during Heinrich events 0 to 4, *Journal of Quaternary Science*, *27*(5), 475–484, doi:10.1002/jqs.2535.

Andrews, J. T., O. T. Gibb, A. E. Jennings, and Q. Simon (2014), Variations in the provenance of sediment from ice sheets surrounding Baffin Bay during MIS 2 and 3 and export to the Labrador Shelf Sea: site HU2008029-0008 Davis Strait, *Journal of Quaternary Science*, *29*(1), 3–13, doi:10.1002/jqs.2643.

Azetsu-Scott, K., A. Clarke, K. Falkner, J. Hamilton, E. P. Jones, C. Lee, B. Petrie, S. Prinsenberg, M. Starr, and P. Yeats (2010), Calcium carbonate saturation states in the waters of the Canadian Arctic Archipelago and the Labrador Sea, *Journal of Geophysical Research*, *115*(C11), C11,021, doi:10.1029/2009JC005917.

Balsam, W. L., B. C. Deaton, and J. E. Damuth (1999), Evaluating optical lightness as a proxy for carbonate content in marine sediment cores, *Marine Geology*, *161*(2), 141–153, doi:10.1016/S0025-3227(99)00037-7.

Bard, E., M. Arnold, J. Mangerud, M. Paterne, L. Labeyrie, J. Duprat, M.-A. Mélières, E. Sønstegaard, and J.-C. Duplessy (1994), The North Atlantic atmosphere-sea surface 14C gradient during the Younger Dryas climatic event, *Earth and Planetary Science Letters*, *126*(4), 275–287, doi:10.1016/0012-821X(94)90112-0.

Bard, E., T. Tuna, Y. Fagault, L. Bonvalot, L. Wacker, S. Fahrni, and H.-A. Synal (2015), AixMICADAS, the accelerator mass spectrometer dedicated to 14C recently installed in Aix-en-Provence, France, *Nuclear Instruments and Methods in Physics Research Section B: Beam Interactions with Materials and Atoms*, *361*, 80–86, doi:10.1016/j.nimb.2015.01.075.

Bauer, J. E., C. E. Reimers, E. R. M. Druffel, and P. M. Williams (1995), Isotopic constraints on carbon exchange between deep ocean sediments and sea water, *Nature*, *373*(6516), 686–689, doi:10.1038/373686a0.

Berger, W. H. (1970), Planktonic Foraminifera: Selective solution and the lysocline, *Marine Geology*, *8*(2), 111–138, doi:http://dx.doi.org/10.1016/0025-3227(70)90001-0.

Blaauw, M., and J. A. Christen (2011), Flexible paleoclimate age-depth models using an autoregressive gamma process, *Bayesian Analysis*, *6*(3), 457–474.

Bond, G., H. Heinrich, W. Broecker, L. Labeyrie, J. McManus, J. Andrews, S. Huon, R. Jantschik, S. Clasen, C. Simet, K. Tedesco, M. Klas, G. Bonani, and S. Ivy (1992), Evidence for massive discharges of icebergs into the North Atlantic ocean during the last glacial period, *Nature*, *360*(6401), 245–249.

Bond, G., W. Broecker, S. Johnsen, J. McManus, L. Labeyrie, J. Jouzel, and G. Bonani (1993), Correlations between climate records from North Atlantic sediments and Greenland ice, *Nature*, *365*(6442), 143–147, doi:10.1038/365143a0.

Bond, G. C., R. Lotti, M. Cheseby, R. Lotti, P. Almasi, P. DeMenocal, P. Priore, H. Cullen, I. Hajdas, G. Bonani, G. H. Denton, W. Karlén, R. B. Alley, W. S. Broecker, T. Fronval, E. Jansen, G. C. Bond, R. Lotti, S. R. Epstein, R. Buchsbaum, H. A. Lowenstam, H. C. Urey, G. Wu, C. Hillaire-Marcel, D. W. Oppo, M. Horowitz, S. J. Lehman, M. S. McCartney, P. A. Mayewski, E. J. Brook, T. Sowers, J. Orchardo, P. Yiou, J. Jouzel, L. D. Keigwin, G. A. Jones, E. Cortijo, P. Yiou, L. Labeyrie, M. Cremer, J. C. Rogers, L. D. Keigwin, D. W. Oppo, S. J. Lehman, S. Rahmstorf, S. Manabe, R. J. Stouffer, T. F. Stocker, D. G. Wright, W. S. Broecker, K. Sakai, W. R. Peltier, E. Tziperman, A. J. Weaver, T. M. C. Hughes, R. T. Sutton, M. R. Allen, Y. Kushnir, P. Pestiaux, I. V. der Mersch, A. Berger, J. C. Duplessy, P. Yiou, H. J. Gudmundsson, E. A. Boyle, L. D. Keigwin, P. Kroopnick, M. J. Bender, G. C. Bond, J. T. Andrews, S. J. Lehman, L. D. Keigwin, L. D. Keigwin, G. A. Jones, T. Fronval, E. Jansen, H. Haflidason, H. P. Sejrup, D. K. Kristensen, S. Johnsen, J. S. Stoner, J. E. T. Channell, C. Hillaire-Marcel, T. V. Lowell, E. Bard, S. D. Woodruff, R. J. Slutz, R. L. Jenne, P. M. Steurer, A. McIntyre, B. Molfino, W. Dansgaard, N. J. Shackleton, J. Imbrie, M. A. Hall, and D. G. Martinson (1995), Iceberg discharges into the north atlantic on millennial time scales during the last glaciation., *Science (New York, N.Y.)*, *267*(5200), 1005–10, doi:10.1126/science.267.5200.1005.

Boudreau, B. P. (1998), Mean mixed depth of sediments: The wherefore and the why, *Limnology and Oceanography*, *43*(3), 524–526, doi:10.4319/lo.1998.43.3.0524.

Briner, J. P., I. Overeem, G. Miller, and R. Finkel (2007), The deglaciation of Clyde Inlet, northeastern Baffin Island, Arctic Canada, *Journal of Quaternary Science*, *22*(3), 223–232, doi:10.1002/jqs.1057.

Briner, J. P., N. P. McKay, Y. Axford, O. Bennike, R. S. Bradley, A. de Vernal, D. Fisher, P. Francus, B. Fréchette, K. Gajewski, A. Jennings, D. S. Kaufman, G. Miller, C. Rouston, and B. Wagner (2016), Holocene climate change in Arctic Canada and Greenland, doi:10.1016/j.quascirev.2016.02.010.

Broecker, W., G. Bond, M. Klas, E. Clark, and J. McManus (1992), Origin of the northern Atlantic's Heinrich events, *Climate Dynamics*, *6*(3-4), 265–273, doi:10.1007/BF00193540.

Broecker, W. S. (1994), Massive iceberg discharges as triggers for global climate change, *Nature*, *372*(6505), 421–424, doi:10.1038/372421a0.

Carlson, A. E., and P. U. Clark (2012), Ice sheet sources of sea level rise and freshwater

discharge during the last deglaciation, *Reviews of Geophysics*, *50*(4), RG4007, doi:10.1029/2011RG000371.

Channell, J., D. Hodell, O. Romero, C. Hillaire-Marcel, A. de Vernal, J. Stoner, A. Mazaud, and U. Röhl (2012), A 750-kyr detrital-layer stratigraphy for the North Atlantic (IODP Sites U1302-U1303, Orphan Knoll, Labrador Sea), *Earth and Planetary Science Letters*, *317-318*, 218–230, doi:10.1016/j.epsl.2011.11.029.

Channell, J. E. T., A. Mazaud, P. Sullivan, S. Turner, and M. E. Raymo (2002), Geomagnetic excursions and paleointensities in the Matuyama Chron at Ocean Drilling Program Sites 983 and 984 (Iceland Basin), *Journal of Geophysical Research: Solid Earth*, *107*(B6), EPM 1–1—-EPM 1–14, doi:10.1029/2001JB000491.

Chung, F. H. (1974), Quantitative interpretation of X-ray diffraction patterns of mixtures. I. Matrix-flushing method for quantitative multicomponent analysis, *Journal of Applied Crystallography*, *7*(6), 519–525, doi:10.1107/S0021889874010375.

Darby, D. A., J. F. Bischof, R. F. Spielhagen, S. A. Marshall, and S. W. Herman (2002), Arctic ice export events and their potential impact on global climate during the late Pleistocene, *Paleoceanography*, *17*(2), 15–1–15–17, doi:10.1029/2001PA000639.

de Groot, A. (2013), Sediment properties and carbonate preservation in two sediment cores from the southern Baffin Bay at the end of the Pleistocene and during the Holocene, Ph.D. thesis, Eberhard-Karls University of Tubingen.

de Vernal, A., C. Hillaire-Marcel, A. Aksu, and P. Mudie (1987), Palynostratigraphy and chronostratigraphy of Baffin Bay deep sea cores: Climatostratigraphic implications, *Palaeogeography, Palaeoclimatology, Palaeoecology*, *61*, 97–105.

de Vernal, A., G. Bilodeau, C. Hillaire-Marcel, and N. Kassou (1992), Quantitative assessment of carbonate dissolution in marine sediments from foraminifer linings vs. shell ratios: Davis Strait, northwest North Atlantic, *Geology*, *20*(6), 527–530, doi:10.1130/0091-7613(1992)020.

de Vernal, A., M. Henry, and G. Bilodeau (1996), Technique de preparation et d'analyse en micropaleontologie. Les Cahiers du GEOTOP Université du Québec à Montréal 3, *Tech. rep.*, GEOTOP Université du Québec à Montréal.

de Vernal, A., A. Rochon, J.-L. Turon, and J. Matthiessen (1997), Organic-walled dinoflagellate cysts: Palynological tracers of sea-surface conditions in middle to high latitude marine environments, *Geobios*, *30*(7), 905–920, doi:10.1016/S0016-6995(97)80215-X.

de Vernal, A., M. Henry, J. Matthiessen, P. J. Mudie, E. Rochon, K. P. Boessenkool, F. E. Erique Eynaud, K. Grøsfjeld, J. E. Guiot, D. Hamel, R. Harland, M. J. Head,

M. Kunz-pirrung, E. Levac, V. Loucheur, O. Peyron, V. Pospelova, T. Radi, J.-l. Turon, E. Voronina, D. Vernal, M. P. J, B. K. P, and R. Head (2001), Dinoflagellate cyst assemblages as tracers of sea-surface conditions in the northern North Atlantic, Arctic and sub-Arctic seas: the new 'n = 677' data base and its application for quantitative palaeoceanographic reconstruction, *Journal of Quaternary Science*, *16*(16), 681–698, doi:10.1002/jqs.659.

de Vernal, A., R. Gersonde, H. Goosse, M.-S. Seidenkrantz, and E. W. Wolff (2013a), Sea ice in the paleoclimate system: the challenge of reconstructing sea ice from proxies - an introduction, *Quaternary Science Reviews*, *79*, 1–8, doi:10.1016/j.quascirev.2013.08.009.

de Vernal, A., C. Hillaire-Marcel, A. Rochon, B. Fréchette, M. Henry, S. Solignac, and S. Bonnet (2013b), Dinocyst-based reconstructions of sea ice cover concentration during the Holocene in the Arctic Ocean, the northern North Atlantic Ocean and its adjacent seas, *Quaternary Science Reviews*, *79*, 111–121, doi:10.1016/j.quascirev.2013.07.006.

Dyke, A., J. Andrews, P. Clark, J. England, G. Miller, J. Shaw, and J. Veillette (2002), The Laurentide and Innuitian ice sheets during the Last Glacial Maximum, *Quaternary Science Reviews*, *21*(1-3), 9–31, doi:10.1016/S0277-3791(01)00095-6.

England, J., N. Atkinson, J. Bednarski, A. Dyke, D. Hodgson, and C. Ó Cofaigh (2006), The Innuitian Ice Sheet: configuration, dynamics and chronology, *Quaternary Science Reviews*, *25*(7-8), 689–703, doi:10.1016/j.quascirev.2005.08.007.

Funder, S. V., K. K. Kjeldsen, K. H. Kjær, and C. O'Cofaigh (2011), *The Greenland ice sheet during the past 300,000 years: a review*, pp. 699–713, Elsevier Science, doi:10.1016/B978-0-444-53447-7.00050-7.

Gibb, O. T. (2014), Paleohydrography of Baffin Bay, Davis Strait, and the northwest Labrador Sea during the last climatic cycle, Ph.D. thesis, UNIVERSITÉ DU QUÉBEC À MONTRÉAL.

Gibb, O. T., C. Hillaire-Marcel, and A. de Vernal (2014), Oceanographic regimes in the northwest Labrador Sea since Marine Isotope Stage 3 based on dinocyst and stable isotope proxy records, *Quaternary Science Reviews*, doi:10.1016/j.quascirev.2013.12.010.

Gibb, O. T., S. Steinhauer, B. Frechette, A. de Vernal, and C. Hillaire-Marcel (2015), Diachronous evolution of sea surface conditions in the Labrador Sea and Baffin Bay since the last deglaciation, *The Holocene*, *25*(12), 1882–1897, doi:10.1177/0959683615591352.

Hald, M., and S. Korsun (1997), Distribution of modern benthic foraminifera from fjords of Svalbard, European Arctic, *The Journal of Foraminiferal Research*, *27*(2).

Hammer, Ø., D. Harper, and P. Ryan (2001), PAST: Paleontological Statistics Software Package for Education and Data Analysis, *Palaeontologia Electronica*, *4*(1).

Harrison, J. C., M. R. St-Onge, O. V. Petrov, S. I. Strelnikov, B. G. Lopatin, F. H. Wilson, S. Tella, D. Paul, T. Lynds, S. P. Shokalsky, C. Hults, K, S. Bergman, H. Jepsen, F, and A. Solli (2011), Geological map of the Arctic, *Tech. rep.*, doi:10.4095/287868.

Heinrich, H. (1988), Origin and consequences of cyclic ice rafting in the Northeast Atlantic Ocean during the past 130,000 years, *Quaternary Research*, *29*(2), 142–152, doi:10.1016/0033-5894(88)90057-9.

Hemming, S. R. (2004), HEINRICH EVENTS : MASSIVE LATE PLEISTOCENE DETRITUS LAYERS OF THE NORTH ATLANTIC AND THEIR GLOBAL CLIMATE IMPRINT, *Marine Geology*, *42*(2003), 1–43, doi:10.1029/2003RG000128.1.INTRODUCTION.

Hilbrecht, H. (1996), Extant planktonic foraminifera and the physical environment in the Atlantic and Indian Oceans, in *Mitteilungen aus dem Geologischen Institut der Eidgen. Technischen Hochschule und der Universität Zürich*.

Hillaire-Marcel, C., and A. de Vernal (2008), Stable isotope clue to episodic sea ice formation in the glacial North Atlantic, *Earth and Planetary Science Letters*, *268*(1), 143–150.

Hiscott, R., A. Aksu, and O. Nielsen (1989), Provenance and dispersal patterns, Pliocene-Pleistocene section at site 645, Baffin Bay, *Proc. Ocean Drill. Program*, *105*, 31–52.

Hodell, D. A., J. E. T. Channell, J. H. Curtis, O. E. Romero, and U. Röhl (2008), Onset of "Hudson Strait" Heinrich events in the eastern North Atlantic at the end of the middle Pleistocene transition (~640 ka)?, *Paleoceanography*, *23*(4), n/a–n/a, doi:10.1029/2008PA001591.

Holland, D. M., R. H. Thomas, B. De Young, M. H. Ribergaard, and B. Lyberth (2008), Acceleration of Jakobshavn Isbrae triggered by warm subsurface ocean waters, *Nature geoscience*, *1*(10), 659.

Jackson, R., A. E. Carlson, C. Hillaire-Marcel, L. Wacker, C. Vogt, and M. Kucera (2017), Asynchronous instability of the North American-Arctic and Greenland ice sheets during the last deglaciation, *Quaternary Science Reviews*, *164*, 140–153, doi:10.1016/j.quascirev.2017.03.020.

Jennings, A., M. Hald, M. Smith, and J. Andrews (2006), Freshwater forcing from the Greenland Ice Sheet during the Younger Dryas: evidence from southeastern Greenland shelf cores, *Quaternary Science Reviews*, *25*(3), 282–298.

Jennings, A., J. Andrews, C. Pearce, L. Wilson, and S. Ólfasdótttir (2015), Detrital carbonate peaks on the Labrador shelf, a 13-7ka template for freshwater forcing from the Hudson Strait outlet of the Laurentide Ice Sheet into the subpolar gyre, *Quaternary Science Reviews*, *107*, 62–80, doi:10.1016/j.quascirev.2014.10.022.

Jennings, A. E., and G. Helgadottir (1994), Foraminiferal assemblages from the fjords and shelf of eastern Greenland, *The Journal of Foraminiferal Research*, *24*(2).

Jennings, A. E., and N. J. Weiner (1996), Environmental change in eastern Greenland during the last 1300 years: evidence from foraminifera and lithofacies in Nansen Fjord, 68Â N, *The Holocene*, *6*(2), 179–191, doi:10.1177/095968369600600205.

Jennings, A. E., N. J. Weiner, G. Helgadottir, and J. T. Andrews (2004), Modern foraminiferal faunas of the southwestern to northern Iceland shelf: Oceanographic and environmental controls, *The Journal of Foraminiferal Research*, *34*(3).

Jennings, A. E., M. E. Walton, C. Ó Cofaigh, A. Kilfeather, J. T. Andrews, J. D. Ortiz, A. De Vernal, and J. A. Dowdeswell (2014), Paleoenvironments during Younger Dryas-Early Holocene retreat of the Greenland Ice Sheet from outer Disko Trough, central west Greenland, *Journal of Quaternary Science*, *29*(1), 27–40, doi:10.1002/jqs.2652.

Jennings, A. E., J. T. Andrews, C. Ó Cofaigh, G. S. Onge, C. Sheldon, S. T. Belt, P. Cabedo-Sanz, and C. Hillaire-Marcel (2017), Ocean forcing of Ice Sheet retreat in central west Greenland from LGM to the early Holocene, *Earth and Planetary Science Letters*, *472*, 1–13, doi:10.1016/j.epsl.2017.05.007.

Kelley, S. E., J. P. Briner, and N. E. Young (2013), Rapid ice retreat in Disko Bugt supported by 10Be dating of the last recession of the western Greenland Ice Sheet, *Quaternary Science Reviews*, *82*, 13–22, doi:10.1016/j.quascirev.2013.09.018.

Kelley, S. E., J. P. Briner, and S. R. H. Zimmerman (2015), The influence of ice marginal setting on early Holocene retreat rates in central West Greenland, *Journal of Quaternary Science*, *30*(3), 271–280, doi:10.1002/jqs.2778.

Kirschvink, J. L. (1980), The least-squares line and plane and the analysis of palaeomagnetic data, *Geophysical Journal International*, *62*(3), 699–718, doi:10.1111/j.1365-246X.1980.tb02601.x.

Knudsen, K.-L., B. Stabell, M.-S. Seidenkrantz, J. Eiriksson, and W. Blake Jr (2008), Deglacial and Holocene conditions in northernmost Baffin Bay: sediments,

foraminifera, diatoms and stable isotopes, *Boreas*, *37*(3), 346–376, doi:10.1111/j.1502-3885.2008.00035.x.

Knutz, P. C., M.-A. Sicre, H. Ebbesen, S. Christiansen, and A. Kuijpers (2011), Multiple-stage deglacial retreat of the southern Greenland Ice Sheet linked with Irminger Current warm water transport, *Paleoceanography*, *26*(3), n/a–n/a, doi:10.1029/2010PA002053.

Korsun, S., and M. Hald (2000), Seasonal dynamics of benthic foraminifera in a glacially fed fjord of Svalbard, European Arctic, *The Journal of Foraminiferal Research*, *30*(4).

Krahmann, G. (2013), Physical oceanography during Maria S. Merian cruise MSM09/2, doi:10.1594/PANGAEA.819207.

Kucera, M., M. Rhein, and K. Gohl (2014), Oceanography and geodynamics in the NW Atlantic and the Baffin Bay-Cruise No.MSM09-July 23-October 29, 2008-Bremen (Germany)-Ponta Delgada (Azores), *Tech. rep.*, doi:10.2312/cr_msm09.

Lagoe, M. B. (1977), Recent benthic Foraminifera from the central Arctic Ocean, *The Journal of Foraminiferal Research*, *7*(2).

Laj, C., C. Kissel, and J. Beer (2004), High Resolution Global Paleointensity Stack Since 75 kyr (GLOPIS-75) Calibrated to Absolute Values, in *Timescales of the internal geomagnetic field*, pp. 255–265, American Geophysical Union, doi:10.1029/145GM19.

Laskar, J., P. Robutel, F. Joutel, M. Gastineau, A. C. M. Correia, and B. Levrard (2004), A long-term numerical solution for the insolation quantities of the Earth, *Astronomy and Astrophysics*, *428*(1), 261–285, doi:10.1051/0004-6361:20041335.

Li, G., D. J. Piper, and D. Calvin Campbell (2011), The Quaternary Lancaster Sound trough-mouth fan, NW Baffin Bay, *Journal of Quaternary Science*, *26*(5), 511–522, doi:10.1002/jqs.1479.

Liu, Q., A. P. Roberts, J. Torrent, C.-S. Horng, and J. C. Larrasoaña (2007), What do the HIRM and S -ratio really measure in environmental magnetism?, *Geochemistry, Geophysics, Geosystems*, *8*(9), n/a–n/a, doi:10.1029/2007GC001717.

Liu, Q., A. P. Roberts, J. C. Larrasoaña, S. K. Banerjee, Y. Guyodo, L. Tauxe, and F. Oldfield (2012), Environmental magnetism: Principles and applications, *Reviews of Geophysics*, *50*(4), RG4002, doi:10.1029/2012RG000393.

Lloyd, J., M. Moros, K. Perner, R. J. Telford, A. Kuijpers, E. Jansen, and D. McCarthy (2011), A 100 yr record of ocean temperature control on the stability of Jakobshavn Isbrae, West Greenland, *Geology*, *39*(9), 867–870, doi:10.1130/G32076.1.

Lloyd, J. M. (2006), Modern distribution of benthic foraminifera from Disko Bugt, West

Greenland., *Journal Of Foraminiferal Research*, *36*(4), 315–+, doi:10.2113/gsjfr.36.4.315.

Lund, D. C., A. C. Mix, and J. Southon (2011), Increased ventilation age of the deep northeast Pacific Ocean during the last deglaciation, *Nature Geoscience*, *4*(11), 771–774, doi:10.1038/ngeo1272.

Mackensen, A., H. Sejrup, and E. Jansen (1985), The distribution of living benthic foraminifera on the continental slope and rise off southwest Norway, *Marine Micropaleontology*, *9*(4), 275–306, doi:10.1016/0377-8398(85)90001-5.

Maclean, B., G. L. Williams, and S. P. Shrivastava (1990), Part 2: Geology of Baffin Bay and Davis Strait, in *Geology of the Continental Margins of Eastern Canada*, vol. 29, pp. 325–348, doi:10.4095/132710.

Marcott, S. A., P. U. Clark, L. Padman, G. P. Klinkhammer, S. R. Springer, Z. Liu, B. L. Otto-Bliesner, A. E. Carlson, A. Ungerer, J. Padman, F. He, J. Cheng, and A. Schmittner (2011), Ice-shelf collapse from subsurface warming as a trigger for Heinrich events., *Proceedings of the National Academy of Sciences of the United States of America*, *108*(33), 13,415–9, doi:10.1073/pnas.1104772108.

Marshall, S. J., and M. R. Koutnik (2006), Ice sheet action versus reaction: Distinguishing between heinrich events and dansgaard-oeschger cycles in the north atlantic, *Paleoceanography*, *21*(2), n/a–n/a, doi:10.1029/2005PA001247, pA2021.

McManus, J. F., R. Francois, J.-M. Gherardi, L. D. Keigwin, and S. Brown-Leger (2004), Collapse and rapid resumption of Atlantic meridional circulation linked to deglacial climate changes., *Nature*, *428*(6985), 834–7, doi:10.1038/nature02494.

Mudie, P. J., and A. E. Aksu (1984), Palaeoclimate of Baffin Bay from 300,000-year record of foraminifera, dinoflagellates and pollen, *Nature*, *312*(5995), 630–634, doi:10.1038/312630a0.

Ò Cofaigh, C., J. A. Dowdeswell, A. E. Jennings, K. A. Hogan, A. Kilfeather, J. F. Hiemstra, R. Noormets, J. Evans, D. J. McCarthy, J. T. Andrews, J. M. Lloyd, and M. Moros (2013), An extensive and dynamic ice sheet on the West Greenland shelf during the last glacial cycle, *Geology*, *41*(2), 219–222, doi:10.1130/G33759.1.

Ó Cofaigh, C., J. T. Andrews, A. E. Jennings, J. A. Dowdeswell, K. A. Hogan, A. A. Kilfeather, and C. Sheldon (2013), Glacimarine lithofacies, provenance and depositional processes on a West Greenland trough-mouth fan, *Journal of Quaternary Science*, *28*(1), 13–26, doi:10.1002/jqs.2569.

Oksman, M., K. Weckström, A. Miettinen, S. Juggins, D. Divine, R. Jackson, R. Telford, N. J. Korsgaard, and M. Kucera (2017), Younger Dryas ice margin retreat triggered by

warming of the ocean surface in central-eastern Baffin Bay, *Nature communications*, (In review).

Ouellet-Bernier, M.-M., A. de Vernal, C. Hillaire-Marcel, and M. Moros (2014), Paleoceanographic changes in the Disko Bugt area, West Greenland, during the Holocene, *The Holocene*, *24*(11), 1573–1583, doi:10.1177/0959683614544060.

Pearce, C., M.-S. Seidenkrantz, A. Kuijpers, G. Massé, N. F. Reynisson, and S. M. Kristiansen (2013), Ocean lead at the termination of the Younger Dryas cold spell., *Nature communications*, *4*, 1664, doi:10.1038/ncomms2686.

Pearce, C., J. T. Andrews, I. Bouloubassi, C. Hillaire-Marcel, A. E. Jennings, J. Olsen, A. Kuijpers, and M.-S. Seidenkrantz (2015), Heinrich 0 on the east Canadian margin: Source, distribution, and timing, *Paleoceanography*, *30*(12), 1613–1624, doi:10.1002/2015PA002884.

Perner, K., M. Moros, J. Lloyd, A. Kuijpers, R. Telford, and J. Harff (2011), Centennial scale benthic foraminiferal record of late Holocene oceanographic variability in Disko Bugt, West Greenland, *Quaternary Science Reviews*, *30*(19), 2815–2826.

Perner, K., M. Moros, A. Jennings, J. Lloyd, and K. Knudsen (2013), Holocene palaeoceanographic evolution off West Greenland, *The Holocene*, *23*(3), 374–387, doi:10.1177/0959683612460785.

Polyak, L., and A. Solheim (1994), Late-and postglacial environments in the northern Barents Sea west of Franz Josef Land, *Polar Research*, *13*(2), 197–207, doi:10.1111/j.1751-8369.1994.tb00449.x.

Polyak, L., S. Korsun, L. A. Febo, V. Stanovoy, T. Khusid, M. Hald, B. E. Paulsen, and D. J. Lubinski (2002), Benthic Foraminiferal Assemblages from the Southern Kara Sea, a River-Influenced Arctic Marine Environment, *The Journal of Foraminiferal Research*, *32*(3).

Rashid, H., R. Hesse, and D. J. Piper (2003), Origin of unusually thick Heinrich layers in ice-proximal regions of the northwest Labrador Sea, *Earth and Planetary Science Letters*, *208*(3), 319–336, doi:10.1016/S0012-821X(03)00030-X.

Rasmussen, S. O., K. K. Andersen, A. M. Svensson, J. P. Steffensen, B. M. Vinther, H. B. Clausen, M.-L. Siggaard-Andersen, S. J. Johnsen, L. B. Larsen, D. Dahl-Jensen, M. Bigler, R. Röthlisberger, H. Fischer, K. Goto-Azuma, M. E. Hansson, and U. Ruth (2006), A new Greenland ice core chronology for the last glacial termination, *Journal of Geophysical Research*, *111*(D6), D06,102, doi:10.1029/2005JD006079.

Reimer, P. (2013a), Selection and Treatment of Data for Radiocarbon Calibration: An

Update to the International Calibration (IntCal) Criteria, *Radiocarbon*, *55*(4), 1923–1945, doi:10.2458/azu_js_rc.55.16955.

Reimer, P. (2013b), IntCal13 and Marine13 Radiocarbon Age Calibration Curves 0-50,000 Years cal BP, *Radiocarbon*, *55*(4), 1869–1887, doi:10.2458/azu_js_rc.55.16947.

Rochon, A., A. de Vernal, J.-L. Turon, J. Matthießen, and M. J. Head (1999), Distribution of recent dinoflagellate cysts in surface sediments from the North Atlantic Ocean and adjacent seas in relation to sea-surface parameters, *American Association of Stratigraphic Palynologists Contribution Series*, *35*, 1–146.

Rytter, F., K. L. Knudsen, M.-S. Seidenkrantz, and J. Eiríksson (2002), MODERN DISTRIBUTION OF BENTHIC FORAMINIFERA ON THE NORTH ICELANDIC SHELF AND SLOPE, *The Journal of Foraminiferal Research*, *32*(3).

Seidenkrantz, M.-S. (1995), Cassidulina teretis Tappan and Cassidulina neoteretis new species (Foraminifera): stratigraphic markers for deep sea and outer shelf areas, *Journal of Micropalaeontology*, *14*(2), 145–157, doi:10.1144/jm.14.2.145.

Seidenkrantz, M.-S., H. Ebbesen, S. Aagaard-Sørensen, M. Moros, J. M. Lloyd, J. Olsen, M. F. Knudsen, and A. Kuijpers (2013), Early Holocene large-scale meltwater discharge from Greenland documented by foraminifera and sediment parameters, *Palaeogeography, Palaeoclimatology, Palaeoecology*, *391*, 71–81, doi:10.1016/j.palaeo.2012.04.006.

Sheldon, C., A. Jennings, J. T. Andrews, K. Hogan, J. A. Dowdeswell, and M.-S. Seidenkrantz (2016), Ice stream retreat following the LGM and onset of the west Greenland current in Uummannaq Trough, west Greenland, *Quaternary Science Reviews*, *147*, 27–46, doi:10.1016/j.quascirev.2016.01.019.

Simon, Q., G. St-Onge, and C. Hillaire-Marcel (2012), Late Quaternary chronostratigraphic framework of deep Baffin Bay glaciomarine sediments from high-resolution paleomagnetic data, *Geochemistry, Geophysics, Geosystems*, *13*(1), doi:10.1029/2012GC004272.

Simon, Q., C. Hillaire-Marcel, G. St-Onge, and J. T. Andrews (2014), North-eastern Laurentide, western Greenland and southern Innuitian ice stream dynamics during the last glacial cycle, *Journal of Quaternary Science*, *29*(1), 14–26, doi:10.1002/jqs.2648.

Sinclair, G., A. Carlson, A. Mix, B. Lecavalier, G. Milne, A. Mathias, C. Buizert, and R. DeConto (2016), Diachronous retreat of the Greenland ice sheet during the last deglaciation, *Quaternary Science Reviews*, *145*, 243–258, doi:10.1016/j.quascirev.2016.05.040.

Stoner, J. S., and G. St-Onge (2007), Chapter Three Magnetic Stratigraphy in Paleoceanography: Reversals, Excursions, Paleointensity, and Secular Variation, in *Proxies in Late Cenozoic Paleoceanography*, *Developments in Marine Geology*, vol. 1, edited by C. Hillaire-Marcel and A. D. Vernal, pp. 99–138, Elsevier, doi:https://doi.org/10.1016/S1572-5480(07)01008-1.

Tang, C. C., C. K. Ross, T. Yao, B. Petrie, B. M. DeTracey, and E. Dunlap (2004), The circulation, water masses and sea-ice of Baffin Bay, *Progress in Oceanography*, *63*(4), 183–228.

Tauxe, L., T. Pick, and Y. S. Kok (1995), Relative paleointensity in sediments: A Pseudo-Thellier Approach, *Geophysical Research Letters*, *22*(21), 2885–2888, doi:10.1029/95GL03166.

Teanby, N., and D. Gubbins (2000), The effects of aliasing and lock-in processes on palaeosecular variation records from sediments, *Geophysical Journal International*, *142*(2), 563–570.

Thiagarajan, N., A. V. Subhas, J. R. Southon, J. M. Eiler, and J. F. Adkins (2014), Abrupt pre-Bølling-Allerød warming and circulation changes in the deep ocean., *Nature*, *511*(7507), 75–8, doi:10.1038/nature13472.

Vilks, G. (1981), Late Glacial-Postglacial Foraminiferal Boundary in Sediments of Eastern Canada, Denmark and Norway, *Geoscience Canada*, *8*(2).

Vogt, C., J. Lauterjung, and R. X. Fischer (2002), Investigation of the Clay Fraction ($<$2 μm) of the Clay Minerals Society Reference Clays, *Clays and Clay Minerals*, *50*(3), 388–400, doi:10.1346/000986002760833765.

Wacker, L., J. Lippold, M. Molnár, and H. Schulz (2013), Towards radiocarbon dating of single foraminifera with a gas ion source, *Nuclear Instruments and Methods in Physics Research Section B: Beam Interactions with Materials and Atoms*, *294*, 307–310, doi:10.1016/j.nimb.2012.08.038.

Waelbroeck, C., L. Labeyrie, E. Michel, J. Duplessy, J. McManus, K. Lambeck, E. Balbon, and M. Labracherie (2002), Sea-level and deep water temperature changes derived from benthic foraminifera isotopic records, *Quaternary Science Reviews*, *21*(1-3), 295–305, doi:10.1016/S0277-3791(01)00101-9.

Winsor, K., A. E. Carlson, G. P. Klinkhammer, J. S. Stoner, and R. G. Hatfield (2012), Evolution of the northeast Labrador Sea during the last interglaciation, *Geochemistry, Geophysics, Geosystems*, *13*(11), n/a–n/a, doi:10.1029/2012GC004263.

Wu, G., and C. Hillaire-Marcel (1994), Accelerator mass spectrometry radiocarbon strati-

graphies in deep Labrador Sea cores: paleoceanographic implications, *Canadian Journal of Earth Sciences*, *31*(1), 38–47.

Young, N. E., J. P. Briner, D. H. Rood, R. C. Finkel, L. B. Corbett, and P. R. Bierman (2013), Age of the Fjord Stade moraines in the Disko Bugt region, western Greenland, and the 9.3 and 8.2 ka cooling events, *Quaternary Science Reviews*, *60*, 76–90, doi: 10.1016/j.quascirev.2012.09.028.

Zonneveld, K. A., G. J. Versteegh, and G. J. de Lange (1997), Preservation of organic-walled dinoflagellate cysts in different oxygen regimes: a 10,000 year natural experiment, *Marine Micropaleontology*, *29*(3), 393–405, doi:10.1016/S0377-8398(96)00032-1.

Zonneveld, K. A., F. Bockelmann, and U. Holzwarth (2007), Selective preservation of organic-walled dinoflagellate cysts as a tool to quantify past net primary production and bottom water oxygen concentrations, *Marine Geology*, *237*(3), 109–126, doi: 10.1016/j.margeo.2006.10.023.

Zreda, M., J. England, F. Phillips, D. Elmore, and P. Sharma (1999), Unblocking of the Nares Strait by Greenland and Ellesmere ice-sheet retreat 10,000 years ago, *Nature*, *398*(6723), 139–142, doi:10.1038/18197.